

ADA037070

Report SAM-TR-76-38

PREDICTING EYE SAFE SEPARATION  
FROM NUCLEAR DETONATIONS

December 1976

Final Report for Period January 1975-January 1976

Approved for public release; distrib

USAF SCHOOL OF AEROSPACE MEDICINE  
Aerospace Medical Division (AFSC)  
Brooks Air Force Base, Texas 78235

NOTICES

This final report was submitted by personnel of the Weapons Effects Branch, Radiation Sciences Division, USAF School of Aerospace Medicine, Aerospace Medical Division, AFSC, Brooks Air Force Base, Texas, under job order 7757-05-27.

When U.S. Government drawings, specifications, or other data are used for any purpose other than a definitely related Government procurement operation, the Government thereby incurs no responsibility nor any obligation whatsoever; and the fact that the Government may have formulated, furnished, or in any way supplied the said drawings, specifications, or other data is not to be regarded by implication or otherwise, as in any manner licensing the holder or any other person or corporation, or conveying any rights or permission to manufacture, use, or sell any patented invention that may in any way be related thereto.

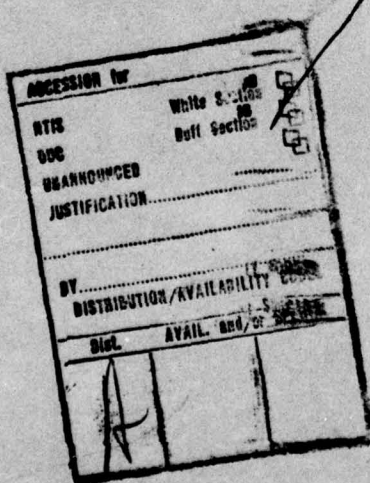
This report has been reviewed by the Information Office (OI) and is releasable to the National Technical Information Service (NTIS). At NTIS, it will be available to the general public, including foreign nations.

This technical report has been reviewed and is approved for publication.

*Everett O. Richey*  
EVERETT O. RICHEY, M.S.  
Project Scientist

*Donald N. Farrar*  
DONALD N. FARRER, Ph.D.  
Supervisor

*Robert G. McIver*  
ROBERT G. MCIVER, Colonel, USAF, MC  
Commander



Unclassified

SECURITY CLASSIFICATION OF THIS PAGE (When Data Entered)

REPORT DOCUMENTATION PAGE		READ INSTRUCTIONS BEFORE COMPLETING FORM
1. REPORT NUMBER 14 SAM-TR-76-38	2. GOVT ACCESSION NO.	3. RECIPIENT'S CATALOG NUMBER 9
4. TITLE (and Subtitle) 6 PREDICTING EYE SAFE SEPARATION DISTANCES FROM NUCLEAR DETONATIONS	5. TYPE OF REPORT & PERIOD COVERED Final <i>rept.</i> Jan 1975 - Jan 1976	
7. AUTHOR(s) 10 Everett G. Richey	8. CONTRACT OR GRANT NUMBER(s)	
9. PERFORMING ORGANIZATION NAME AND ADDRESS USAF School of Aerospace Medicine (RAW) Aerospace Medical Division (AFSC) Brooks AFB, Texas 78235	10. PROGRAM ELEMENT, PROJECT, TASK AREA & WORK UNIT NUMBERS 62202F 7757-05-27	
11. CONTROLLING OFFICE NAME AND ADDRESS USAF School of Aerospace Medicine (RAW) Aerospace Medical Division (AFSC) Brooks AFB, Texas 78235	12. REPORT DATE 11 December 1976	13. NUMBER OF PAGES 112
14. MONITORING AGENCY NAME & ADDRESS (if different from Controlling Office) 12 115p. 16 7757	15. SECURITY CLASS. (of this report) Unclassified	
16. DISTRIBUTION STATEMENT (of this Report)  Approved for public release; distribution unlimited.		
17. DISTRIBUTION STATEMENT (of the abstract entered in Block 20, if different from Report) 17 05		
18. SUPPLEMENTARY NOTES		
19. KEY WORDS (Continue on reverse side if necessary and identify by block number) Flashblindness Retinal burns Nuclear-flash eye effects Nuclear safe separation distances		
20. ABSTRACT (Continue on reverse side if necessary and identify by block number) Effects of retinal burns and flashblindness caused by eye exposure to nuclear flashes are reviewed, and mathematical concepts and equations used to predict eye safe separation distances (SSD) from low-altitude nuclear detonations are developed. A computer program using these concepts and equations has been prepared, and predicted results are compared with Operation Dominic experimental results. Effects on predicted SSD are shown for attenuation of the nuclear flash thermal energy by a B-1 windscreen and by sunglasses. Predicted SSD for both retinal burns and flashblindness, for day and night conditions, are shown for detonation		

317000

JB

**Unclassified**

SECURITY CLASSIFICATION OF THIS PAGE(When Data Entered)

Item 20 - Abstract - Continued:

yields from 0.01 to 10,000 kt; for detonation altitudes of 1, 10, and 30 kft; and for visibilities of 5 and 25 naut. miles.

This method for predicting SSD to prevent nuclear-flash retinal burns and flashblindness is recommended for use by the Air Force.

**Unclassified**

SECURITY CLASSIFICATION OF THIS PAGE(When Data Entered)

## CONTENTS

	<u>Page</u>
INTRODUCTION .....	3
DISCUSSION .....	5
Weapon Characteristics .....	5
Atmospheric Transmission .....	6
Interaction of Radiation Energy with the Eye .....	7
Chorioretinal Burns .....	8
Visual Effects of Chorioretinal Burns .....	9
Flashblindness .....	12
MATHEMATICAL MODEL .....	14
Chorioretinal Burns .....	15
Calculation of Retinal Exposure .....	15
Calculation of Transmission .....	20
Determination of Chorioretinal Burn Threshold .....	28
Iteration Convergence Procedure .....	31
Flashblindness .....	32
Calculation of Effective Luminous Exposure .....	32
Flashblindness Criteria .....	38
Irradiance and Total Exposure at Plane and Cornea .....	41
CONCLUSIONS AND RECOMMENDATIONS .....	42
REFERENCES .....	51
APPENDIXES .....	55
A -- Retinal Burn and Flashblindness SSD; Day; 25-Naut.-Mile (46.3-km) Visibility .....	57
B -- Retinal Burn and Flashblindness SSD; Day; 5-Naut.-Mile (9.3-km) Visibility .....	71
C -- Retinal Burn and Flashblindness SSD; Night; 25-Naut.-Mile (46.3-km) Visibility .....	85
D -- Retinal Burn and Flashblindness SSD; Night; 5-Naut.-Mile (9.3-km) Visibility .....	99

LIST OF ILLUSTRATIONS

<u>FIGURE</u>		<u>Page</u>
1 -- Distribution of Energy in a Nuclear Detonation .....		5
2 -- Apparent Fireball-Surface Temperature vs. Time .....		6
3 -- Schematic Drawing of Eye .....		8
4 -- Visual Acuity vs. Distance from Fovea .....		10
5 -- Schematic Retinal Burns and Scotomata .....		11
6 -- Schematic Retinal Nerve Fibers .....		12
7 -- Schematic Visual-Field Defects .....		13
8 -- Flashblindness vs. Exposure and Task Luminance .....		14
9 -- Scaled Fireball Diameter vs. Scaled Time .....		18
10 -- Geometry for Determining Atmospheric Transmission .....		22
11 -- Retinal Burn Thresholds for Monkeys .....		29
12 -- Flashblindness Recovery Times .....		41
13 -- Predicted and Experimental Retinal Burn Threshold Distances for Rabbits .....		43
14 -- Predicted Retinal Burn SSD vs. Observer Altitude for Unprotected Observers .....		45
15 -- Predicted Flashblindness SSD vs. Observer Altitude for Unprotected Observers .....		46
16 -- Predicted Retinal Burn SSD vs. Observer Altitude for Protected Observers .....		46
17 -- Predicted Flashblindness SSD vs. Observer Altitude for Protected Observers .....		47
18 -- Predicted Retinal Burn SSD vs. Observer Altitude for Protected Observers .....		47
19 -- Predicted Flashblindness SSD vs. Observer Altitude for Protected Observers .....		48
20 -- Predicted Retinal Burn SSD vs. Time for Unprotected and Protected Observers .....		49
21 -- Predicted Flashblindness SSD vs. Time for Unprotected and Protected Observers .....		50

## PREDICTING EYE SAFE SEPARATION DISTANCES FROM NUCLEAR DETONATIONS

### INTRODUCTION

The thermal energy released in a nuclear detonation can cause visual impairment in personnel who view such detonations without adequate eye protection. This impairment may be temporary, as in flashblindness, or permanent, as in chorioretinal burns. The extent and duration of these eye effects depend on exposure conditions and, because the eye focuses the causative radiant energy, can be a serious hazard at extreme distances—far greater than the range at which any other direct effects are a biological hazard (11). The first reported case of a human retinal burn caused by a nuclear detonation occurred during the Hiroshima atomic explosion (37). Although the need for eye protection was recognized and protective goggles were worn at the first atomic bomb test in 1942 and all subsequent tests, there is a history of eye injury to personnel engaged in nuclear weapons testing who viewed detonations without proper eye protection. Six cases were reported in 1956 (42), and two others after the high-altitude detonations in October 1962 (17).

Early experiments in flashblindness concluded that this was not a major problem with nominal-yield detonations (20 kt) during daylight hours (12), but that recovery of useful vision at very low light levels could require as long as 11 minutes following exposure to a nuclear detonation (13). Experiments during Operation Upshot-Knothole in 1953 (14) concluded that a pilot would be able to perform typical visual tasks required in flying his aircraft within 60 seconds following exposure under the test conditions.

Operating modern high-performance military equipment, however, is a complex task requiring good vision even under favorable circumstances. During critical periods of mission performance, vision loss for even a few seconds may negate the mission and result in a loss of personnel and equipment. When the probability of viewing nuclear detonations from hostile activities in a nuclear war is combined with the probability of viewing our own nuclear detonations, visual impairment caused by these detonations becomes a problem of prime importance to the military services. Predictions of nuclear-flash eye effects are required for operational planning and for evaluating existing or proposed eye-protection devices.

Early efforts to predict eye safe separation distances were simplified approximations, hampered by lack of data on the thermal emission of nuclear detonations, atmospheric attenuation and scattering, and the interaction of thermal energy with the eye. In 1962, predictions of retinal burn

threshold distances were used with considerable success to position experimental animals during Operations Dominic and Fishbowl. Flashblindness and retinal burn threshold distances from low-yield nuclear detonations, and a method for calculating these distances, were published in 1966 (39, 40). As more experimental data became available and computer programs were developed, many flashblindness and retinal burn safe separation curves were published in 1967 (4). In 1968 and 1969, the curves were updated as additional experimental data became available and computer programs were improved (5, 6, 47). In 1972, a mathematical model to predict flashblindness, based on a theoretical treatment of photopigment bleaching and regeneration, was published (20).

Computer programs to solve the heat-diffusion equation for the eye have been developed and incorporated in retinal burn prediction programs, generally called Temperature Models (7, 36, 48). The use of these programs, however, has been handicapped by lack of definitive data relating predicted time-temperature profiles in the retina to retinal damage and visual impairment.

The U.S. Air Force presently uses an Exposure Model for predicting retinal burn and flashblindness safe distances from low-altitude nuclear detonations. This model relates calculated retinal exposures to retinal effects observed in humans and experimental animals. An iterative-type computer program calculates the eye safe separation distance to prevent either retinal burns or flashblindness, or both. Eye safe separation distance (SSD), as used in this report, is the minimum distance, measured on the earth's surface between detonation ground zero and the point directly under the observer, at which the observer may view the nuclear fireball without permanent retinal damage or more than 10 seconds recovery time from flashblindness.

The method used to calculate the retinal burn safe distance is essentially the same as used in the past. Much of the discussion and mathematical development can be found scattered in references 4, 5, 6, 41, and 47. The discussion and development are repeated here to gather in one report information on the interaction of radiant energy with the eye, the development and solution of equations to calculate the radiant energy reaching the retina, and the use of this information to predict safe distances to prevent retinal burns. The computer program has been completely rewritten to (1) simplify the program and increase computer efficiency, (2) divide the spectrum of the radiant energy considered into 14 bands, (3) account for the constriction of the pupil after exposure to the nuclear flash, (4) enable input of visibility, and (5) update the constants and threshold data.

The method used to determine the flashblindness safe distance compares a calculated exposure to the experimentally determined exposure required for a given recovery time, but the method of calculating the exposure is different from that used in previous flashblindness prediction models.

The purpose of this report is to describe the interaction of radiant energy with the eye, show the development and solution of mathematical concepts used in the Exposure Model, and present curves of eye SSD predictions for different detonations and exposure conditions. Nuclear detonation characteristics, atmospheric transmission, and pertinent aspects of the physiology of the eye are discussed briefly to acquaint the reader with the basic concepts involved and to relate retinal exposure to impairment of visual function.

## DISCUSSION

### Weapon Characteristics

Much of the energy in a nuclear detonation is emitted as thermal energy (light and heat), which is responsible for chorioretinal burns and flashblindness. Figure 1 shows the distribution of energy from a fission weapon in a typical air burst. For air bursts below 15,240 m (50,000 ft), 30% to 40% of the total energy is emitted as thermal energy (25). At low altitudes a nuclear detonation forms a gaseous fireball and essentially

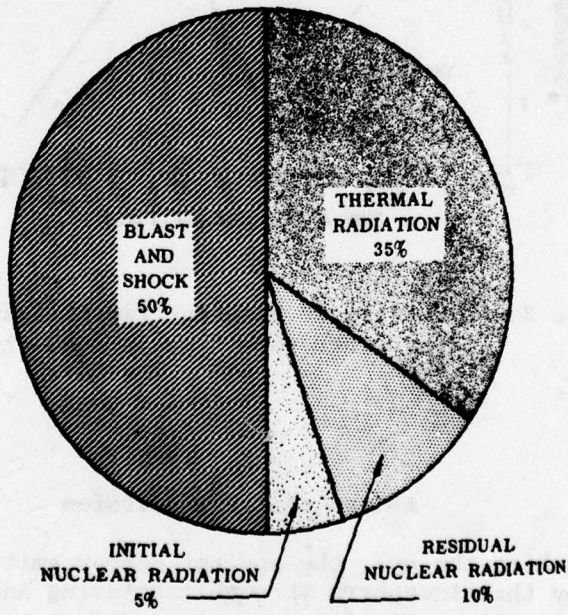


Figure 1. Distribution of energy in a typical air burst of a fission weapon at an altitude below 30,480 m (100,000 ft).

all of the thermal energy is emitted in two pulses. Figure 2 shows, as a function of time, the apparent surface temperature of a 20-kt detonation at low altitude (25). The first pulse is relatively short and contains only about 1% of the total energy, but may produce flashblindness or a chorioretinal burn. As the detonation altitude increases, more of the thermal energy appears in the first pulse until, for very high altitude detonations, essentially all of the thermal energy is emitted in a single, very short pulse.

The amount of thermal energy reaching an observer depends upon the weapon design, detonation yield and altitude, observer altitude and distance, and characteristics of the intervening atmosphere. Estimating the thermal energy that will reach an observer is a major problem in predicting nuclear-flash eye effects, and accounts for much of the uncertainty in prediction results.

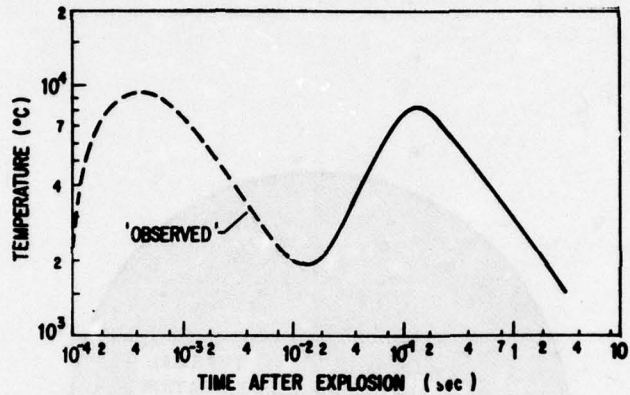


Figure 2. Variation of apparent fireball surface temperature with time in a 20-kt explosion.

#### Atmospheric Transmission

Before reaching the eye, the radiant energy emitted by the fireball is attenuated by the atmosphere through scattering and absorption processes. Atmospheric attenuation is a complex subject because of the variety of phenomena and situations that can be involved. In general, attenuation of radiant energy by the atmosphere depends upon the composition,

characteristics, and distribution of the atmosphere in the path between the detonation and observer, and the spectrum of the radiation energy. These atmospheric factors vary with time and geographic location and are difficult or impossible to predict with any accuracy. For the problem of retinal burns, considering all phenomena involved or accounting for the full range of situations and variations which can occur does not appear necessary (6); thus, consideration has been limited to the unscattered, or image-forming, radiation. For the flashblindness problem, consideration has been limited to the unscattered and single-scattered radi-

#### Interaction of Radiation Energy with the Eye

Thermal energy and light concentrated on the retina by the eye lens system can result in either permanent injury to the retina (chorioretinal burns) or temporary visual impairment (flashblindness). Normally, however, permanent injury to the retina occurs only if the source of energy or a specular reflection is in the field of vision so that an image of the source is formed on the retina. Because the eye focuses the radiant energy, the distance at which retinal damage can occur may be much greater than the distances at which skin burns or other direct effects are a hazard. This results from the fact that both the irradiance (energy per unit area per unit time) incident on the eye and the area of the fireball image on the retina are inversely proportional to the square of the distance from the fireball. As a result, the irradiance at the retina in the image of the fireball is independent of the distance from the fireball--except for the attenuation introduced by the atmosphere. Fortunately, atmospheric attenuation increases with distance, so distance does provide protection.

Scattering of light by the atmosphere and by clouds or other non-specular-reflecting surfaces can result in sufficient luminous exposure to cause flashblindness even though the fireball is not in the field of vision. Normally, however, the distance at which flashblindness occurs is greater if the fireball is in the visual field than if it is not, and the distance is maximum when the fireball is in the center of the visual field. As with chorioretinal burns, atmospheric attenuation decreases the distance at which flashblindness occurs, and distance does provide protection. The distance at which flashblindness occurs may be greater than, equal to, or less than the distance at which permanent retinal damage occurs, depending upon the conditions of exposure and the luminance and complexity of the visual task to be performed following the exposure.

At low levels of illumination the pupil of the eye normally enlarges to admit more light. Thus, the pupil is larger and allows more thermal energy from the fireball to enter the eye at dusk or night than in daylight. Also, only radiation received prior to closing the eyes in a reflexive blink contributes to chorioretinal burns and flashblindness. As a result, both the ambient light condition and blink reflex time must be considered in predicting eye safe distances (6).

### Chorioretinal Burns

A schematic drawing of the human eye is shown in Figure 3. For purposes of discussion, the eye may be compared to a camera. Radiant energy received by the eye is refracted by the cornea, anterior chamber,

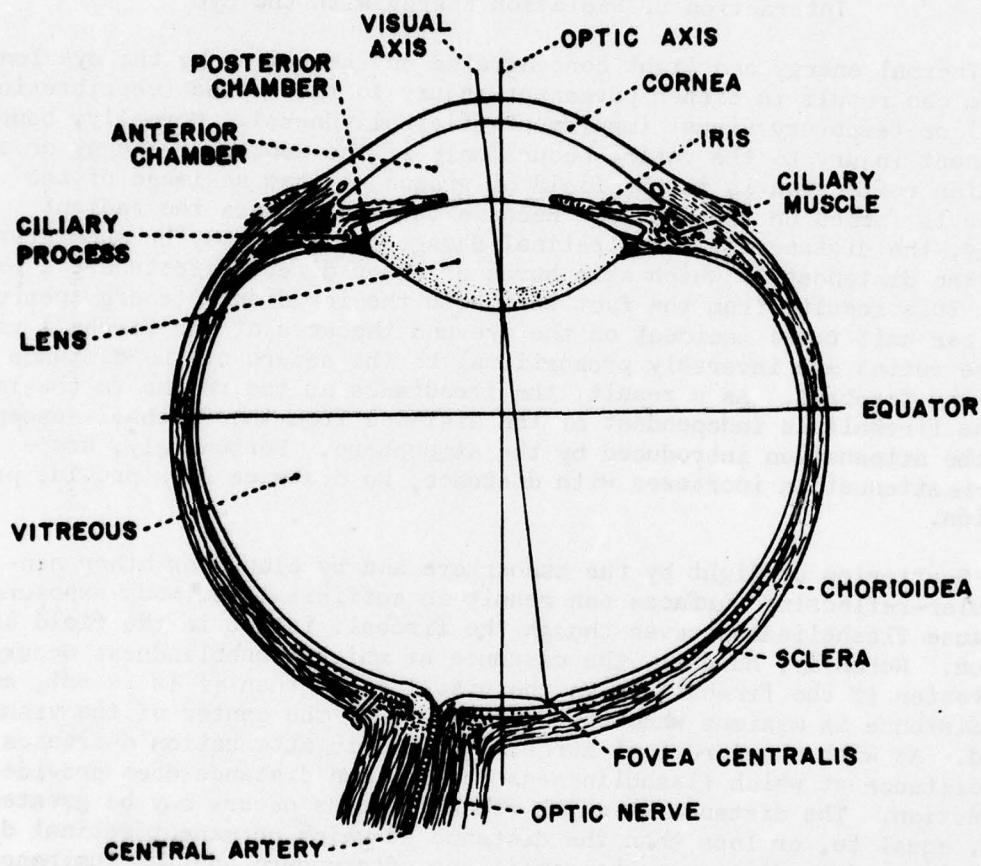


Figure 3. Schematic drawing of the eye.

lens, and vitreous so that it is focused on the retina where an image of the fireball is produced. Heat, generated in the retina and adjacent structures by the radiant energy, will in time diffuse from the area in which the image is focused and will also be conducted from the area by the flow of blood in the vascular bed. If the rate at which the heat is generated in an area is greater than the rate at which it is dissipated, the temperature will increase. If the temperature exceeds the biologic tolerances, permanent injury to the photoreceptors (rods and cones), optical nerve tissue, and other structures in the retina and choroid may result, with a subsequent permanent loss of vision in the area involved. Current research efforts are attempting to define threshold temperatures, but relatively little reliable quantitative information exists at present. Until more knowledge is gained in this area, threshold criteria must be based upon visible retinal changes, histopathologic findings, or loss of function.

#### Visual Effects of Chorioretinal Burns

The visual impairment caused by a retinal burn depends on the size, severity, and location of the burn. The size of the image, which influences the size of the burn, depends on the visual angle subtended by the object; i.e., the size of the fireball and its distance from the observer. The severity of the burn depends, in general, upon the amount by which the exposure exceeds the threshold exposure (6). The visual impairment is determined by the location of the burn; e.g., a large burn in the fovea will seriously affect visual acuity, since the fovea is used for high acuity and color recognition. A burn in the periphery will have less effect on visual acuity and, barring complications, can result in a scotoma, or blind spot, that is not normally noticeable.

The curves in Figure 4 show the visual acuity of the retina, for three different levels of luminance of the test letter, as a function of angular distance from the fovea along the horizontal meridian in a temporal direction (33). Visual acuity of the retina in this area is slightly greater than in the nasal direction or along the vertical meridian for an equal angular displacement from the fovea.

From Figure 4, it can be estimated that burns exactly centered in each fovea and large enough to include the central 2.5° visual field will reduce visual acuity to about 60% of normal (20/33 on the Snellen scale) for brightly lighted tasks. In theory, if the central 10° visual field were destroyed, the acuity would be 30% of normal (20/65). Even if the central 20° visual field were destroyed (an extremely unlikely situation), visual acuity would be reduced only to approximately 10% of normal (about 20/200). This theoretical reduction in visual acuity, however, does not appear to agree with what little data are available. Two individuals who sustained foveal burns during Operation Fishbowl (17) suffered a larger decrease in visual acuity than that estimated from Figure 4. Data from rhesus monkeys indicate a reduction in visual acuity which is less than

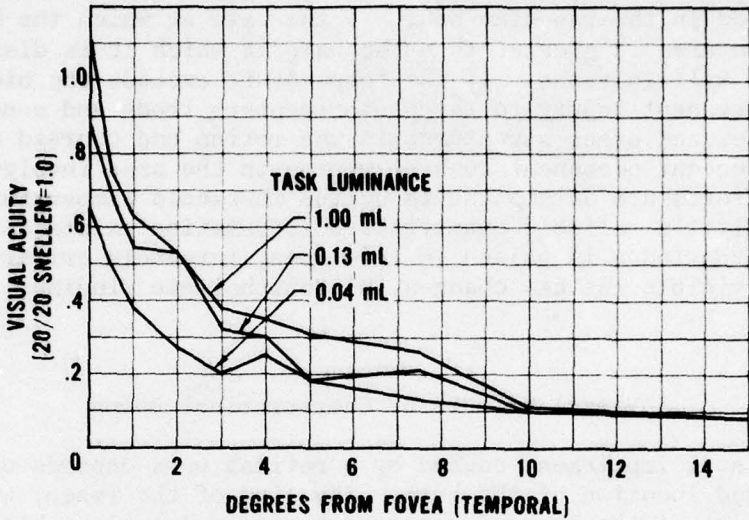
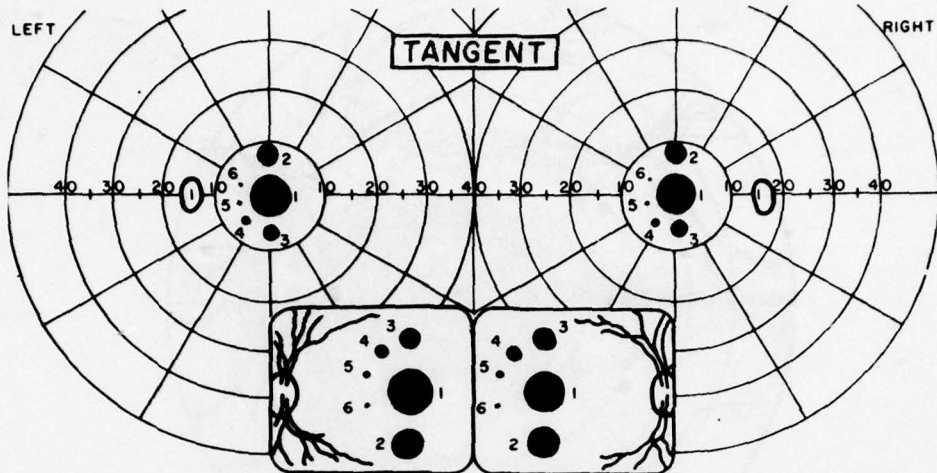


Figure 4. Visual acuity as a function of angular distance from the fovea in a temporal direction for three task luminance levels.

expected for small (less than  $2.5^{\circ}$ ) lesions, and greater than expected for large (more than  $6^{\circ}$ ) lesions centered on the fovea. More experimental data are needed to better define the visual loss due to retinal burns in the foveal area.

A schematic drawing of central-field defects and the burns responsible for these defects is shown in Figure 5. The burns (Nos. 1 to 6) are shown in the region of the macula as they would appear in size and relation to the optic nerve. Burns having corresponding numbers result from a bilateral view of a single source. Corresponding scotomata are plotted on the field charts. If centered on the fovea, the centrally located 1.8-mm ( $6^{\circ}$ ) burn is estimated to cause a permanent reduction of visual acuity to approximately 40% of normal. Visual acuity would probably be no better than 20/50 even after the edema had subsided. Burns located off the fovea should not reduce acuity, but only produce blind spots.

Extrafoveal burns may produce visual defects that are significantly different from foveal burns. A lesion of the nerve fiber layer produces a visual defect corresponding to the area served by the affected fibers and not to the area of the lesion. Thus, a small severe burn near the



1. - 1.8 mm MACULAR BURN CAUSING CENTRAL SCOTOMA OF 6°
2. - 1.35 mm MACULAR BURN CAUSING PARACENTRAL SCOTOMA OF 4.5°
3. - .9 mm MACULAR BURN CAUSING PARACENTRAL SCOTOMA OF 3°
4. - .45 mm MACULAR BURN CAUSING PARACENTRAL SCOTOMA OF 1.5°
5. - .15 mm MACULAR BURN CAUSING PARACENTRAL SCOTOMA OF 0.5°
6. - .07 mm MACULAR BURN CAUSING PARACENTRAL SCOTOMA OF 0.25°

Figure 5. Schematic drawing of bilateral retinal burns from viewing a high-intensity source of radiant energy and the visual-field defects (scotomata) resulting from these lesions.

disc could result in an extensive visual-field defect as well as a localized scotoma at the site of the burn. The course of the nerve fibers of the retina is shown schematically in Figure 6, and Figure 7 shows estimated visual-field defects resulting from damage to nerve fiber bundles (6).

Vision loss resulting from retinal burns, although permanent and uncorrectable, does not take the form of total blindness. Retinal burns can cause some vision impairment in the form of blind spots, but complete visual incapacitation as a result of retinal burns is not likely. Two individuals who sustained relatively large and severe foveal burns during Operation Fishbowl recovered 20/25 and 20/60 bilateral visual acuity (17). Experiments to investigate the effects of retinal burns on visual acuity could not detect, in trained monkeys, a decrease in visual acuity following retinal exposures unless an ophthalmoscopically visible lesion involving the fovea and 800-1000  $\mu\text{m}$  in diameter was produced (24).

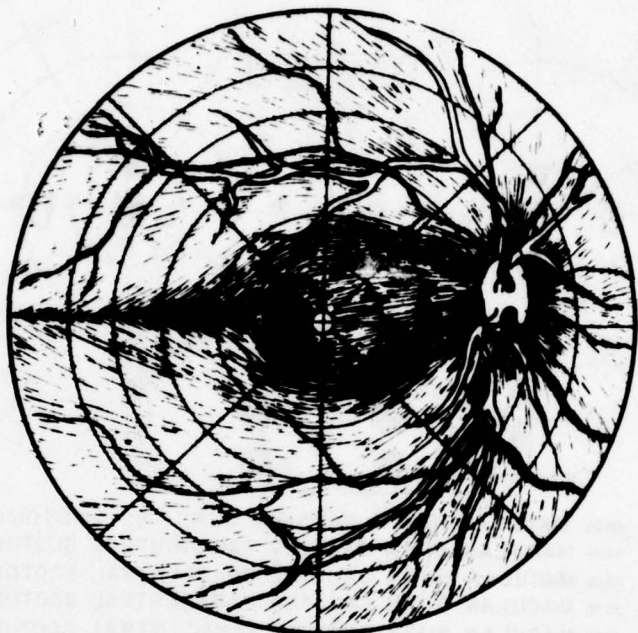


Figure 6. Schematic drawing of the nerve fibers of the retina.

#### Flashblindness

Flashblindness is the temporary visual impairment caused by exposure to a short, high-intensity flash of light, and recovery time is the time required to regain a specified level of visual function after the flash. When a recovery time is specified, the visual task or visual capability desired must also be specified because the time required to recover depends upon the level of visual performance desired.

High-intensity light flashes imaged on the retina produce afterimages with the same angular size and shape as the source of the light flash. The initially perceived brightness of an afterimage appears to be related to the amount of photopigment bleached by the light stimulus, and the decrease in afterimage brightness with time seems to be related to the regeneration of the photopigments. The afterimage is projected as either a bright or dark area (depending upon the luminance of the background) in the visual field and reduces the contrast in a scene within

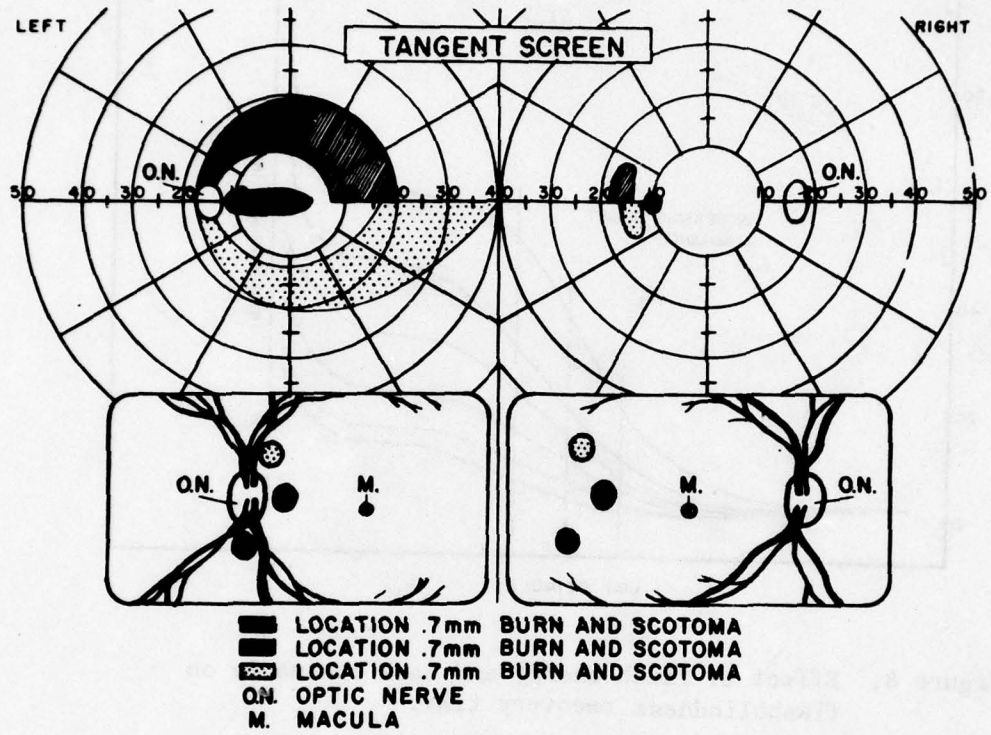


Figure 7. Schematic drawing of the visual-field defects resulting from injury to nerve fiber bundles at the indicated locations.

the area occupied by the afterimage. For an object to be seen "through" the afterimage, the object must be of sufficient brightness and size to create a detectable contrast. Detail that can be detected prior to a flash is indistinguishable against the background of the afterimage until the afterimage decays to a brightness level that permits perceivable contrast. If the detail is sufficiently coarse, however, it may be perceived and recognized by peripheral vision; i.e., "looking around" the afterimage. In general, therefore, recovery time depends upon the integrated luminous energy imaged on the retina, the size of the flash image on the retina, and the luminance of and visual acuity required by the subsequent visual task (6).

The general form of recovery time as a function of flash energy (stimulus) and task (target) luminance, assuming a constant flash duration, is shown in Figure 8 (10). Very low flash energies have little

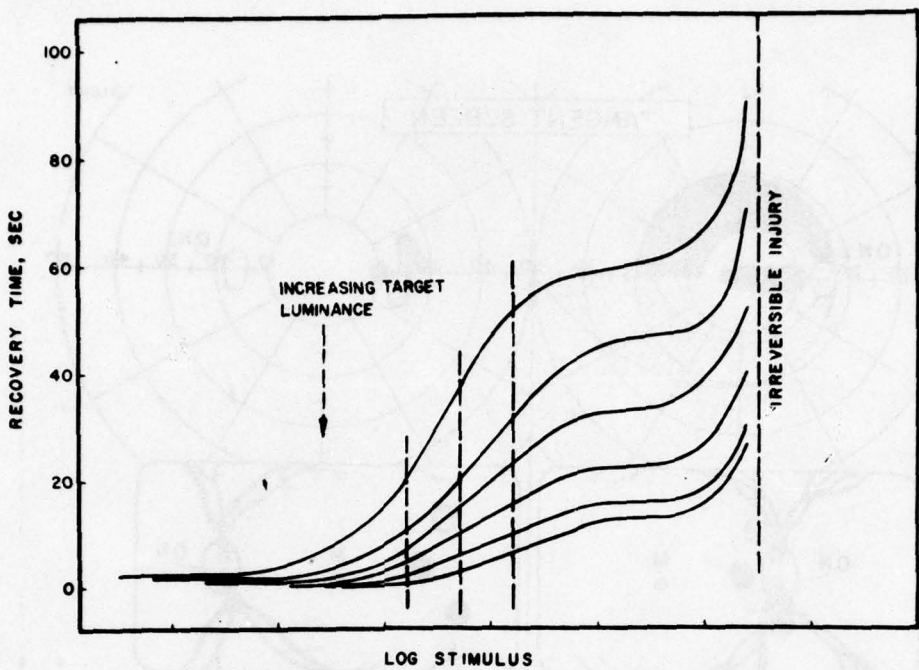


Figure 8. Effect of flash energy and task luminance on flashblindness recovery time.

effect on visual function. As the flash energy increases, the recovery time increases until maximum bleaching of the photopigment occurs, after which the recovery time changes very little with increasing flash energy. As the flash energy approaches the threshold for retinal damage, however, recovery time increases rapidly until injury occurs, at which time visual function in the injured area is lost permanently.

For a given flash energy, recovery time decreases as the luminance of the required visual task increases. Recovery times can be significantly reduced by increasing the task luminance.

#### MATHEMATICAL MODEL

The Exposure Model relates the calculated retinal exposure (QR) to the experimentally determined retinal burn threshold exposure (QRT); and when the two are equal, a burn is predicted. Thus, a retinal burn threshold distance is determined by calculating the distance at which  $QR = QRT$ . Similarly, the safe separation distance is the distance at which  $QR = QRA$ , where QRA is an allowable (safe) retinal exposure, determined by dividing the burn threshold value by an appropriate safety factor; i.e.,  $QRA = QRT/SF$ .

The calculated effective luminous exposure (QEC) is related to the experimentally determined effective threshold luminous exposure (QAT), which produces the allowable flashblindness recovery time for the specified ambient light and visual task conditions. The flashblindness threshold distance, then, is the distance at which QEC = QAT; and the safe separation distance is the distance at which QEC = QAT/SF.

### Chorioretinal Burns

#### Calculation of Retinal Exposure

When the eye is exposed to a nuclear flash as a time-varying source of radiant energy, the retinal exposure (QR) is

$$QR = \int_t HR_t \times dt \quad (\text{cal/m}^2) \quad (1)$$

where

$$t = \text{time} \quad (\text{sec})$$

$$HR_t = \text{retinal irradiance as a function of time } (\text{cal/m}^2\text{-sec})$$

The retinal irradiance ( $HR_t$ ) is

$$HR_t = \int_\lambda HR_{t\lambda} \times d\lambda \quad (\text{cal/m}^2\text{-sec}) \quad (2)$$

where

$$\lambda = \text{wavelength} \quad (\text{m})$$

$$HR_{t\lambda} = \text{spectral retinal irradiance as a function of time} \quad (\text{cal/m}^2\text{-sec-m})$$

If we assume the source is isotropic and at a distance which is large compared to the diameter of the source, then the spectral retinal irradiance ( $HR_{t\lambda}$ ) is

$$HR_{t\lambda} = \left\{ \pi \times N_{t\lambda} \times AFB_t / (4 \times \pi \times D^2) \right\} \times (AP_t / AI_{Dt}) \times T_{Dt\lambda} \quad (3)$$

where

$$N_{t\lambda} = \text{spectral radiance of the fireball as a function of time} \quad (\text{cal/m}^2\text{-sec-m-sr})$$

$$AFB_t = \text{area of the fireball as a function of time} \quad (\text{m}^2)$$

$$D = \text{distance from observer to center of fireball} \quad (\text{m})$$

$AP_t$  = area of the pupil as a function of time  $(m^2)$

$AI_{Dt}$  = area of the retinal image of the source as a function of time and distance  $(m^2)$

$T_{Dt\lambda}$  = spectral transmission of the intervening atmosphere, windows or canopies, eye-protection devices, and the ocular media as a function of time and distance

(dimensionless)

but

$$AFB_t = \pi \times FD_t^2 \quad (m^2)$$

$$AP_t = (\pi/4) \times PD_t^2 \quad (m^2)$$

$$AI_{Dt} = (\pi/4) \times DI_{Dt}^2 \quad (m^2)$$

$$DI_{Dt} = FL \times FD_t/D \quad (m)$$

where

$$FD_t = \text{fireball diameter as a function of time} \quad (m)$$

$$PD_t = \text{pupil diameter as a function of time} \quad (m)$$

$$DI_{Dt} = \text{image diameter as a function of time and distance} \quad (m)$$

$$FL = \text{effective focal length of eye} \quad (m)$$

$= 0.017 \text{ m for human}$

Substituting in equation 3 and rearranging, we have

$$\begin{aligned} HR_{t\lambda} &= (\pi/4) \times (PD_t/FL)^2 \times N_{t\lambda} \times T_{Dt\lambda} \\ &= OMEGAR_t \times N_{t\lambda} \times T_{Dt\lambda} \end{aligned} \quad (\text{cal}/m^2 \cdot \text{sec} \cdot m) \quad (4)$$

$$\text{Where } OMEGAR_t = (\pi/4) \times (PD_t/FL)^2$$

The spectral radiance ( $N_{t\lambda}$ ) is calculated from

$$N_{t\lambda} = P_{t\lambda} / (\pi \times FD_t)^2 \quad (\text{cal}/m^2 \cdot \text{sec} \cdot m \cdot sr) \quad (5)$$

where

$$P_{t\lambda} = \text{spectral power of the source as a function of time} \quad (\text{cal}/\text{sec} \cdot m)$$

The spectral power ( $P_{t\lambda}$ ) is calculated from

$$P_{t\lambda} = A_{t\lambda} \times W^{B_{t\lambda}} \quad (\text{cal/sec-m}) \quad (6)$$

where

$$W = \text{detonation yield} \quad (\text{kt})$$

$$A_{t\lambda} \text{ and } B_{t\lambda} = \text{derived functions of } \lambda \text{ and } t\text{star}$$

and the scaled time (tstar) is calculated from

$$t\text{star} = t/t_{2\text{max}} \quad (\text{dimensionless}) \quad (7)$$

where

$$t_{2\text{max}} = \text{time to second thermal maximum} \quad (\text{sec})$$

$$= 0.037 \times W^{0.47} \times (\text{RHOD/RHOS})^{0.282} \quad (\text{sec}) \quad (8)$$

$$\text{RHOD} = \text{standard air density at detonation altitude} \quad (\text{kg/m}^3)$$

$$\text{RHOS} = \text{standard air density at sea level} \quad (\text{kg/m}^3) \\ = 1.225 \text{ kg/m}^3 \quad (45)$$

The fireball diameter ( $FD_t$ ) is calculated from

$$FD_t = 0.3504 \times FDS_t \times W^{0.35} \times (\text{RHOS/RHOD})^{0.13} \quad (\text{m}) \quad (9)$$

where

$$FDS_t = \text{scaled fireball diameter as a function of time (a derived function of tstar) (Fig. 9)}$$

The coefficients (A) and exponents (B) as functions of scaled time for 10 wavelength bands, the scaled fireball diameter (FDS) as a function of scaled time, and the scaling equations (equations 6, 8, 9) all were derived from experimental data and some theoretical considerations and should be valid for yields of 0.01 to 10,000 kt and detonation altitudes of 0 to 15,240 m (50,000 ft) (6). The coefficients (A) and exponents (B) for 14 wavelength bands were derived from those for 10 bands by least-square curve-fitting techniques.

In general, only that part of the spectrum between  $3.6 \times 10^{-7}$  and  $1.35 \times 10^{-6}$  m (360 to 1350 nm) reaches the retina of the human eye. Energy outside this part of the spectrum is almost totally absorbed by the intervening cornea, lens, and ocular media and need not be considered in calculating retinal irradiance and exposure. In this model, the spectrum from  $3.55 \times 10^{-7}$  to  $1.378 \times 10^{-6}$  m is used and is divided into the 14 discrete wavelength bands listed in Table 1.

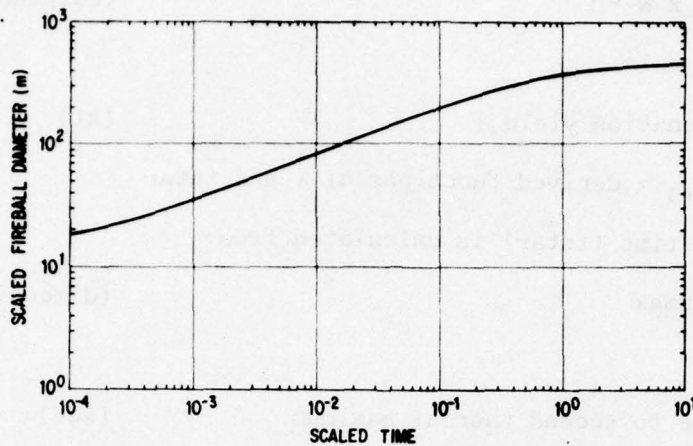


Figure 9. Scaled fireball diameter as a function of scaled time.

TABLE 1. CENTER WAVELENGTH AND BANDWIDTH FOR EACH SPECTRAL BAND

Spectral band number	Center wavelength (meters)	Bandwidth (meters)
1	3.68 E-7	2.6 E-8
2	3.97 E-7	3.2 E-8
3	4.32 E-7	3.8 E-8
4	4.735 E-7	4.5 E-8
5	5.205 E-7	4.9 E-8
6	5.675 E-7	4.5 E-8
7	6.13 E-7	4.6 E-8
8	6.625 E-7	5.3 E-8
9	7.20 E-7	6.2 E-8
10	7.89 E-7	7.6 E-8
11	8.725 E-7	9.1 E-8
12	9.755 E-7	1.15 E-7
13	1.107 E-6	1.48 E-7
14	1.2795 E-6	1.97 E-7

The radiance of the nuclear fireball in each wavelength band and the fireball diameter are assumed to increase uniformly prior to scaled time  $t_{star} = 5 \times 10^{-4}$ . After scaled time  $t_{star} = 10$ , the radiance and size of the fireball are such that the retinal irradiance is negligible. The real times ( $t$ ) at which the spectral radiance and retinal irradiance are calculated advance in an arbitrary logarithmic progression of 7 steps per

decade (1, 1.5, 2, 2.5, 3, 5, 7) from  $1.5 \times 10^{-6}$  to 10 seconds. The first real time used for a particular detonation yield and altitude is the first, in this progression, that results in a scaled time of  $5 \times 10^{-4}$  or greater. The succeeding times are then taken in order from the progression, up to the smaller of  $10 \times t_{2\max}$  or 10 seconds.

For a given detonation yield and altitude, equation 8 is used to determine  $t_{2\max}$ . Then, introducing the subscripts i and j to designate specific time steps and wavelength bands, respectively, in the general equations 1 to 9, equation 7 is used to determine  $t_{\text{star}_i}$  for all times  $t_i$  of interest. When  $t_{\text{star}_i}$  is known, then  $A_{ij}$ ,  $B_{ij}$ , and  $FDS_i$  are determined from tabular data, equation 6 is used to compute  $P_{ij}$  for each time  $t_i$  and wavelength  $\lambda_j$ , and equation 9 is used to compute  $FD_i$  for each time  $t_i$ . The radiance for time  $t_i$  and wavelength  $\lambda_j$  then is, from equation 5,

$$N_{ij} = P_{ij} / (\pi \times FD_i)^2 \quad (\text{cal/m}^2\text{-sec-m-sr}) \quad (10)$$

When the eye is exposed to a bright flash of light, the pupil, after a reaction time, starts to contract unless it is already fully constricted. For times  $t_i$  greater than 0.3 sec, the diameter of the pupil ( $PD_i$ ) (35) is given by

$$PD_i = PD - 0.00408 \times (t_i - 0.3) \quad (\text{m}) \quad (11)$$

where

$$\begin{aligned} PD &= \text{pupil diameter before the flash} && (\text{m}) \\ &= 0.007 \text{ m (night)} \text{ or } 0.003 \text{ m (day)} \end{aligned}$$

$$0.00408 = \text{rate of constriction of the pupil} \quad (\text{m/sec})$$

$$0.3 = \text{reaction time} \quad (\text{sec})$$

and  $PD_i$  is limited to  $PD_i \geq 0.003 \text{ m}$ .

The retinal irradiance for each time of interest at distance D is, from equations 2 and 4,

$$HR_{Di} = OMEGAR_i \sum_{j=1}^{14} N_{ij} \times T_{Dij} \times \Delta\lambda_j \quad (\text{cal/m}^2\text{-sec}) \quad (12)$$

where

$$\Delta\lambda_j = \text{bandwidth of wavelength band } j \quad (\text{m})$$

and, from equation 1, the total retinal exposure up to time  $t_k$  at distance D, is

$$QR_{Dk} = \sum_{i=1}^k 0.5 \times (HR_{Di} + HR_{Di-1}) \times \Delta t_i \quad (\text{cal/m}^2) \quad (13)$$

where

$0.5 \times (HR_{Di} + HR_{Di-1})$  = the average irradiance  $\text{m}^{-2}$   
for time step i ( $\text{cal/m}^2\text{-sec}$ )

$\Delta t_i$  = the duration of time step i (sec)

$$= t_i - t_{i-1}$$

This completes the calculation of the retinal exposure except for determining the spectral transmission ( $T_{Dij}$ ).

#### Calculation of Transmission

The total spectral transmission, as noted earlier, is composed of the spectral transmission of (1) the ocular media, TREYE; (2) any windows or canopies between the observer and fireball, TRCAN; (3) any eye-protection devices used, which may be of the fixed-filter type, TRFXFL, or the dynamic-filter type that may vary with time, TRDNFL; and (4) the atmosphere between the observer and the fireball, TRATM. TREYE, TRCAN, and TRFXFL are functions of wavelength; TRDNFL is a function of both wavelength and time; and TRATM is a function of wavelength and distance. Since the radiant energy passes serially through these various filters, the transmission at distance D, time  $t_i$ , and wavelength  $\lambda_j$ , is

$$T_{Dij} = TREYE_j \times TRATM_{Dj} \times TRCAN_j \times TRFXFL_j \times TRDNFL_{ij} \quad (\text{dimensionless}) \quad (14)$$

The spectral transmission of the ocular media of the human eye is taken from reference 9; values for TRCAN and TRFXFL must be measured or obtained from technical reports for the specific canopy and/or filter of interest. Values for TRDNFL are calculated for each dynamic filter considered, for each time and wavelength of interest.

Narrow-beam transmission through the atmosphere is assumed, and only attenuation by dry-air and water-vapor scattering is considered. Water-vapor absorption and the effects of dust and other contaminants are not considered in this model (6, 32). The transmission through this simplified atmosphere for wavelength  $\lambda_j$  and distance D is given by

$$TRATM_{Dj} = \exp -(SCAIR_j \times AIRM_D + SCWAT_j \times WATM_D) \quad (\text{dimensionless}) \quad (15)$$

where

SCAIR = spectral mass scattering coefficient  
for dry air  $(\text{m}^2/\text{kg})$

**SCWAT** = spectral mass scattering coefficient for water vapor  $(\text{m}^2/\text{kg})$

**AIRM** = air mass between observer and detonation  $(\text{kg}/\text{m}^2)$

**WATM** = water vapor mass between observer and detonation  $(\text{kg}/\text{m}^2)$

The spectral mass scattering coefficients for dry air and water vapor were calculated from data in reference 32. The air mass and water-vapor mass are calculated by

$$\text{AIRM} = \int_D \text{RHO}_H \times dP \quad (\text{kg}/\text{m}^2) \quad (16)$$

and

$$\text{WATM} = \int_D \text{WVD}_H \times dP \quad (\text{kg}/\text{m}^2) \quad (17)$$

where

**RHO<sub>H</sub>** = air density as a function of altitude H  $(\text{kg}/\text{m}^3)$

**WVD<sub>H</sub>** = water-vapor density as a function of altitude H  $(\text{kg}/\text{m}^3)$

**dP** = element of slant path between observer and detonation  $(\text{m})$

**H** = altitude of element dP  $(\text{m})$

**D** = slant range between observer and detonation  $(\text{m})$

The slant range (D) is calculated, using the cosine law, from

$$D = [(BA + RE)^2 + (OA + RE)^2 - 2 \times (BA + RE) \\ \times (OA + RE) \times \cos a]^{1/2} \quad (\text{m}) \quad (18)$$

where (see Fig. 10)

**BA** = detonation altitude  $(\text{m})$

**OA** = observer altitude  $(\text{m})$

**RE** = mean radius of the earth  $(\text{m})$   
= 6,371,326 m (45)

**a** = S/RE  $(\text{radians})$

**S** = surface distance between ground zero and the point directly under observer  $(\text{m})$

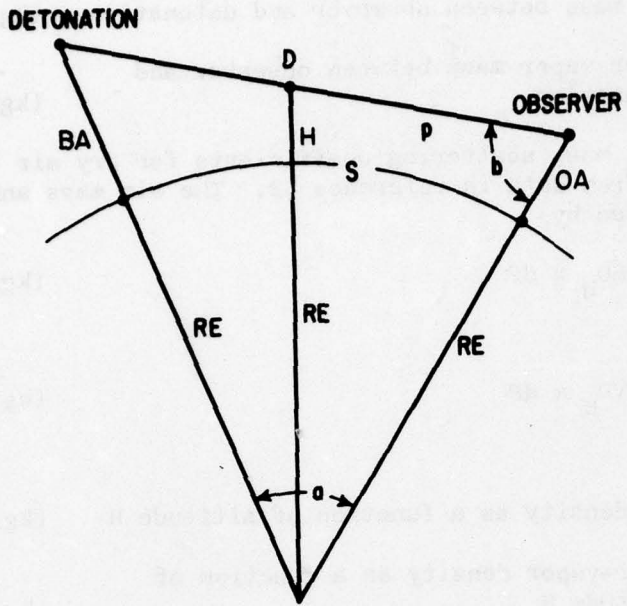


Figure 10. Geometry for calculation of slant range, air mass, water mass, and atmospheric transmission.

Similarly, the altitude ( $H$ ) of element  $dP$  is

$$H = [P^2 + (OA + RE)^2 - 2 \times P \times (OA + RE) \times \cos b]^{1/2} - RE \quad (m) \quad (19)$$

where

$P$  = distance from observer to element  $dP$   
under consideration (m)

$b$  = angle, at observer, between the line of sight to  
the detonation and the line to the center of the earth (radians)

The angle  $b$  is not known, but  $\cos b$  is

$$\cos b = [D^2 + (OA + RE)^2 - (BA + RE)^2] / [2 \times D \times (OA + RE)]$$

Substituting in equation 19 and simplifying, we have

$$H = [(P/D) \times (BA + RE)^2 + \{1 - (P/D)\} \times (OA + RE)^2 - (P/D) \times \{1 - (P/D)\} \times D^2]^{1/2} - RE \quad (m) \quad (20)$$

where

P/D = the fractional part of the distance from the observer to the fireball at which the element dP is located.

If the slant path from the observer to the fireball intercepts the horizon for a given detonation altitude, observer altitude, and surface distance, the altitude (H) calculated by equation 20 will be negative and all calculations for that set of conditions are terminated with a note that the safe distance is beyond the horizon.

The U.S. and ICAO standard atmosphere is a mixture of isothermal and adiabatic layers of clean dry air (43), and the air density ( $\rho_H$ ) at altitude H is given by

$$\rho_H = \rho_{OB} \times (1 + LM \times GH'/TB)^{-[1 + go \times M/(R \times LM)]} \quad (\text{kg/m}^3) \quad (21)$$

when  $LM \neq 0$ . When  $LM = 0$ , the air density is given by

$$\rho_H = \rho_{OB} \times \exp[-go \times M \times GH'/(R \times TB)] \quad (\text{kg/m}^3) \quad (22)$$

where

$\rho_{OB}$  = standard air density at bottom of air layer B  $(\text{kg/m}^3)$

$LM$  = lapse rate for layer B  $(^\circ\text{K}/\text{m})$

$TB$  = temperature (kinetic) at bottom of layer B  $(^\circ\text{K})$

$go$  = acceleration of gravity at sea level and  
45° latitude  $(\text{m/sec}^2)$   
= 9.80665  $\text{m/sec}^2$  (45)

$M$  = mean molecular weight of air (below 90,000 m)  $(\text{kg/kmol})$   
= 28.966  $\text{kg/kmol}$  (45)

$R$  = gas constant  $(\text{J/kmol-}^\circ\text{K})$   
=  $8.31434 \times 10^3 \text{ J/kmol-}^\circ\text{K}$  (45)

$GH'$  =  $GH - GHB$  = geopotential altitude within layer B (m)

$GH$  = geopotential altitude for geometric altitude H (m)

$GHB$  = geopotential altitude at bottom of air layer B (m)

These equations are used for geopotential altitudes less than 90,000 m. The air below 20 km is divided into 2 layers; layer 1 extending from the surface to a geopotential altitude of 11 km, and layer 2 extending from 11 to 20 km. From reference 45, we have for layer 1

$$\rho_{OB} = 1.225 \text{ kg/m}^3$$

$$L_M = -0.0065 \text{ } ^\circ\text{K/m}$$

$$T_B = 288.16 \text{ } ^\circ\text{K}$$

and for layer 2

$$\rho_{OB} = 0.36391 \text{ kg/m}^3$$

$$L_M = 0$$

$$T_B = 216.66 \text{ } ^\circ\text{K}$$

Substituting in equations 21 and 22 we obtain

$$\rho_{OH} = 1.225 \times (2.2557 \times 10^{-5} \times GH)^{4.2562} \text{ (kg/m}^3\text{)} \quad (23)$$

for geopotential altitudes (GH) from 0 to  $1.1 \times 10^4$  m and

$$\rho_{OH} = 0.36391 \times \exp [-1.5769 \times 10^{-4} \times (GH - 1.1 \times 10^4)] \text{ (kg/m}^3\text{)} \quad (24)$$

for geopotential altitudes from  $1.1 \times 10^4$  to  $2 \times 10^4$  m.

The geopotential altitude (GH) is (43)

$$GH = \int_0^H (g/g_0) \times dH \quad (25)$$

where

$$g = \text{acceleration of gravity as a function of altitude and latitude} \text{ (m/sec}^2\text{)}$$

The geopotential altitude is approximated by (32)

$$GH = H \times RE / (H + RE) \text{ (m)} \quad (26)$$

This approximation neglects forces due to the earth's rotation and changes in the gravitational constant with altitude and latitude. It is, however, accurate within  $+0.2\%$  at the equator and  $-0.3\%$  at the pole, and is almost exactly correct at  $40^\circ$ - $45^\circ$  latitude. The standard air density calculated with this approximate geopotential altitude is accurate to  $+1\%$  at the pole and  $-0.65\%$  at the equator for a geometric altitude of 20,000 m when compared to the standard air density calculated with the true geopotential altitude. As the geometric altitude decreases or the latitude approaches  $40^\circ$ - $45^\circ$ , the error decreases.

Simpson's one-third rule (21) is used for an approximate numerical integration of the air mass in the slant path from the observer to the detonation (equation 16). Thus

$$\int_0^D \rho_{H} \times dP \cong A = (D/3n) \times [\rho_{H_0} + 4\rho_{H_1} + 2\rho_{H_2} + 4\rho_{H_3} + \dots + 4\rho_{H_{n-1}} + \rho_{H_n}] \quad (\text{kg/m}^2) \quad (27)$$

where

$n$  = any even integer = number of intervals into which the slant path is divided

$\rho_{H_0}, \rho_{H_1}, \rho_{H_2}$ , etc. = air density at intervals along the slant path  $(\text{kg/m}^3)$

Thus,

$$\begin{aligned} A &= (D/3n) \times [\rho_{H_0} + \rho_{H_n} + 4 \times (\rho_{H_1} + \rho_{H_3} + \dots + \rho_{H_{n-1}}) \\ &\quad + 2 \times (\rho_{H_2} + \rho_{H_4} + \dots + \rho_{H_{n-2}})] \\ &= (D/3n) \times [\rho_{H_0} + \rho_{H_n} + 2 \times (\rho_{H_1} + \rho_{H_2} + \dots + \rho_{H_{n-1}}) \\ &\quad + 2 \times (\rho_{H_1} + \rho_{H_3} + \dots + \rho_{H_{n-1}})] \end{aligned}$$

and we have

$$\begin{aligned} \text{AIRM} &\cong (D/3n) \times (\rho_{H_0} + \rho_{H_n} + 2 \times \sum_{k=1}^{n-1} \rho_{H_k} \\ &\quad + 2 \times \sum_{k=1}^{n/2} \rho_{H_{2k-1}}) \quad (\text{kg/m}^2) \quad (28) \end{aligned}$$

Standard reference books on computer methods give iterative algorithms for this type of equation. The iteration is continued until the relative error between the air masses for two successive iterations is equal to or less than  $5 \times 10^{-6}$ .

Meteorological range (visibility) is "that distance for which the contrast transmission of the atmosphere is two percent," (34) and the defining equation is

$$\text{VIS} = -\ln(0.02)/X_0 \quad (\text{m}) \quad (29)$$

where

$X_0$  = the linear extinction coefficient of the atmosphere at sea level for radiation of 550-nm wavelength  $(1/\text{m})$

This model assumes that the coefficient  $X_0$  has two components, that is

$$X_0 = X_{AIR}(550) + X_{WAT}(550) \quad (1/m) \quad (30)$$

where

$X_{AIR}(550)$  = linear extinction coefficient for clean dry air scattering of 550-nm-wavelength radiation (1/m)

$X_{WAT}(550)$  = linear extinction coefficient for water-vapor scattering of 550-nm-wavelength radiation (1/m)

The linear extinction coefficients are

$$X_{AIR}(550) = SCAIR(550) \times RHOS \quad (1/m) \quad (31)$$

$$X_{WAT}(550) = SCWAT(550) \times WVDO \quad (1/m) \quad (32)$$

where

$$\begin{aligned} SCAIR(550) &= \text{mass-scattering coefficient of clean dry air} \\ &\quad \text{for 550-nm-wavelength radiation} \quad (m^2/kg) \\ &= 8.809 \times 10^{-6} \text{ m}^2/\text{kg} \quad (32) \end{aligned}$$

$$\begin{aligned} RHOS &= \text{standard sea-level air density} \quad (kg/m^3) \\ &= 1.225 \text{ kg/m}^3 \quad (45) \end{aligned}$$

$$\begin{aligned} SCWAT(550) &= \text{mass-scattering coefficient of water vapor for} \\ &\quad \text{550-nm-wavelength radiation} \quad (m^2/kg) \\ &= 2.919 \times 10^{-3} \text{ m}^2/\text{kg} \quad (32) \end{aligned}$$

$$WVDO = \text{sea-level water-vapor density} \quad (kg/m^3)$$

Substituting these values in equation 29 and solving for WVDO, we obtain

$$WVDO = (1.34 \times 10^3 / VIS) - 3.697 \times 10^{-3} \quad (kg/m^3) \quad (33)$$

Equation 33 is used to determine the sea-level water-vapor density for the visibility of interest.

The water-vapor density (WVD) is assumed to decrease exponentially with altitude as

$$WVD = WVDO \times \exp(WVLR \times H) \quad (kg/m^3) \quad (34)$$

where

$$WVLR = \text{water-vapor lapse rate} \quad (1/m)$$

From measurements made in the Pacific during the weapons tests of 1962, WVLR had an average value of  $-5.754 \times 10^{-4}/m$  for an average sea-level water-vapor density of  $1.957 \times 10^{-2} \text{ kg/m}^3$ . Water-vapor lapse rates for different values of WVD0 are calculated assuming that the water-vapor density at an altitude of  $1.524 \times 10^4 \text{ m}$  (50,000 ft) is the same for all values of WVD0. Thus we have

$$WVD1 = WVD2 = WVD01 \times \exp(H \times WVLR1) = WVD02 \times \exp(H \times WVLR2)$$

or

$$WVD01/WVD02 = \exp(H \times (WVLR2 - WVLR1)) \quad (35)$$

where

$WVD01$  and  $WVD02$  = sea-level water-vapor density for conditions 1 and 2, respectively  $(\text{kg/m}^3)$

$WVLR1$  and  $WVLR2$  = water-vapor lapse rate for conditions 1 and 2, respectively  $(1/\text{m})$

$WVD1$  and  $WVD2$  = water-vapor density at altitude  $H$  for conditions 1 and 2, respectively  $(\text{kg/m}^3)$

$$\begin{aligned} H &= \text{altitude at which } WVD1 = WVD2 \\ &= 1.524 \times 10^4 \text{ m} \end{aligned}$$

Using the average values listed above for condition 1 and solving equation 35 for  $WVLR2$ , we have

$$WVLR2 = -\ln(WVD02) \times 6.56 \times 10^{-5} \sim 8.335 \times 10^{-4} \quad (1/\text{m}) \quad (36)$$

which is the desired lapse rate (WVLR) in terms of the sea-level water-vapor density (WVD0).

The integration of the water mass in the slant path from the observer to the detonation, equation 17, is approximated by numerical integration using Simpson's one-third rule in exactly the same manner as used for the air mass. Thus, we have

$$\begin{aligned} WATM &\cong (D/3n) \times (WVD_0 + WVD_n + 2 \times \sum_{k=1}^{n-1} WVD_k \\ &\quad + 2 \times \sum_{k=1}^{n/2} WVD_{2k-1}) \quad (\text{kg/m}^2) \quad (37) \end{aligned}$$

This equation is solved concurrently with equation 28 for the air mass, using the same number of subintervals (n). Since the water mass converges more rapidly than the air mass, the test on the air mass is sufficient for termination of both iterations.

Thus, for a given visibility, detonation altitude, observer altitude, and surface distance, equations 33 and 36 are used to calculate the water-vapor density and water-vapor lapse rate, and equation 18 is used to calculate the slant range. Equations 28 and 37 are used to calculate the air mass and water mass, respectively, in the slant path, using equations 20, 23 or 24, 26, and 34 to calculate the values of air density and water-vapor density at intervals along the slant path. The spectral transmission of the atmosphere along the slant path is then calculated using equation 15, and the total spectral transmission ( $T_{Dij}$ ) from the fireball to the retina is then calculated using equation 14.

#### Determination of Chorioretinal Burn Threshold

The retinal burn threshold exposure (QRT) is determined from measured threshold values required to produce ophthalmoscopically visible damage in rhesus monkey eyes (36). The experimental data were fitted with the equation

$$QRT = (E_t / DI^2) + (K_t / DI) + Q_t \quad (\text{cal/m}^2) \quad (38)$$

where

$$DI = \text{image diameter} \quad (\text{m})$$

E, K, and Q are functions of exposure time derived from the experimental data (47, 49) and are entered as tabular values. Figure 11 shows the resulting threshold curves for exposure times between  $10^{-4}$  and 10 seconds.

The burn threshold data were obtained from laboratory exposures using a single pulse of approximately constant irradiance and fixed image size, but the retinal exposure from a nuclear detonation below 15,240 m (50,000 ft) is received in two pulses of continuously varying irradiance and image diameter. As a consequence, the two are not directly comparable and some modification is necessary before a meaningful comparison is possible.

The approach used here is to approximate the actual exposure with an exposure calculated as if it had occurred under conditions similar to those in the laboratory; i.e., a fixed-size, square-pulse exposure. (This approach has been tested in the laboratory with good results (7)). This is accomplished by determining an effective image diameter (DEFF) for exposure time t, and assuming that the entire exposure occurs at the maximum retinal irradiance (HRMAX) experienced during the exposure. To

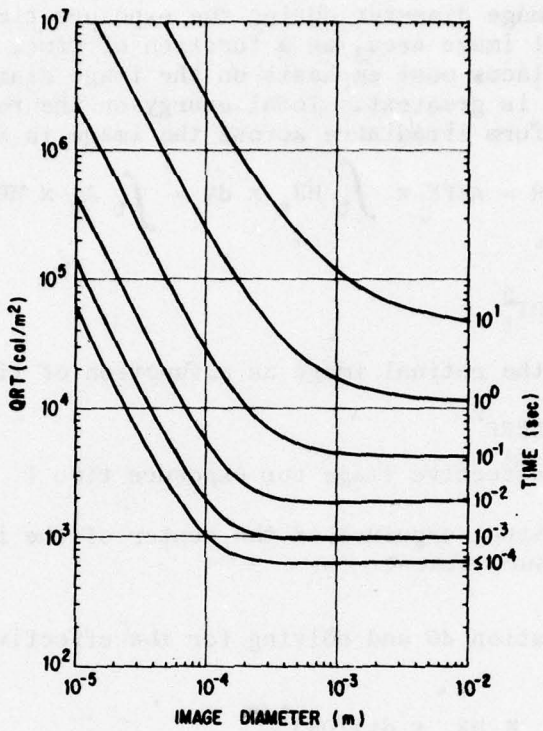


Figure 11. Threshold retinal exposure for ophthalmoscopically visible damage for rhesus monkeys as a function of geometrical image diameter for several exposure times.

conserve the retinal exposure (QR), an effective exposure time (TEFF) is determined from

$$TEFF = QR/HRMAX \quad (\text{sec}) \quad (39)$$

The effective exposure time is calculated for each cumulative time and is used in determining E, K, and Q for use in equation 38 to determine the burn threshold. Since the total energy in the first pulse is less than 1% of the total energy in the second pulse, the retinal exposure during the first pulse is neglected for exposure times greater than the time to the first thermal minimum; i.e., QR and HRMAX are set to zero at the beginning of the second pulse.

The effective image diameter during the exposure time is determined by weighting the actual image area, as a function of time, with the retinal irradiance. This places most emphasis on the image diameters that exist when the irradiance is greatest. Total energy on the retina (ENRG) is conserved and a uniform irradiance across the image is assumed.

$$ENRG = AEFF \times QR = AEFF \times \int_t HR_t \times dt = \int_t A_t \times HR_t \times dt \quad (cal) \quad (40)$$

where

$$A_t = (\pi/4) \times DI_t^2 \quad (m^2)$$

= area of the retinal image as a function of time

$$AEFF = (\pi/4) \times DEFF^2 \quad (m^2)$$

= area of effective image for exposure time t

QR = total retinal exposure at the center of the image  
for exposure time t

(cal/m<sup>2</sup>)

Substituting in equation 40 and solving for the effective image diameter, we obtain

$$DEFF = [(\int_t DI_t^2 \times HR_t \times dt)/QR]^{1/2} \quad (m) \quad (41)$$

Thus, the effective image diameter for time  $t_k$  at distance D is

$$DEFF_{Dk} = [(\sum_{i=1}^k \{0.5 \times (DI_{Di} + DI_{Di-1})\}^2 \times 0.5 \times (HR_{Di} + HR_{Di-1}) \times \Delta t_i)/QR_{Dk}]^{1/2} \quad (m) \quad (42)$$

but

$$DI_{Di} = FL \times FD_i/D \quad (m)$$

$$DI_{Di-1} = FL \times FD_{i-1}/D \quad (m)$$

$$FD_{AVE_i} = 0.5 \times (FD_i + FD_{i-1}) \quad (m)$$

$$DQR_{Di} = 0.5 \times (HR_{Di} + HR_{Di-1}) \times \Delta t_i \quad (cal/m^2)$$

where

$DI_{Di}$  and  $DI_{Di-1}$  = image diameter at distance D and times  
 $t_i$  and  $t_{i-1}$ , respectively (m)

$FD_i$  and  $FD_{i-1}$  = fireball diameter at times  $t_i$  and  
 $t_{i-1}$ , respectively (m)

$HR_{Di}$  and  $HR_{Di-1}$  = retinal irradiance at distance D and times  
 $t_i$  and  $t_{i-1}$ , respectively (cal/m<sup>2</sup>-sec)

Substituting in equation 42 and rearranging, we obtain

$$DEFF_{Dk} = FL \left[ \left( \sum_{i=1}^k FD_{AVE_i}^2 \times DQR_{Di} \right) / QR_{Dk} \right]^{1/2} / D \quad (m) \quad (43)$$

The effective exposure time from equation 39 is used to determine  $E_t$ ,  $K_t$ , and  $Q_t$  from tables. These values and the effective image diameter from equation 43 are used in equation 38 to calculate the retinal burn threshold value for the conditions of the exposure.

This completes the calculation of the retinal exposure and the burn threshold exposure. In practice, an iterative procedure finds the horizontal range at which the two are equal, and this is the predicted threshold distance. For a predicted safe distance, the program finds the distance at which the retinal exposure equals the burn threshold divided by a safety factor.

#### Iteration Convergence Procedure

The minimum safe distance is calculated for each time ( $t_i$ ) of interest for each observer altitude ( $OA_n$ ). The observer altitudes used are from 0 to 15,240 m (50,000 ft) in increments of 1,524 m (5,000 ft), with the constraint that one observer altitude must equal the detonation altitude. An initial safe distance of 18.52 m (0.01 naut. miles) is estimated for each observer altitude.

To determine the minimum safe distance ( $SDIST_{ni}$ ) for observer altitude ( $OA_n$ ) and time ( $t_i$ ), the safe distance for the same altitude and previous time ( $t_{i-1}$ ) is used as a first estimate (XDIST) except for the first time ( $t_i$ ), in which case the initial estimate of 18.52 m is used. The retinal exposure ( $QR_{Di}$ ) and allowable retinal exposure ( $QRA_{Di}$ ) for time ( $t_i$ ) and the estimated distance are calculated as previously described. If this estimated safe distance is too large (i.e.,  $QR_{Di} < QRA_{Di}$ ), the calculation is terminated and the estimated safe distance is accepted as the safe distance for that observer altitude and time. This

precludes calculating a safe distance less than 18.52 m or less than a previously calculated safe distance for that observer altitude.

If the estimated safe distance (XDIST) is too small (i.e.,  $QR_{Di} > QRA_{Di}$ ), then XDIST is successively multiplied by  $2^k$  ( $k=1, 2, 3, \dots$ ) until  $QR_{Di} < QRA_{Di}$ . Then the distance  $XDIST \times 2^k$  is successively decremented and/or incremented (according to  $QR_{Di} < QRA_{Di}$  or  $QR_{Di} > QRA_{Di}$ ) by an amount  $XDIST \times 2^{k-1}/2^m$  ( $m = 1, 2, 3, \dots$ ) until the retinal exposure is within 1% of the allowable exposure; i.e.,  $|QR_{Di} - QRA_{Di}| / QRA_{Di} \leq 0.01$ , or until the last increment (or decrement) is less than 0.1% of  $XDIST \times 2^k$ , with the constraint that

$$20 \text{ m} \leq 0.001 \times XDIST \times 2^k \leq 500 \text{ m}$$

The distance at which either of these criteria is met is the minimum SSD. If the minimum SSD for a given time and observer altitude results in a line of sight to the detonation which intercepts the earth's surface, the safe distance is listed as being beyond the horizon for that and all subsequent times for that observer altitude.

This procedure is repeated until the predicted retinal burn safe distance for each time step and observer altitude has been determined.

#### Flashblindness

#### Calculation of Effective Luminous Exposure

When the eye is exposed to a nuclear flash as a time-varying source of radiant energy, the effective luminous exposure (QEC), in effective troland-sec, is

$$QEC = \int_t VS_t \times dt \quad (\text{tdeff-sec}) \quad (44)$$

where

$$t = \text{time} \quad (\text{sec})$$

$$VS_t = \text{effective visual stimulus as a function of time} \quad (\text{tdeff})$$

and the effective visual stimulus is

$$VS_t = \int_\lambda VS_{t\lambda} \times d\lambda \quad (\text{tdeff}) \quad (45)$$

where

$$\lambda = \text{wavelength} \quad (\text{m})$$

$$VS_{t\lambda} = \text{effective spectral visual stimulus as a function of time} \quad (\text{tdeff/m})$$

The troland (td) is defined as the visual stimulation produced by viewing a luminance of  $1 \text{ cd/m}^2$  through a pupil with an area of  $1 \text{ mm}^2$ , and the area of larger entrance pupils should be corrected for the Stiles-Crawford effect (16). Thus, using the equivalence  $1 \text{ cd/m}^2 = 1 \text{ lm/m}^2\text{-sr}$  (45), the effective spectral visual stimulation from viewing a nuclear detonation at distance D, at time  $t_i$ , and wavelength  $\lambda_j$ , is

$$VS_{Dij} = 10^6 \times (\pi/4) \times (PDEFF_i)^2 \times B_{ij} \times TM_{Dij} \quad (\text{tdeff/m}) \quad (46)$$

where

$PDEFF_i$  = effective pupil diameter at time  $t_i$  (m)

$B_{ij}$  = source luminance at time  $t_i$  and wavelength  $\lambda_j$  ( $\text{lm/m}^2\text{-m-sr}$ )

$TM_{Dij}$  = transmission of all media between the source and the eye at distance D, time  $t_i$ , and wavelength  $\lambda_j$  ( $= T_{Dij}/T_{REYE_j}$ , see eqn 14) (dimensionless)

and time step i and wavelength band j are as described previously (Calculation of Retinal Exposure).

The effective pupil diameter (30) at time  $t_i$  is calculated from

$$PDEFF_i = [PD_i^2 \times (1 + PD_i^2 \times (4.17 \times 10^7 \times PD_i^2 - 1.06 \times 10^4))]^{1/2} \quad (\text{m}) \quad (47)$$

where

$PD_i$  = pupil diameter at time  $t_i$  and is calculated as described for equation 11 (m)

The luminance of the source (22) at time  $t_i$  and wavelength  $\lambda_j$ , is given by

$$B_{ij} = 680 \times V_j \times 4.184 \times N_{ij} \\ = 2845.12 \times V_j \times N_{ij} \quad (\text{lm/m}^2\text{-m-sr}) \quad (48)$$

where

680 = theoretical maximum possible luminous efficiency of a source for photopic vision (29) (lm/W)

$V_j$  = photopic relative visibility function at wavelength  $\lambda_j$  (calculated from data in ref 29) (dimensionless)

4.184 = W-sec/cal (45)

$N_{ij}$  = radiance of source at time  $t_i$  and wavelength  $\lambda_j$ , and is calculated as described previously  
 (eqns 5 through 10) (cal/m<sup>2</sup>-sec-m-sr)

Equation 46 is adequate to define the effective spectral visual stimulus from a source which subtends a large visual angle ( $10^\circ$  or larger) and is close to the eye, conditions which usually exist in laboratory experiments to determine flashblindness recovery times. Under these conditions, the luminous energy distribution on the retina is essentially uniform within the geometric image of the source, and scattered radiation is negligible.

When the unprotected eye is exposed to a nuclear detonation at or near safe distances, however, the visual angle subtended by the source may be quite small (less than  $1^\circ$ ) and the distance considerable. Under these conditions, the luminous energy distribution on the retina is far from uniform and extends well beyond the limits of the geometric image. Also, the contribution from scattered radiation usually will not be negligible. The effects of this nonuniform energy distribution and the scattered radiation are enhanced by the fact that we are interested in the flashblindness recovery time, hence the visual stimulation, at a point on the retina  $4.5 \times 10^{-4}$  m from the center of the geometric image (for a centrally fixated source) rather than at the center of the image (see Flashblindness Criteria section).

The effective retinal illuminance due to direct (unscattered) radiation from a nuclear detonation at distance  $D$ , time  $t_i$ , and wavelength  $\lambda_j$ , is (see eqns 3 and 4)

$$ERD_{Dij} = (\pi/4) \times (PDEFF_i/FL)^2 \times B_{ij} \times TM_{Dij} \times TREYE_j \quad (1m/m^2) \quad (49)$$

or

$$(\pi/4) \times (PDEFF_i)^2 \times B_{ij} \times TM_{Dij} = FL^2 \times ERD_{Dij}/TREYE_j \quad (50)$$

and substituting in equation 46, we obtain

$$VSD_{Dij} = 10^6 \times FL^2 \times ERD_{Dij}/TREYE_j \quad (tdeff/m) \quad (51)$$

which is the effective spectral visual stimulation due to direct (unscattered) radiation as a function of the effective spectral retinal illuminance.

The derivation of equation 49 assumes an isotropic source and its solution yields the effective spectral retinal illuminance due to direct radiation, for a uniformly illuminated retinal image as calculated by methods of geometric optics; i.e., the eye is assumed to be a perfect optical system. We know, however, that the eye is not a perfect optical system.

According to Fourier Transform Theory (31), when a uniformly radiating source with circular projected area is focused on the retina, the effective spectral illuminance ( $ERDF_{\lambda}$ ) at a point on the retina is given by

$$ERDF_{\lambda}(r,b) = ERD_{\lambda} \times 2\pi b \times \int_0^{\infty} T(\omega) \times J_1(2\pi b\omega) \times J_0(2\pi r\omega) \times d\omega \quad (lm/m^2-m) \quad (52)$$

where

$ERD_{\lambda}$  = effective spectral retinal illuminance within a uniformly illuminated image as calculated by methods of geometric optics; i.e., eqn 49  $(lm/m^2-m)$

$J_1$  = Bessel function of the first kind and order 1 (dimensionless)

$J_0$  = Bessel function of the first kind and order 0 (dimensionless)

$b$  = radius of the image of the source calculated by methods of geometric optics (m)

$r$  = retinal distance of the point from the center of the image (m)

=  $4.5 \times 10^{-4}$  m (see Flashblindness Criteria section)

$\omega$  = spatial frequency (1/m)

$T(\omega)$  = modulation transfer function of the optical system of the eye (dimensionless)

White (48) proposed a transfer function of the form  $T(\omega) = \exp(-a\omega)$ , with  $a = 2.5 \times 10^{-5}$  m for the human eye in the spectral region considered here ( $\lambda = 3.55 \times 10^{-7}$  to  $1.35 \times 10^{-6}$  m). Substituting in equation 52 we have, for the effective spectral illuminance at a point on the retina which is  $r$  meters from the center of the geometric image of radius  $b$  meters,

$$ERDF_{\lambda}(r,b) = ERD_{\lambda} \times 2\pi b \times \int_0^{\infty} \exp(-a\omega) \times J_1(2\pi b\omega) \times J_0(2\pi r\omega) \times d\omega \quad (lm/m^2-m) \quad (53)$$

Apparently the integral in equation 53 does not have a rigorous solution and must be evaluated by numerical integration, which is a relatively lengthy process (1 to 2 min) even on modern fast computers and is not practical in an iterative-type program which may require thousands of solutions. So the function is normalized to 1 at  $r = 0$  (i.e., the center of the image), a table of normalized values is constructed, and logarithmic interpolation within this table yields normalized values of the effective spectral retinal illuminance for different values of  $b$ . The normalized function,  $EN(r,b)$ , is

$$EN(r,b) = ERDF_{\lambda}(r,b)/ERDF_{\lambda}(0,b) \quad (\text{dimensionless}) \quad (54)$$

where  $\text{ERDF}_\lambda(0, b)$  is the effective spectral retinal illuminance at the center of the image ( $r = 0$ ). But when  $r = 0$ , the Bessel function  $J_0(2\pi r \omega) = 1$ , and we have

$$\text{ERDF}_\lambda(0, b) = \text{ERD}_\lambda \times 2\pi b \times \int_0^\infty \exp(-a\omega) \times J_1(2\pi b\omega) \times d\omega \quad (\text{lm/m}^2\text{-m}) \quad (55)$$

which has the solution (44)

$$\text{ERDF}_\lambda(0, b) = \text{ERD}_\lambda \times (1 - 1/[1 + (2\pi b/a)^2]^{1/2}) \quad (\text{lm/m}^2\text{-m}) \quad (56)$$

Substituting in equation 54 from equations 53 and 56, we obtain

$$\begin{aligned} \text{EN}(r, b) &= 2\pi b \times \int_0^\infty \exp(-a\omega) \times J_1(2\pi b\omega) \times J_0(2\pi r\omega) \\ &\quad \times d\omega / (1 - 1/[1 + (2\pi b/a)^2]^{1/2}) \quad (\text{dimensionless}) \end{aligned} \quad (57)$$

and since all of the quantities in equation 57 are independent of wavelength, one table of normalized values can be used for all 14 wavelength bands in this model. Equation 57 was used to construct a table of  $\text{EN}(r, b)$  for  $r = 4.5 \times 10^{-4}$  m and a range of values of  $b$ . Interpolation within this table yields  $\text{EN}(r, b)$  for desired values of  $b$ , and the effective spectral retinal illuminance is calculated from

$$\text{ERDF}_\lambda(r, b) = \text{ERDF}_\lambda(0, b) \times \text{EN}(r, b) \quad (\text{lm/m}^2\text{-m}) \quad (58)$$

Substituting in equation 51 from equations 58, 56, 57, and 49, we obtain

$$\begin{aligned} \text{VSD}_{Dij}(r, b_{Di}) &= 10^6 \times \text{FL}^2 \times \text{ERDF}_{Dij}/\text{TREYE}_j \\ &= 10^6 \times \text{FL}^2 \times \text{ERDF}_{Dij}(0, b_{Di}) \times \text{EN}(r, b_{Di})/\text{TREYE}_j \\ &= \text{OMEGAF}_i \times B_{ij} \times \text{TM}_{Dij} \times A_{Di} \times \text{EN}(r, b_{Di}) \quad (\text{tdeff/m}) \end{aligned} \quad (59)$$

where

$$\text{OMEGAF}_i = 10^6 \times (\pi/4) \times (\text{PDEFF}_i)^2$$

$$A_{Di} = 1 - 1/[1 + (2\pi b/a)^2]^{1/2}$$

Solution of equation 59 gives the effective visual stimulation due to direct (unscattered) radiation at distance  $D$ , time  $t_i$ , and wavelength  $\lambda_j$ , for a point on the retina ( $r$ ) which is  $4.5 \times 10^{-4}$  m from the center of the source image. Radiation scattered by the atmosphere, however, contributes to the visual stimulation and for small image radii may contribute significantly at the point  $r = 4.5 \times 10^{-4}$  m.

Calculating the scattering of radiant or luminous energy by the atmosphere is a subject of considerable complexity with an almost infinite range of variables. Programs using Monte Carlo techniques to predict

atmospheric scattering for specific model atmospheres are available (1, 46). These programs, however, require considerable computer time and are not practical for use in iterative-type calculations.

This model neglects the multiple-scattered radiation and calculates the visual stimulation due to radiation which has experienced only a single scattering event in the atmosphere. The atmospheric model used is the same as that described in the Calculation of Transmission section. It is recognized that this will result in considerable error in the calculation of the scattered light at large distances, but the result at distances less than 10 km (5.4 naut. miles) should closely approximate the correct answer. A better approximation must await the development of calculational techniques for the multiple-scattering problem which will be practical for use in iterative-type calculations.

For a point on the retina which is  $4.5 \times 10^{-4}$  m from the center of the source image, it can be shown (8) that the effective visual stimulation due to single atmospheric scattering is

$$VSS_{Dij} = -8.344 \times OMEGAF_i \times (FD_i/D)^2 \times B_{ij} \times TM_{Dij} \\ \times \ln(TRATM_{Dj}) \quad (tdeff/m) \quad (60)$$

where

$\ln(TRATM)$  = natural logarithm of the atmospheric transmission (dimensionless), and all other variables are as previously described and calculated.

The total effective visual stimulus for a point on the retina ( $r = 4.5 \times 10^{-4}$  m), due to wavelength  $\lambda_j$ , is the sum of the visual stimuli due to direct and scattered radiation. Thus

$$VS_{Dij} = VSD_{Dij}(r, b_{Di}) + VSS_{Dij} \quad (tdeff/m) \quad (61)$$

and from equations 45, 59, and 60, the effective visual stimulus at distance D and time  $t_i$  is

$$VS_{Di} = \sum_{j=1}^{14} VS_{Dij} \times \Delta\lambda_j \\ = OMEGAF_i \times EN(r, b_{Di}) \times A_{Di} \times \sum_{j=1}^{14} B_{ij} \times TM_{Dij} \times \Delta\lambda_j \\ + OMEGAF_i \times (-8.344) \times (FD_i/D)^2 \sum_{j=1}^{14} B_{ij} \times TM_{Dij} \times \ln(TRATM_{Dj}) \\ \times \Delta\lambda_j \quad (tdeff) \quad (62)$$

and from equation 44, the calculated effective visual exposure up to time  $t_k$  at distance D is

$$QEC_{Dk} = \sum_{i=1}^k 0.5 \times (VS_{Di} + VS_{Di-1}) \times \Delta t_i \quad (td_{eff}-sec) \quad (63)$$

The calculated visual exposure (QEC) resulting from the solution of equation 63 is compared with the allowable visual exposure (QAT), and the distance for which

$$QEC_{Dk} = QAT/SF$$

is defined as the flashblindness safe distance for exposure time  $t_k$ .

#### Flashblindness Criteria

According to Czeh et al. (19), flashblindness recovery time (T) following exposure to a bright flash of light can be predicted by the empirical equation

$$\begin{aligned} T = & \text{antilog} [7.000922 - 0.34826531 \times \log L + 0.0086512441 \times (\log L)^2 \\ & + 0.0099458175 \times (\log L)^3 - 1.1146726 \times A + 4.5215008 \times A^2 \\ & - 1.4977985 \times A^3 - 4.1308911 \times \log ET + 0.76585211 \times (\log ET)^2 \\ & - 0.042097964 \times (\log ET)^3] \quad (\text{sec}) \end{aligned} \quad (64)$$

where

antilog and log are to base 10

$$L = \text{recovery task luminance} \quad (mL)$$

$$7.586 \times 10^{-3} \leq L \leq 1.914 \times 10^4$$

$$A = \text{visual acuity required by recovery task} \quad (1/\text{min})$$

$$0.08 \leq A \leq 0.33$$

$$ET = \text{visual exposure} \quad (td\text{-sec})$$

$$3.164 \times 10^4 \leq ET \leq 8.913 \times 10^7$$

The data used in developing this equation were all obtained using centrally fixated light flashes which subtended a relatively large visual angle ( $7.5^\circ$ - $15^\circ$  in most cases), and the subject was required to identify the task target by seeing it through the afterimage. A nuclear fireball, however, subtends a relatively small visual angle ( $0.5^\circ$ - $3^\circ$ ) at distances where the fireball can be safely viewed with no protection for the eye. Also, considerable visual information can be obtained by parafoveal (peripheral) vision; i.e., by "looking around" the afterimage, particularly when the afterimage is small.

Richey, predicting flashblindness safe separation distances in 1966 (39), viewed a standard altimeter at a distance of 76 cm (30 in)--average eye-to-instrument distance in fighter aircraft--following exposure to centrally fixated flashes of bright light. No difficulty was experienced in reading the altimeter when the afterimages subtended visual angles of  $3^{\circ}$  or less, even though individual numbers, when fixated directly, could not be identified through the afterimages. As the visual angle subtended by the afterimages increased from  $3^{\circ}$ , the altimeter became increasingly difficult to read until, at  $10^{\circ}$ , a great deal of concentration and repeated peripheral scanning were required to determine the altitude to the nearest 30.5 m (100 ft). A pilot, however, cannot concentrate on a single instrument to the exclusion of all else.

Thus, rather arbitrarily, a centrally located afterimage subtending a visual angle of at least  $3^{\circ}$  was chosen as the condition necessary for a significant reduction in a pilot's ability to read his major flight instruments.

Cushman (18), using three aircraft instruments as the recovery target, found that, by looking around the afterimage from a centrally fixated high-intensity flash: (1) the altimeter could be seen almost immediately with sufficient detail to determine if the indicated altitude was increasing or decreasing when the flash subtended a visual angle of  $15^{\circ}$  or less; (2) the gyrocompass could be seen almost immediately with sufficient detail to determine the indicated heading when the flash subtended a visual angle of  $5^{\circ}$  or less; and (3) a  $3^{\circ}$  afterimage interfered with reading the airspeed indicator. Other investigators (7, 36), using visual acuity gratings and Sloan-Snellen letters as the recovery target, found that  $2^{\circ}$  was the maximum visual angle subtended by a centrally fixated afterimage which would allow using peripheral vision to read their recovery targets. There is no known data, however, defining the visual acuity required by a pilot to maintain control of his aircraft during short periods of flashblindness.

Hill and Chisum (28) reported the results of an in-flight study in which pilots flying an F-9F were blindfolded while the aircraft was in various flight attitudes. They concluded that the maximum time the pilot could maintain safety-of-flight for the worst test condition ( $180^{\circ}$  point of a slow roll) was 5 seconds. The criterion for loss of safety-of-flight was the subjective opinion of a check pilot. The same investigators, however, reporting the data from a similar experiment using the same test equipment and procedures but different pilots and check pilots, found that safety-of-flight was maintained for more than 15 seconds (the longest time tested) for various aircraft attitudes (15).

Alder (2) exposed experienced pilots to a centrally fixated light flash subtending a visual angle of about  $5^{\circ}$  in a C-131A/T-29 flight simulator. All flashes were presented under night conditions, during instrument-landing-system approaches or controlled turns, and usually during an emergency procedure due to a simulated malfunction of some aircraft system.

Glide slope graphs (for flashes during approaches) and plotted courses (for flashes during turns) were reviewed by the simulator instructor. When the mean recovery time was 30 seconds, 37.5% of the glide slope graphs deviated beyond usual limits; but when the mean recovery time was 7.5 seconds, only 6.3% were beyond usual limits. When the mean recovery time was 27 seconds, 48.6% of the plotted courses were beyond usual limits; but when the recovery time was 11 seconds, only 16.7% were beyond usual limits.

Hamilton (26) exposed pilots in a B-52 flight simulator to a centrally fixated flash subtending a visual angle of about  $5.5^{\circ}$  and producing a mean recovery time of 32 seconds. Immediately after the flash, which occurred during straight and level flight, the pilot attempted to make a  $30^{\circ}$  left bank, maintaining altitude and airspeed. Airspeed, altitude, and degree of pitch and bank were reported at 6-sec intervals up to 24 seconds. The airspeed, altitude, and degree of pitch did not differ significantly from control results 18 seconds after the flash, but the degree of bank did differ significantly 12 seconds after the flash.

Alder and Hamilton (3) exposed pilots in a F-106B aircraft to a centrally fixated flash subtending a visual angle of  $7.5^{\circ}$  and producing a mean recovery time of 20 seconds. When flashed, the pilot was flying on instruments (hood closed) in a  $60^{\circ}$  right bank, maintaining altitude and airspeed, and was to continue the maneuver as long as possible after the flash. No statistical analysis was made (equipment failure resulted in insufficient data), but the data available indicated little evidence of loss of control of the aircraft for 20 seconds following the flash.

In view of the above, it seems conservative to use a recovery time of 10 seconds or more from a centrally fixated afterimage subtending a visual angle of  $3^{\circ}$  or more as a criterion for flashblindness that will interfere with a pilot's ability to control his aircraft. Such an afterimage will have a retinal radius of  $4.5 \times 10^{-4}$  m.

From Figure 8 and equation 64, visual task luminance is seen as an important variable in determining recovery time and must be defined before the luminous exposure resulting in 10-sec recovery time can be determined. An average instrument luminance of 0.07 mL is used for nighttime conditions (2, 27) and 20 mL for daytime conditions (38). From Figure 4, a required visual acuity of 0.33 (20/60) is estimated.

Substituting these values in equation 64 and solving graphically (Fig. 12), we obtain  $4.65 \times 10^5$  td-sec and  $3.2 \times 10^7$  td-sec as the visual exposures necessary to produce 10-sec recovery time for night and day conditions, respectively. Correcting these values for the effective pupil diameters (eqn 47), we obtain QAT =  $2.69 \times 10^5$  tdeff-sec and  $2.9 \times 10^7$  tdeff-sec as the allowable effective visual exposures for night and day, respectively, for 10-sec recovery time.

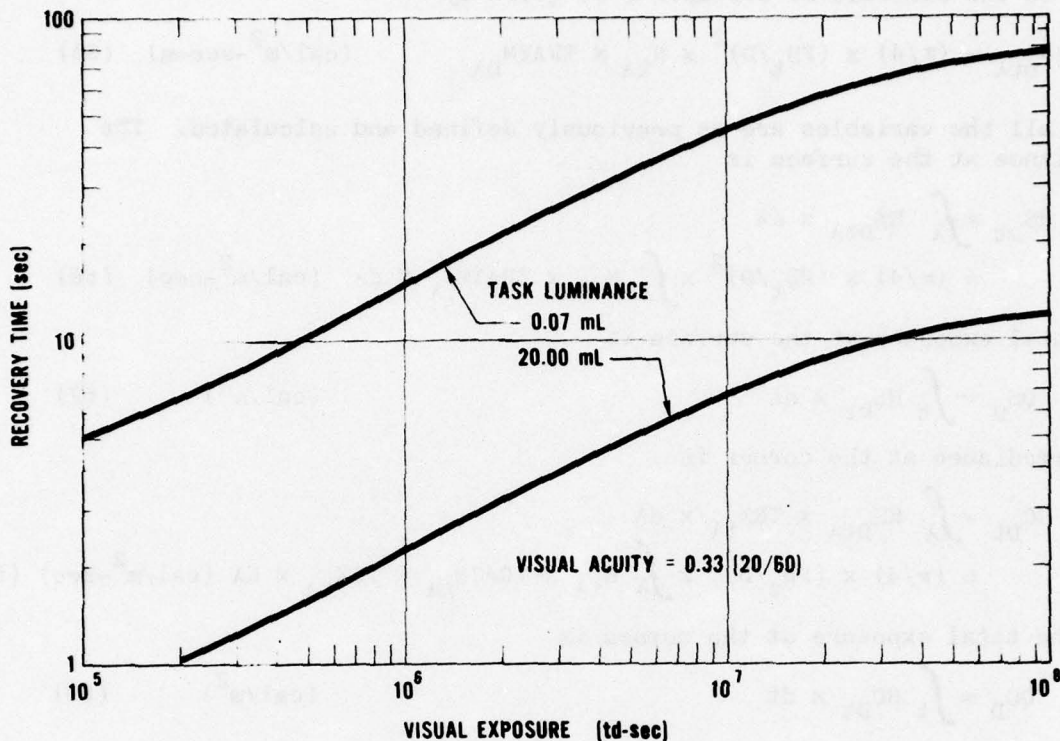


Figure 12. Flashblindness recovery time for a visual acuity of 0.33 (20/60 Snellen) as a function of visual exposure for task luminances of 0.07 and 20 mL.

With this information the visual exposure of the eye and the allowable exposure for flashblindness, as defined for the criteria above, can be determined. In practice, an iterative procedure finds the horizontal range at which the two are equal for the predicted threshold distance. When a predicted safe distance is desired, the allowable exposure is divided by a safety factor. The iteration convergence procedure is the same as that previously described for determining the retinal burn threshold or safe distance.

#### Irradiance and Total Exposure at Plane and Cornea

When a predicted eye safe separation distance is calculated for a specific set of conditions, the maximum irradiance and total exposure at the surface of the aircraft (or other enclosure) and at the cornea are frequently of concern, particularly when an eye-protection device is used.

The spectral irradiance ( $HS_{Dt\lambda}$ ) at a surface normal to the line of sight to the fireball at distance D is given by

$$HS_{Dt\lambda} = (\pi/4) \times (FD_t/D)^2 \times N_{t\lambda} \times TRATM_{D\lambda} \quad (\text{cal}/m^2\text{-sec-m}) \quad (65)$$

where all the variables are as previously defined and calculated. The irradiance at the surface is

$$\begin{aligned} HS_{Dt} &= \int_{\lambda} HS_{Dt\lambda} \times d\lambda \\ &= (\pi/4) \times (FD_t/D)^2 \times \int_{\lambda} N_{t\lambda} \times TRATM_{D\lambda} \times d\lambda \quad (\text{cal}/m^2\text{-sec}) \end{aligned} \quad (66)$$

the total exposure at the surface is

$$QS_D = \int_t HS_{Dt} \times dt \quad (\text{cal}/m^2) \quad (67)$$

the irradiance at the cornea is

$$\begin{aligned} HC_{Dt} &= \int_{\lambda} HS_{Dt\lambda} \times TRX_{t\lambda} \times d\lambda \\ &= (\pi/4) \times (FD_t/D)^2 \times \int_{\lambda} N_{t\lambda} \times TRATM_{D\lambda} \times TRX_{t\lambda} \times d\lambda \quad (\text{cal}/m^2\text{-sec}) \end{aligned} \quad (68)$$

and the total exposure at the cornea is

$$QC_D = \int_t HC_{Dt} \times dt \quad (\text{cal}/m^2) \quad (69)$$

where

$$TRX_{t\lambda} = TRCAN_{\lambda} \times TRFXFL_{\lambda} \times TRDNFL_{t\lambda} \quad (\text{dimensionless})$$

all as previously defined and calculated.

In practice, the retinal burn and/or flashblindness safe distance is calculated for each time step. Then, for whichever of these distances is greater for that time step, the irradiance at the surface of the aircraft and cornea is calculated for all time steps. The aircraft and corneal surfaces are assumed to be normal to the line of sight to the fireball with an unobstructed view of the fireball (except for the filters considered). The maximum irradiance for each surface is stored and printed. The total exposure is calculated as if the surface were at the specified distance from 0 to  $10 \times t_{2\max}$  or 10 seconds, whichever is shorter.

#### CONCLUSIONS AND RECOMMENDATIONS

This Exposure Model was used with pertinent rabbit-eye information to predict retinal burn threshold distances for rabbits for conditions under which rabbits were exposed during Operation Dominic in 1962. The results are shown in Figure 13, with the distances at which retinal burns were

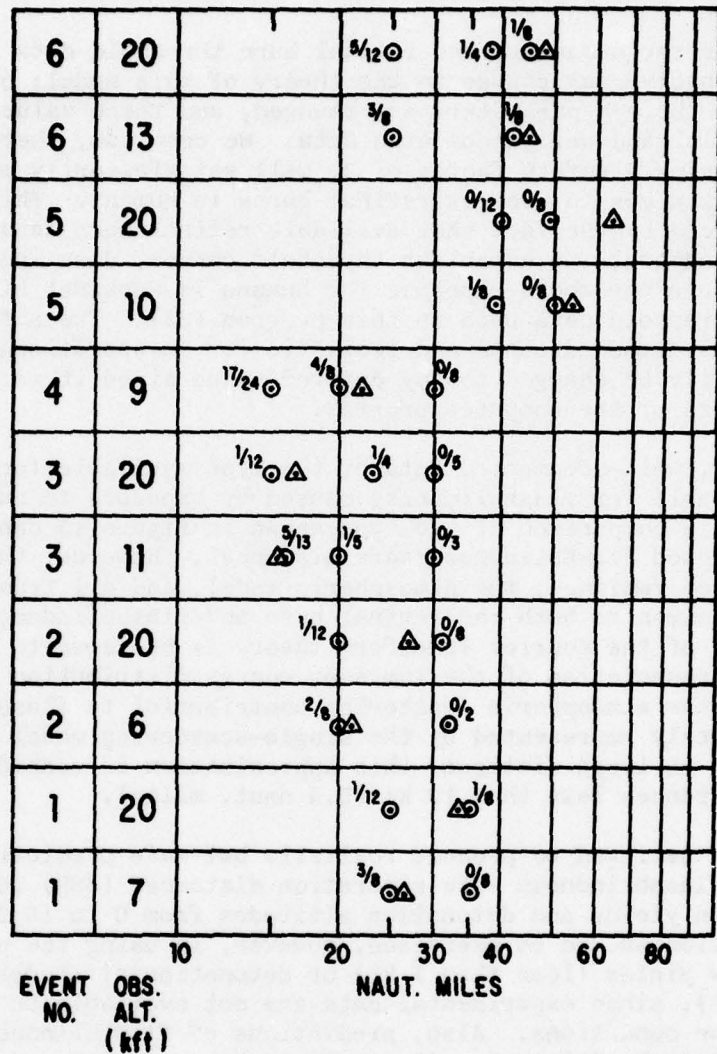


Figure 13. Using Operation Dominic exposure conditions for rabbits, burns produced are compared to predicted retinal burn threshold distances.

$\odot$  = Distance at which rabbits were exposed

$a/b$  = Number of rabbits with retinal burns/  
number of rabbits exposed

$\Delta$  = Predicted retinal burn threshold distance  
for rabbits

produced. The excellent agreement between predicted and experimental results indicates that this Exposure Model will satisfactorily predict, for rabbits, retinal burn threshold distances from nuclear detonations.

Using data for the human eye and retinal burn threshold data for monkeys does not involve any change in the theory of this model; only tabular values for the eye parameters are changed, and these values are based on experimental and well-documented data. We conclude, therefore, that this model, using a safety factor of 2, will satisfactorily predict safe separation distances to prevent retinal burns in humans. This conclusion is reinforced by the fact that available retinal burn data for humans, while not adequate to establish threshold curves, does indicate that the retinal burn threshold exposure for humans is somewhat higher than the monkey threshold data used in this program (23). The safety factor of 2 is considered adequate and realistic for an operational situation but can easily be changed to any desired value since it is one of the input parameters of the computer program.

Unfortunately, well-documented data of the type available for retinal burns is not available for flashblindness caused by exposure to nuclear detonations. Thus a comparison of the type shown in Figure 13 cannot be made for the predicted flashblindness safe distances. However, the calculation of the source radiance, the atmospheric model, and all transmission calculations are common to both the retinal burn and flashblindness predictions. The use of the Fourier Transform theory is believed to result in a realistic representation of the luminous energy distribution on the retina. Although the atmospheric scattering contribution to flashblindness is not accurately represented by the single-scattering model used here, particularly at large distance, this approximation is considered reasonable for distances less than 10 km (5.4 naut. miles).

This model is believed to produce realistic but safe predictions of retinal burn and flashblindness safe separation distances (SSD) for 10-kt to 10-Mt detonation yields and detonation altitudes from 0 to 15,240 m (50,000 ft). Caution should be exercised, however, in using the predictions for very low yields (less than 1 kt) or detonation altitudes above 7,620 m (25,000 ft), since experimental data are not available to test the model for those conditions. Also, predictions of flashblindness SSD greater than about 50 km (27 naut. miles) should be used with caution. This model is not adequate and should not be used to predict flashblindness SSD for conditions that will result in a large amount of scatter from surfaces; e.g., observer and detonation between water or snow-covered ground and low-altitude cloud cover or between two solid cloud layers.

To increase confidence in predictions of eye SSD, additional data are needed to (1) better define fireball diameters and spectral radiance as a function of yield, altitude, and time, (2) better define the visual acuity required by a pilot to maintain temporary control of his aircraft during periods of partial flashblindness, (3) determine an acceptable

maximum recovery time to that visual acuity, and (4) determine the maximum size afterimage which will not preclude that visual acuity. Also, a multiple-scattering model practical for use in an iterative-type program is needed.

Figures 14 and 15 show predicted retinal burn and flashblindness SSD, respectively, for a 100-kt daytime detonation at 304.8 m (1,000 ft) and a visibility of 46.3 km (25 naut. miles). SSD is shown for three assumed

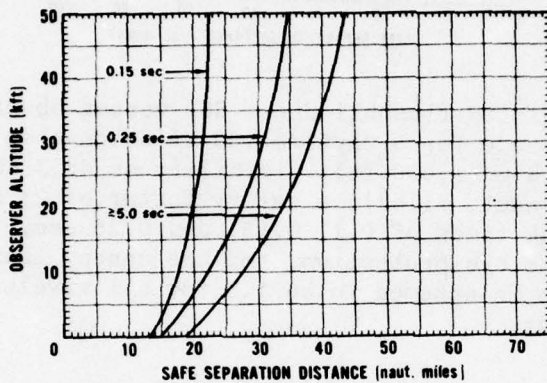
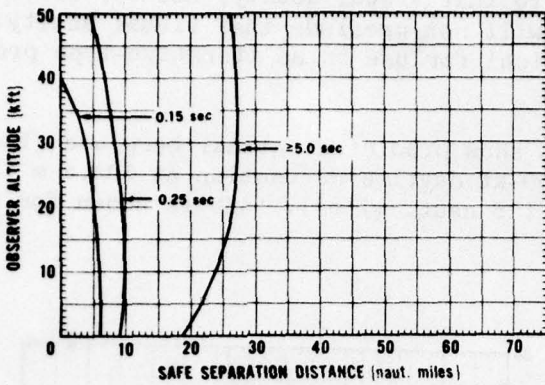
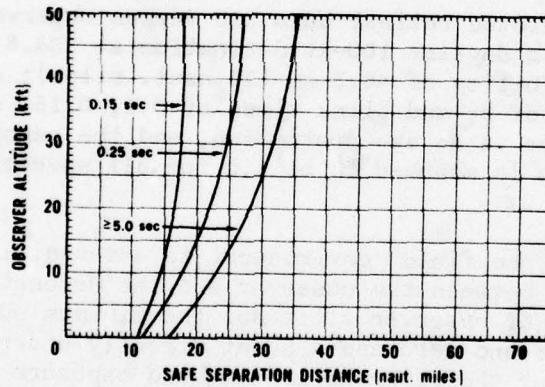


Figure 14. Predicted retinal burn SSD versus observer altitude for a daytime 100-kt detonation at 304.8 m (1,000 ft); visibility of 46.3 km (25 naut. miles); a safety factor of 2; and blink times of 0.1, 0.15, and 0.25 sec. There is no eye protection, and the canopy transmission is assumed to be 1.0 for all wavelength bands.

blink times, and a "free field" environment is assumed; i.e., there is no windscreen or canopy between the observer and the detonation. Each curve shows, as a function of observer altitude, the minimum surface distance between detonation ground zero and a point directly under the observer which will be safe for the given blink time and exposure conditions. A safety factor of 2 was used. Figures 16 and 17 show the predicted SSD for the same conditions as Figures 14 and 15 except that the observer is assumed to be looking through a B-1 windscreen that is perpendicular to the line of sight to the fireball. Comparing Figures 14 and 15 with 16 and 17, the eye protection afforded by the B-1 windscreen is readily apparent. Figures 18 and 19 show the SSD for the same exposure conditions as Figures 16 and 17 except that the observer is assumed to be wearing a pair of Air Force N-15 sun glasses, and demonstrate the effectiveness of this readily available eye protection.



**Figure 15.** Predicted flashblindness SSD versus observer altitude for a daytime 100-kt detonation at 304.8 m (1,000 ft); visibility of 46.3 km (25 naut. miles); a safety factor of 2; and blink times of 0.1, 0.15, and 0.25 sec. There is no eye protection, and the canopy transmission is assumed to be 1.0 for all wavelength bands.



**Figure 16.** Predicted retinal burn SSD versus observer altitude for a daytime 100-kt detonation at 304.8 m (1,000 ft); visibility of 46.3 km (25 naut. miles); a safety factor of 2; and blink times of 0.1, 0.15, and 0.25 sec. There is no eye protection and the observer is assumed to be looking through a B-1 windscreens that is perpendicular to the line of sight to the fireball.

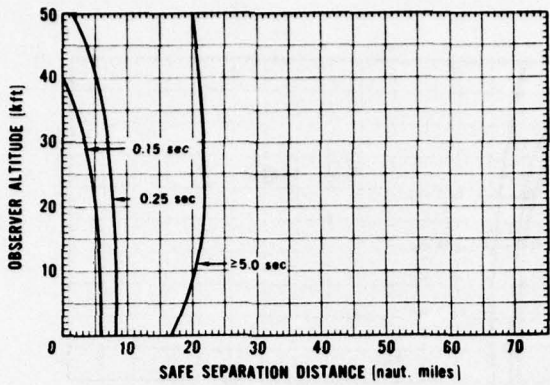


**Figure 17.** Predicted flashblindness SSD versus observer altitude for a daytime 100-kt detonation at 304.8 m (1,000 ft); visibility of 46.3 km (25 naut. miles); a safety factor of 2; and blink times of 0.1, 0.15, and 0.25 sec. There is no eye protection and the observer is assumed to be looking through a B-1 windscreens that is perpendicular to the line of sight to the fireball.

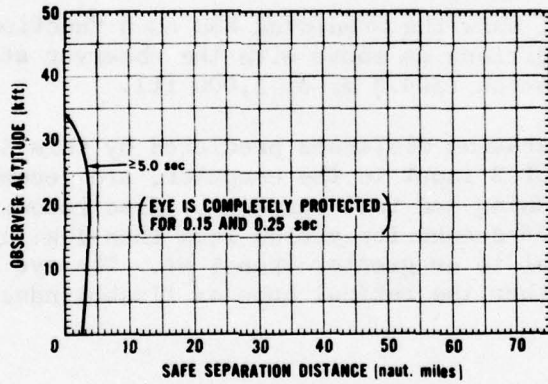


**Figure 18.** Predicted retinal burn SSD versus observer altitude for a daytime 100-kt detonation at 304.8 m (1,000 ft); visibility of 46.3 km (25 naut. miles); a safety factor of 2; and blink times of 0.1, 0.15, and 0.25 sec. The observer is assumed to be wearing a pair of Air Force N-15 sun glasses and looking through a B-1 windscreens that is perpendicular to the line of sight to the fireball.

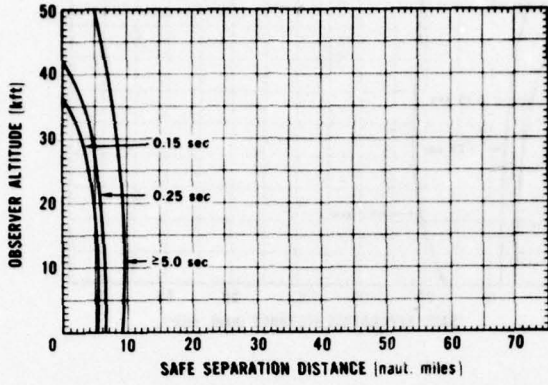


**Figure 19.** Predicted flashblindness SSD versus observer altitude for a daytime 100-kt detonation at 304.8 m (1,000 ft); visibility of 46.3 km (25 naut. miles); a safety factor of 2; and blink times of 0.1, 0.15, and 0.25 sec. The observer is assumed to be wearing a pair of Air Force N-15 sun glasses and looking through a B-1 windscreens that is perpendicular to the line of sight to the fireball.

Figures 20 and 21 show the predicted SSD as a function of time for the same exposure conditions as above with the observer at the same altitude as the detonation (304.8 m, or 1,000 ft).

The eye safe separation distances predicted by this Exposure Model, with a safety factor of 2 input to the computer, are recommended for Air Force operational planning and test purposes. Also recommended for use is a blink time of 0.25 second for yields less than 1 Mt and of 0.35 second for yields equal to or greater than 1 Mt. The eye safe separation distance should be either the retinal burn or flashblindness SSD, whichever is greater.

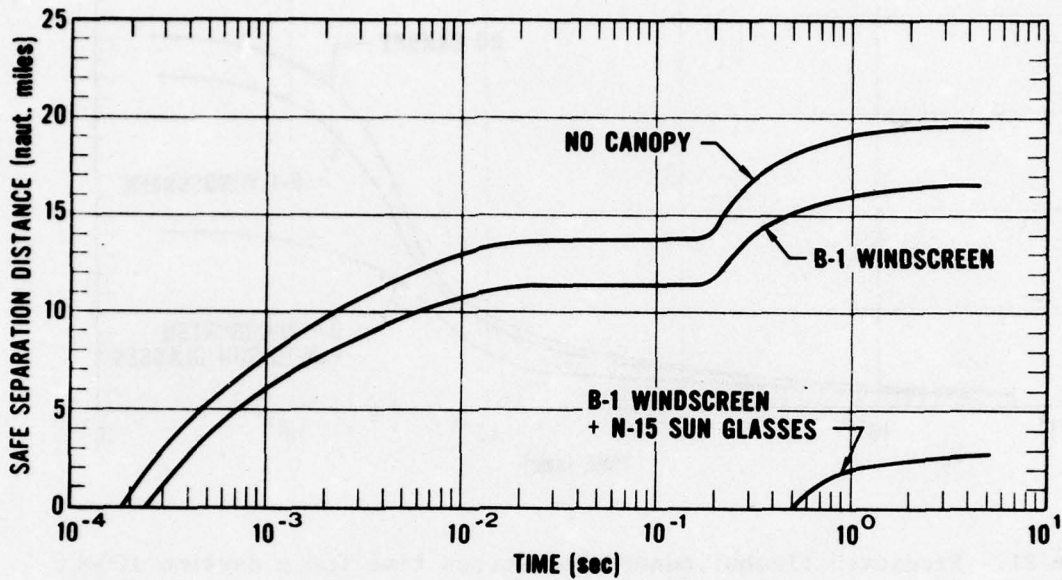


Figure 20. Predicted retinal burn SSD versus time for a daytime 100-kt detonation at 304.8 m (1,000 ft); visibility of 46.3 km (25 naut. miles); a safety factor of 2; and an observer altitude of 304.8 m (1,000 ft). The observer's eye is assumed to be completely unprotected, to be protected by a B-1 windscreens, and to be protected by a B-1 windscreens plus N-15 sun glasses.

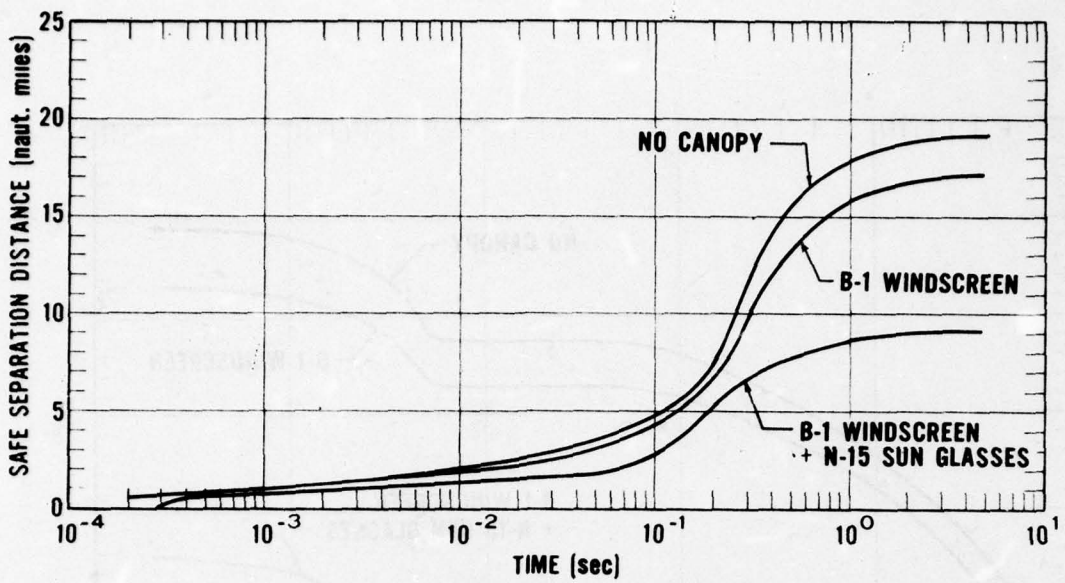


Figure 21. Predicted flashblindness SSD versus time for a daytime 100-kt detonation at 304.8 m (1,000 ft); visibility of 46.3 km (25 naut. miles); a safety factor of 2; and an observer altitude of 304.8 m (1,000 ft). The observer's eye is assumed to be completely unprotected, to be protected by a B-1 windscreens, and to be protected by a B-1 windscreens plus N-15 sun glasses.

#### ACKNOWLEDGMENT

I wish to express my appreciation to Dr. Ralph G. Allen for his generous advice in deriving the mathematical concepts and general content of this report and to Mr. H. Neal Keiser for his assistance in the computer programming and the numerous computer runs performed.

#### REFERENCES

1. Albanese, R. A. USAFSAM/Biometrics Division, Brooks AFB, Tex. Personal communication, 1975.
2. Alder, A. V. C131-A/T-29 flight simulator flashblindness study. SAM-TR-65-75 (DDC AD 577 332L), Oct 1965.
3. Alder, A. V., and J. E. Hamilton. F-106B aircraft flashblindness experiment. SAM-TR-67-41 (DDC AD 659 718), July 1967.
4. Allen, R. G., Jr., et al. Nuclear-flash eye-effects technical report for military planners. Final report, USAF Contract No. AF41 (609)-2900 (DDC AD 659 145), Technology Inc., Life Sciences Div., San Antonio, Tex., Feb 1967.
5. Allen, R. G., Jr., et al. Calculation of retinal burn and flashblindness safe separation distances. Final report, USAF Contract No. F41609-67-C-0040 (DDC AD 668 549), Technology Inc., Life Sciences Div., San Antonio, Tex., Jan 1968.
6. Allen, R. G., Jr., et al. The calculation of retinal burn and flashblindness safe separation distances. SAM-TR-68-106 (DDC AD 680 842), Sep 1968.
7. Allen, R. G., Jr., et al. Research to obtain eye-effects data and develop a mathematical model for eye-effects predictions. Final report, USAF Contract No. F41609-70-C-0007 (DDC AD 882 847), Technology Inc., Life Sciences Div., San Antonio, Tex., Dec 1970.
8. Allen, R. G., Jr. USAFSAM/Radiobiology Division, Brooks AFB, Tex. Personal communication, 1975.
9. Boettner, L. A. Spectral transmission of the eye. Final report, Contract No. AF41(609)-2966 (DDC AD 663 246), University of Michigan, Ann Arbor, Mich., July 1967.
10. Brown, J. L. Experimental investigation of flashblindness. Human Factors 6:503 (1964).
11. Buettner, K., and H. W. Rose. Eye hazards from an atomic bomb. Sight Sav Rev 23:1 (1953).
12. Byrnes, V. A. Flashblindness. WT-341, Operation Buster, Project 4.3, Air Force Special Weapons Projects, Washington, D.C., Mar 1952.
13. Byrnes, V. A. Flashblindness. WT-530, Operation Snapper, Project 4.5 Air Force Special Weapons Projects, Washington, D.C., Mar 1953.

14. Byrnes, V. A., et al. Ocular effects of thermal radiation from atomic detonation--flashblindness and chorioretinal burns. WT-745, Operation Upshot-Knothole, Project 4.5, Air Force Special Weapons Projects, Washington, D.C., Nov 1955.
15. Chisum, G. T., and J. H. Hill. Eye protection for nuclear weapons delivery pilots; inflight research studies to obtain quantitative performance data. Report No. NADC-MA-L6106 (DDC AD 253 426), Naval Air Development Center, Johnsville, Pa., Mar 1961.
16. Committee on Colorimetry: Optical Society of America. The science of color. New York: Crowell Co., 1953.
17. Culver, J. F., et al. Human chorioretinal burns following high-altitude nuclear detonations. Proc. 35th Annual Scientific Meeting of the AMA, May 1964.
18. Cushman, W. H. Effect of flash field size on flashblindness in an aircraft cockpit. Aerosp Med 42:6 (1971).
19. Czeh, R. S., A. W. Casper, and E. C. Segraves, Jr. A mathematical model of flashblindness. Final report, contract No. AF41(609)-2644, General Electric Co., Oklahoma City, Okla., Oct 1965.
20. Development of a theoretical flashblindness model. Final report, Contract No. DASA 01-70-C-0008, Technology Inc., Life Sciences Div., San Antonio, Tex., Nov 1972.
21. Dwight, H. B. Tables of integrals and other mathematical data (3d ed). New York: Macmillan Co., 1957.
22. Electro-Optics handbook. Radio Corporation of America, Aerospace Systems Division, Burlington, Mass., 1968.
23. Elgin, S., D. O. Robbins, and D. R. Cavonius. Threshold for permanent functional and morphological visible damage in human retinas using visible radiation. Final report, USAF Contract No. F41609-69-C-0027 (DDC AD 735 802), Eye Research Foundation, Bethesda, Md., May 1971.
24. Farrer, D. N., et al. Effects of threshold macular lesions and sub-threshold macular exposures on visual performance in rhesus monkeys. Am Indus Hyg Assoc J 30:123 (1969).
25. Glasstone, S. (ed). The effects of nuclear weapons (rev. ed.). Washington: U.S. Government Printing Office, 1962.
26. Hamilton, J. E. B-52D mobile flight simulator flashblindness experiment. SAM-TR-67-67 (DDC AD 663 230), Sep 1967.

27. Handbook for instructions for aerospace personnel subsystem design (HIAPSD), AFSC Manual 80-3, July 1961; Supplemental report, 15 April 1965.
28. Hill, J. H., and G. T. Chisum. Eye protection for nuclear weapons delivery pilots; inflight research studies to obtain quantitative performance data. Report No. NADC-MA-L6035 (DDC AD 257 372), Naval Air Development Center, Johnsville, Pa., Sep 1960.
29. Kingslake, R. Applied optics and optical engineering, Vol I. New York: Academic Press, 1965.
30. LeGrand, Y. Light, color, and vision. Approved translation by R. W. G. Hunt, et al. New York: Wiley and Sons, Inc., 1957.
31. Linfoot, E. H. Fourier methods in optical image evaluation. New York: Focal Press, 1964.
32. List, R. J. Smithsonian meteorological tables (6th rev. ed.). Washington: Smithsonian Institution, 1971.
33. Mandelbaum, J., and L. L. Sloan. Peripheral visual acuity. Am J Ophthalmol 30:581 (1947).
34. Middleton, W. E. K. Vision through the atmosphere. Toronto: University of Toronto Press, 1958.
35. Miller, N. D. Visual recovery from high-intensity flashes. II. Final report, Contract No. AF41(609)-2426 (DDC AD 642 731), Ohio State University Research Foundation, Columbus, Ohio, July 1966.
36. Miller, N. D., et al. Evaluation of eye hazards from nuclear detonations. I. Retinal burns and flashblindness. Final report, USAF Contract No. F41609-68-C-0023 (DDC AD 697 425), Technology Inc., Life Sciences Div., San Antonio, Tex., Nov 1969.
37. Oyama, A., and T. Sasaki. A case of burn of the cornea and retina by atomic bomb. Ganko Rinsho Iho 40:177 (1946). Cited in D. G. Cogan, S. F. Martin, and S. J. Kimura. Survey of A-bomb survivors in Japan. Report of Atomic Bomb Casualty Commission, Nov 1949.
38. Pitts, D. G., and L. R. Loper. Ambient and cockpit luminance measurements. Aerosp Med 34:145 (1963).
39. Richey, E. O. Prediction of eye safe separation distances. Presented at AGARD Symposium on Loss of Vision from High-Intensity Light, Paris, France (DDC AD 634 723), Mar 1966.
40. Richey, E. O. Threshold distances for retinal burns from low-yield nuclear detonations. SAM-TR-66-49 (DDC AD 641 188), July 1966.

27. Handbook for instructions for aerospace personnel subsystem design (HIAPSD), AFSC Manual 80-3, July 1961; Supplemental report, 15 April 1965.
28. Hill, J. H., and G. T. Chisum. Eye protection for nuclear weapons delivery pilots; inflight research studies to obtain quantitative performance data. Report No. NADC-MA-L6035 (DDC AD 257 372), Naval Air Development Center, Johnsville, Pa., Sep 1960.
29. Kingslake, R. Applied optics and optical engineering, Vol I. New York: Academic Press, 1965.
30. LeGrand, Y. Light, color, and vision. Approved translation by R. W. G. Hunt, et al. New York: Wiley and Sons, Inc., 1957.
31. Linfoot, E. H. Fourier methods in optical image evaluation. New York: Focal Press, 1964.
32. List, R. J. Smithsonian meteorological tables (6th rev. ed.). Washington: Smithsonian Institution, 1971.
33. Mandelbaum, J., and L. L. Sloan. Peripheral visual acuity. Am J Ophthalmol 30:581 (1947).
34. Middleton, W. E. K. Vision through the atmosphere. Toronto: University of Toronto Press, 1958.
35. Miller, N. D. Visual recovery from high-intensity flashes. II. Final report, Contract No. AF41(609)-2426 (DDC AD 642 731), Ohio State University Research Foundation, Columbus, Ohio, July 1966.
36. Miller, N. D., et al. Evaluation of eye hazards from nuclear detonations. I. Retinal burns and flashblindness. Final report, USAF Contract No. F41609-68-C-0023 (DDC AD 697 425), Technology Inc., Life Sciences Div., San Antonio, Tex., Nov 1969.
37. Oyama, A., and T. Sasaki. A case of burn of the cornea and retina by atomic bomb. Ganko Rinsho Iho 40:177 (1946). Cited in D. G. Cogan, S. F. Martin, and S. J. Kimura. Survey of A-bomb survivors in Japan. Report of Atomic Bomb Casualty Commission, Nov 1949.
38. Pitts, D. G., and L. R. Loper. Ambient and cockpit luminance measurements. Aerosp Med 34:145 (1963).
39. Richey, E. O. Prediction of eye safe separation distances. Presented at AGARD Symposium on Loss of Vision from High-Intensity Light, Paris, France (DDC AD 634 723), Mar 1966.
40. Richey, E. O. Threshold distances for retinal burns from low-yield nuclear detonations. SAM-TR-66-49 (DDC AD 641 188), July 1966.

41. Richey, E. O., and N. E. Lof. Predicting safe distances to prevent retinal burns from nuclear detonations. SAM-TR-75-30 (DDC AD-A 017 797), Dec 1975.
42. Rose, H. W., et al. Human chorioretinal burns from atomic fireballs. AMA Arch Ophthalmol 55:205-210 (1956).
43. U.S. standard atmosphere, 1962. Washington: U.S. Government Printing Office, Superintendent of Documents, 1962.
44. Watson, G. N. A treatise on the theory of Bessel functions (2d ed.). Cambridge: University Press, 1958.
45. Weast, R. C. (ed). Handbook of chemistry and physics (55th ed.) Chemical Rubber Co. Press, Cleveland, Ohio, 1974-1975.
46. Wells, M. B., and W. B. Blattner. Sky brightness calculations for 450, 550, and 650 nm wavelength point isotropic sources in model atmospheres. I. Description of calculations. Report RRA-T7203-I, Radiation Research Associates, Fort Worth, Tex., Mar 1972.
47. White, T. J., et al. Evaluation of eye hazards from nuclear detonations. II. Safe separation distance predictions. Final report, USAF Contract No. F41609-68-C-0023 (DDC AD 697 425), Technology Inc., Life Sciences Div., San Antonio, Tex., Nov 1969.
48. White, T. J. Observer distances for nuclear events. I. Model for observer distances for retinal burn criteria. DASIAC-SR-125, General Electric -- TEMPO, Santa Barbara, Calif., Mar 1973.
49. White, T. J. Technology Inc., San Antonio, Tex. Personal communication, 1972.

## APPENDIXES

### INTRODUCTION

Appendices A through D show safe separation distances for retinal burns and flashblindness, as calculated by the method described in this report and using a safety factor of 2, for thirteen yields (0.01, 0.03, 0.1, 0.3, 1, 3, 10, 30, 100, 300, 1000, 3000, and 10,000 kt), three detonation altitudes (1, 10, and 30 kft; 0.3, 3, and 9.1 km), two visibilities (5 and 25 naut. miles; 9.3 and 46.3 km) and for day and night conditions (3- and 7-mm pupil diameter, respectively). Blink time is the parameter between curves, and curves for 0.10-, 0.15-, 0.25-, 0.5-, 1-, and 5-sec blink times are included except where impractical because of closely spaced curves or no changes. All calculations assumed a "free field" condition; i.e., no eye-protection devices, no windscreens or canopies, and no intervening or scattering materials, except the atmosphere, in or near the line of sight to the fireball. In addition, a worst-case exposure is assumed; i.e., the observer is looking directly at the fireball.

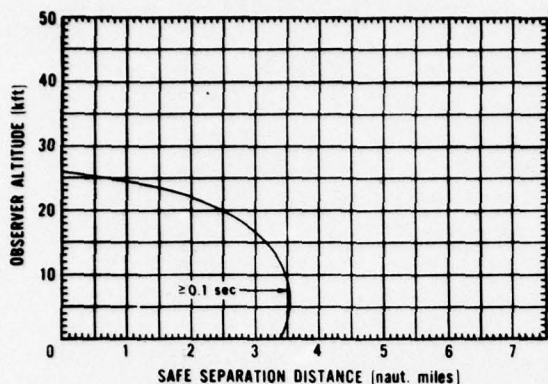
Within each appendix the figures are presented in the order of increasing yield and detonation altitude. The figures show the SSD (naut. miles) plotted versus the observer altitude (kft), with blink time (sec) as the parameter between curves. The SSD is the minimum distance on the earth's surface, between the detonation ground zero and a point directly beneath the observer, at which the observer is considered to be safe from the eye hazard for the exposure conditions considered. The eye safe separation distance is either the retinal burn or flashblindness safe distance, whichever is greater for the blink time and exposure conditions considered.

APPENDIX A: RETINAL BURN AND FLASHBLINDNESS SSD FOR DAY AND  
25-NAUT.-MILE (46.3-KM) VISIBILITY

Curves in Figures A-1 through A-39 show minimum SSD plotted vs. observer altitude for retinal burns and flashblindness during daylight (3-mm pupil dia.) and 25-naut.-mile visibility for detonation yields, altitudes, and blink times as indicated.

PRECEDING PAGE BLANK NOT FILMED

Retinal Burn SSD



Flashblindness SSD

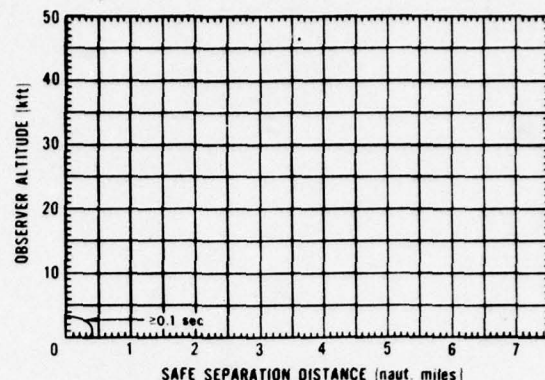


Figure A-1. 0.01 kt detonated at 1 kft (0.3 km).

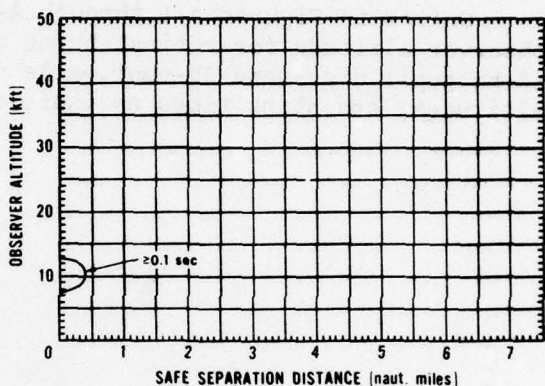
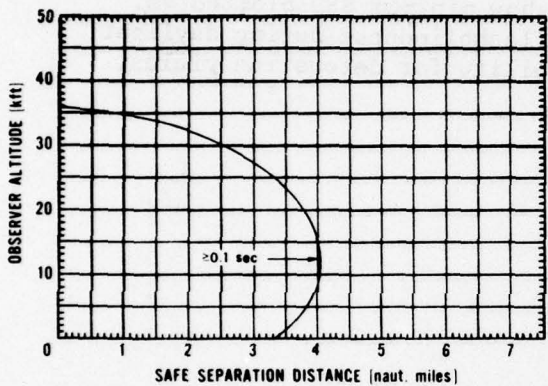


Figure A-2. 0.01 kt detonated at 10 kft (3 km).

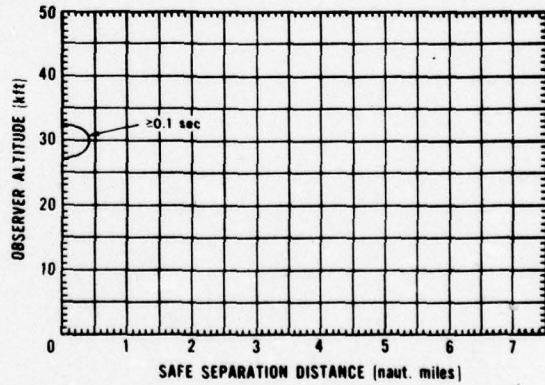
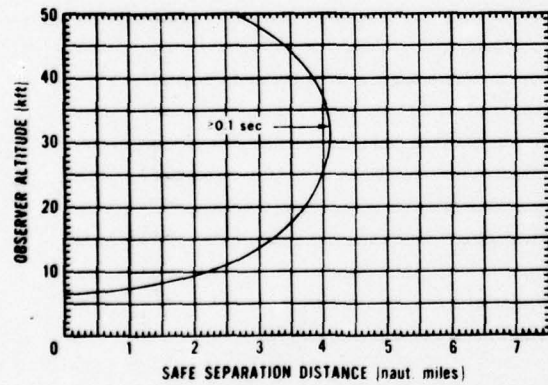
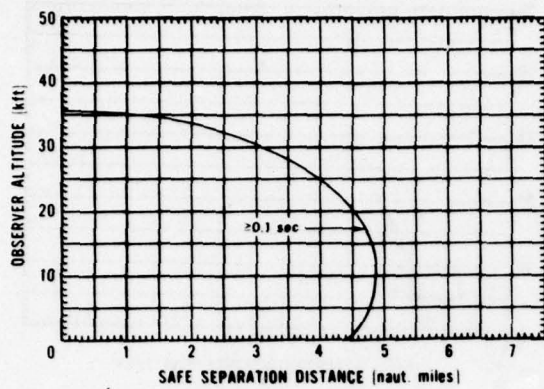


Figure A-3. 0.01 kt detonated at 30 kft (9.1 km).

Retinal Burn SSD



Flashblindness SSD

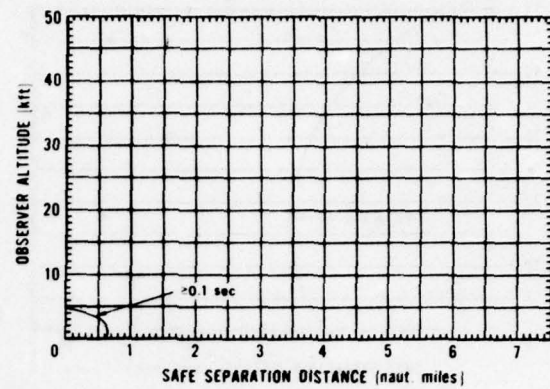


Figure A-4. 0.03 kt detonated at 1 kft (0.3 km).

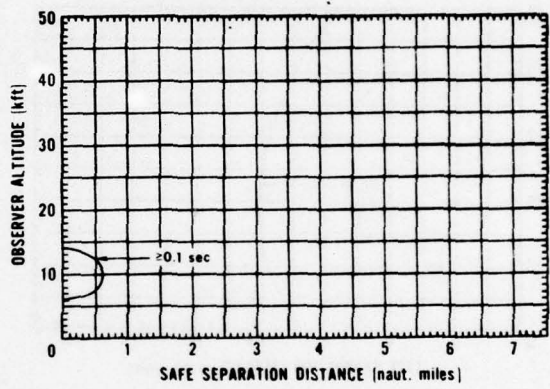
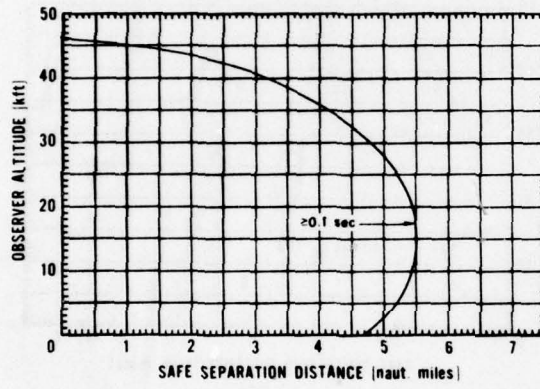


Figure A-5. 0.03 kt detonated at 10 kft (3 km).

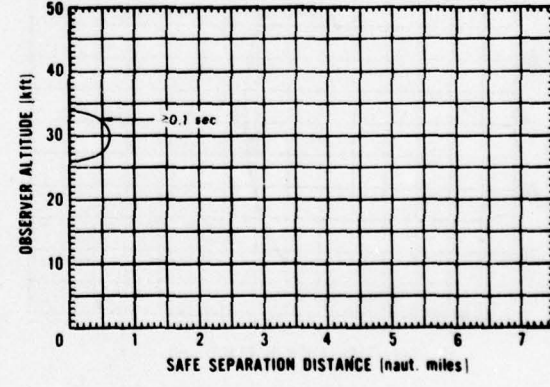
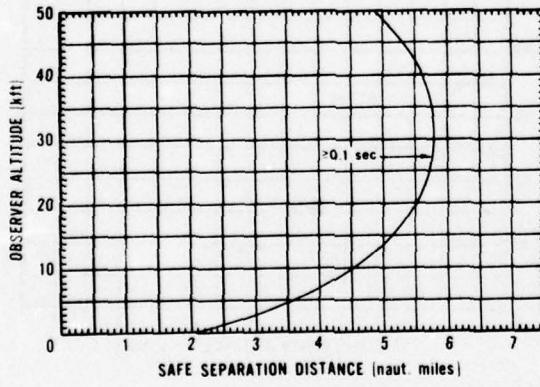
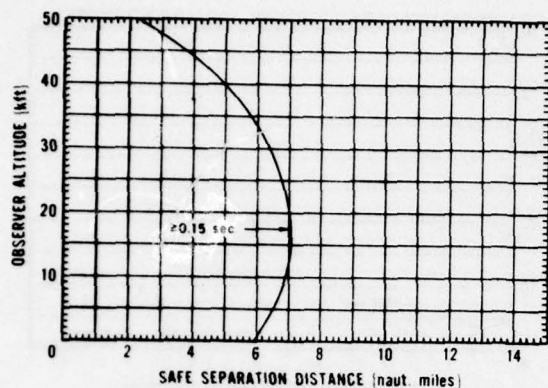


Figure A-6. 0.03 kt detonated at 30 kft (9.1 km).

Retinal Burn SSD



Flashblindness SSD

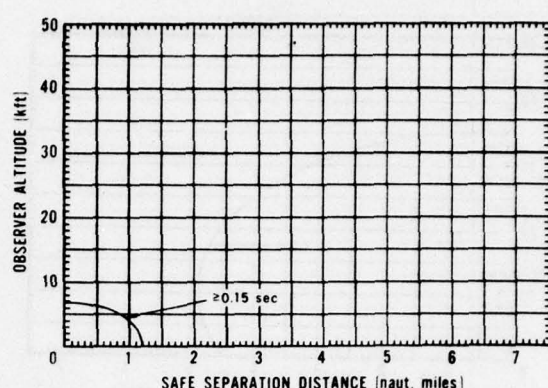


Figure A-7. 0.1 kt detonated at 1 kft (0.3 km).

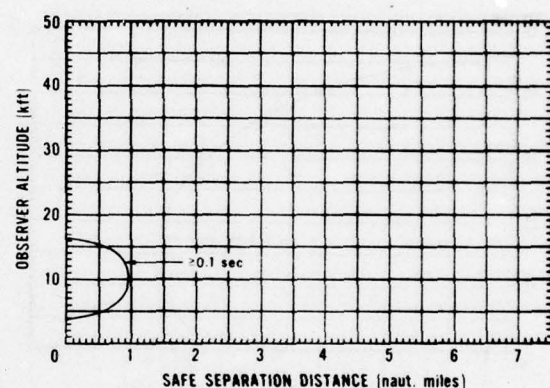
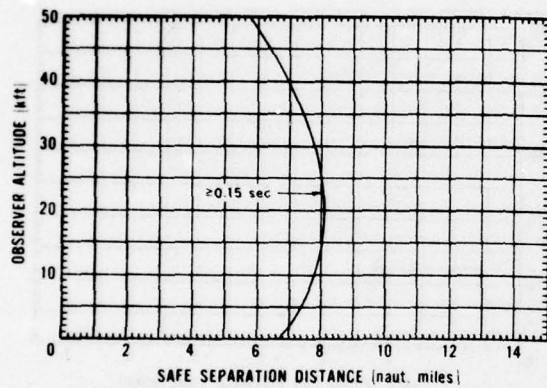


Figure A-8. 0.1 kt detonated at 10 kft (3 km).

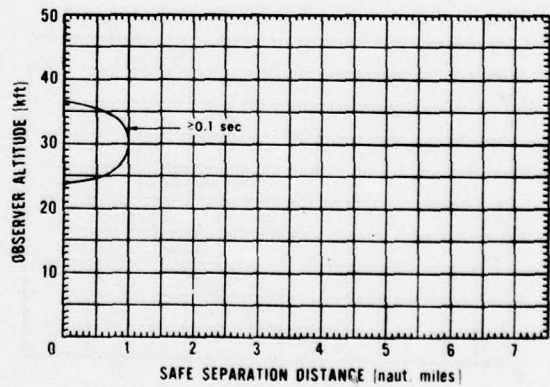
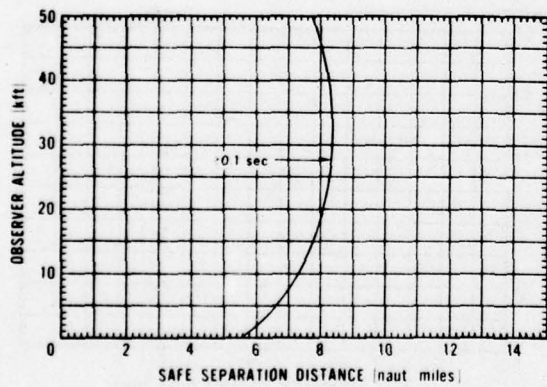
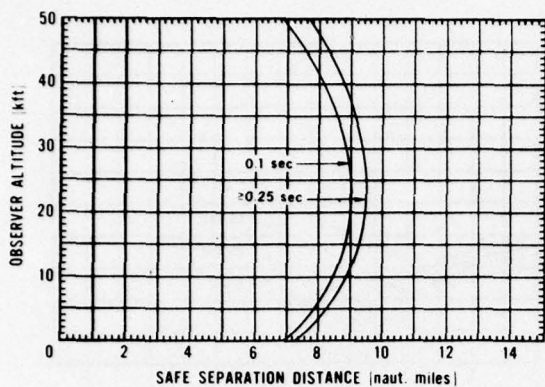


Figure A-9. 0.1 kt detonated at 30 kft (9.1 km).

Retinal Burn SSD



Flashblindness SSD

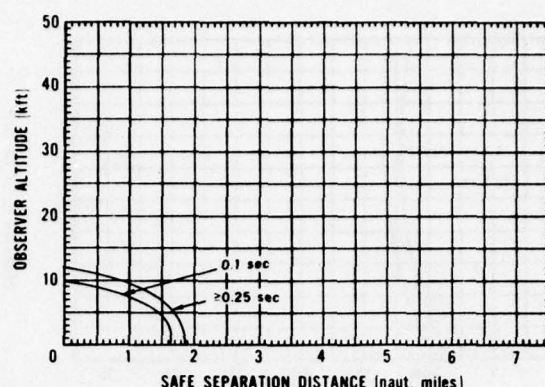


Figure A-10. 0.3 kt detonated at 1 kft (0.3 km).

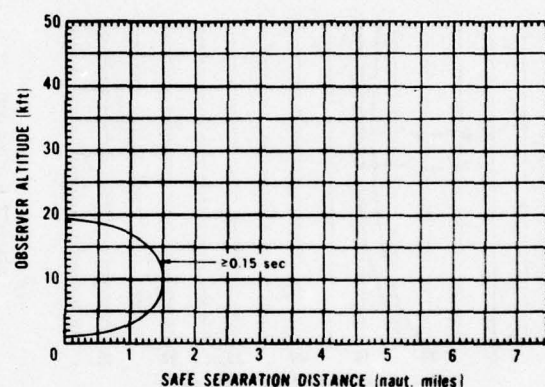
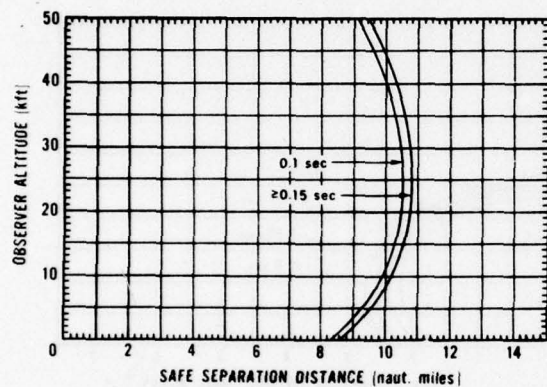


Figure A-11. 0.3 kt detonated at 10 kft (3 km).

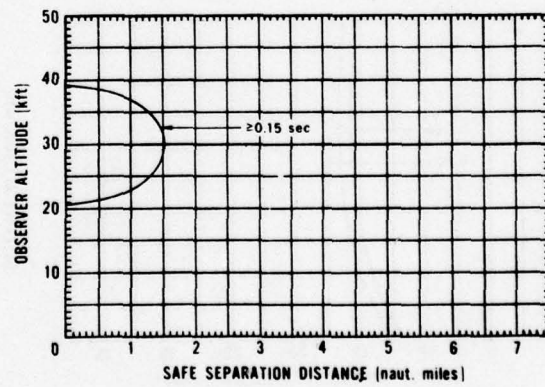
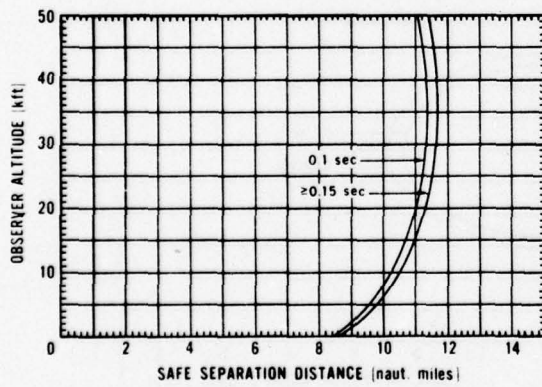
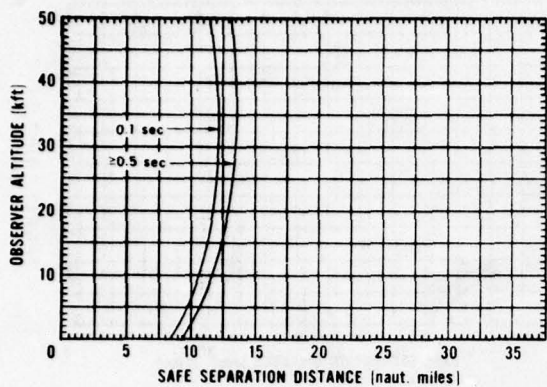


Figure A-12. 0.3 kt detonated at 30 kft (9.1 km).

Retinal Burn SSD



Flashblindness SSD

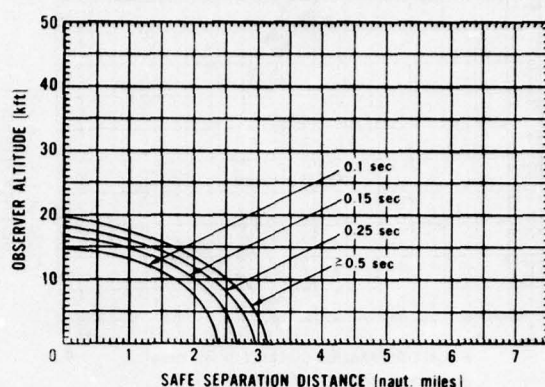


Figure A-13. 1 kt detonated at 1 kft (0.3 km).

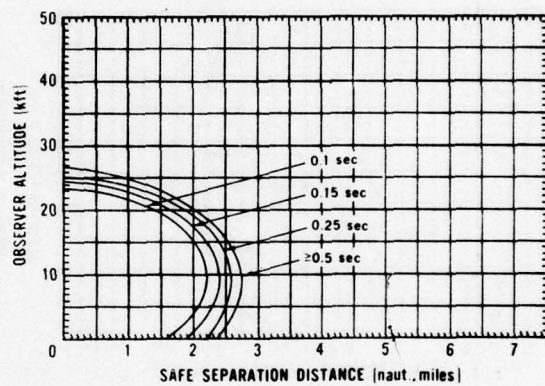
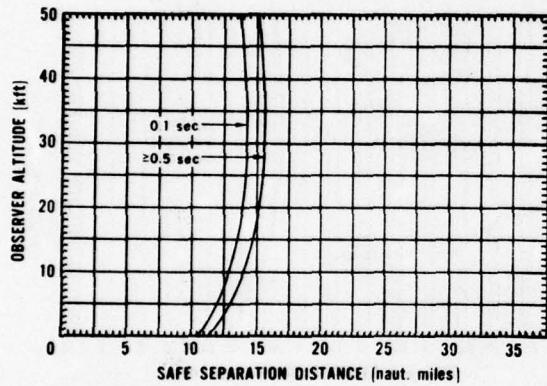


Figure A-14. 1 kt detonated at 10 kft (3 km).

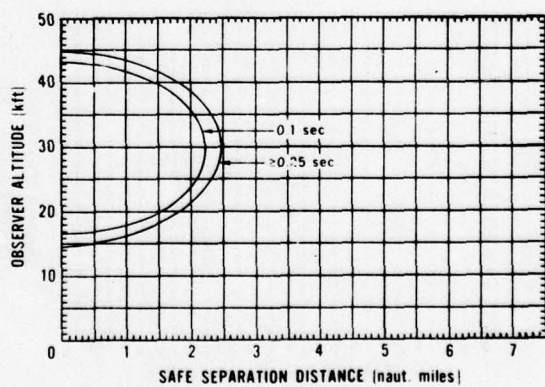
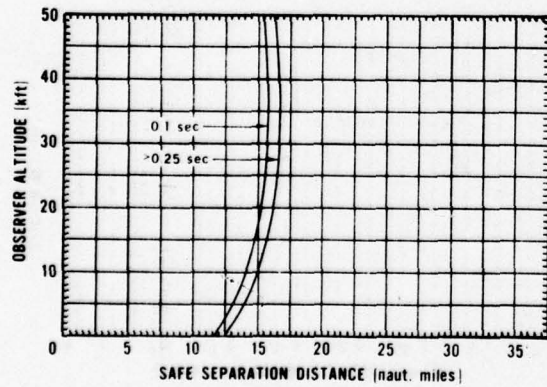
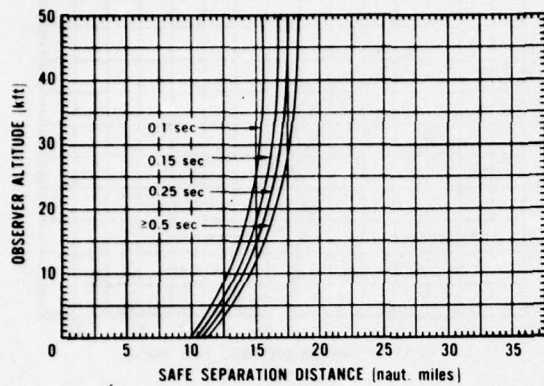


Figure A-15. 1 kt detonated at 30 kft (9.1 km).

Retinal Burn SSD



Flashblindness SSD

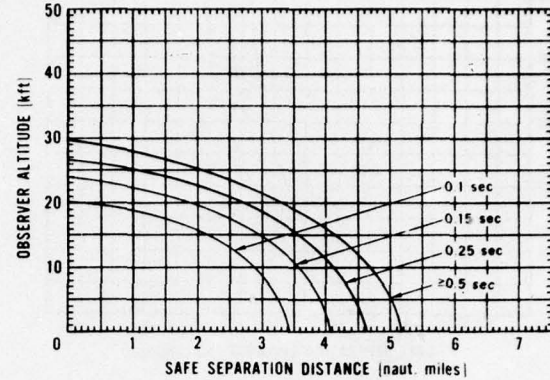


Figure A-16. 3 kt detonated at 1 kft (0.3 km).

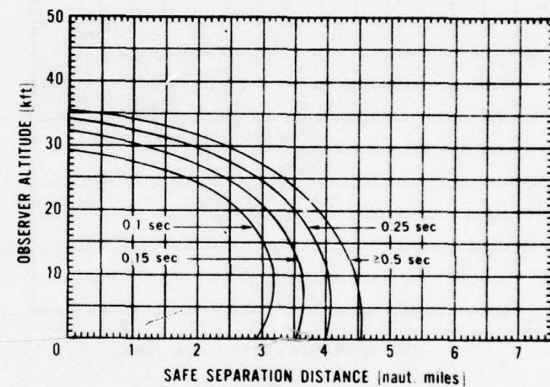
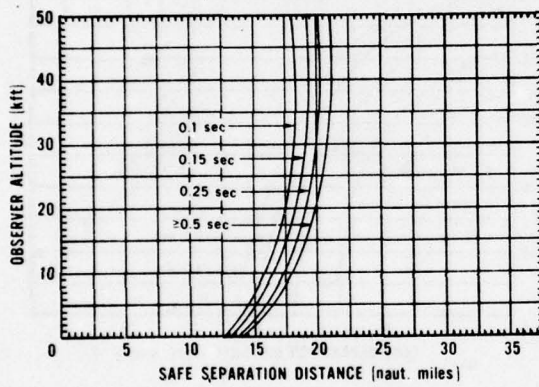


Figure A-17. 3 kt detonated at 10 kft (3 km).

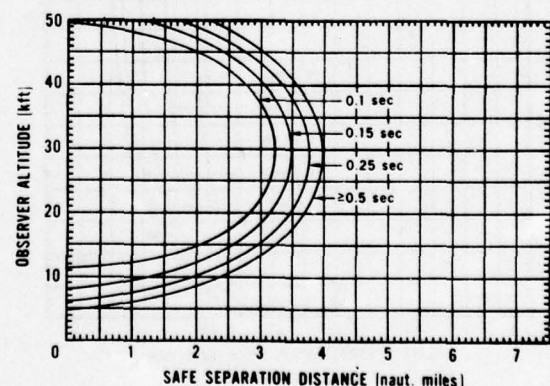
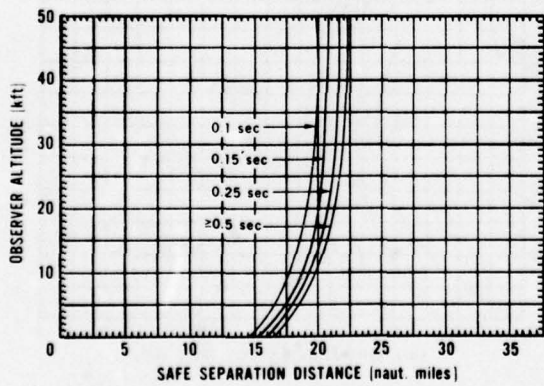
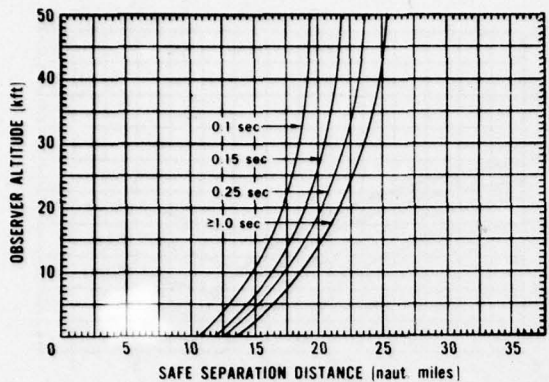


Figure A-18. 3 kt detonated at 30 kft (9.1 km).

**Retinal Burn SSD**



**Flashblindness SSD**

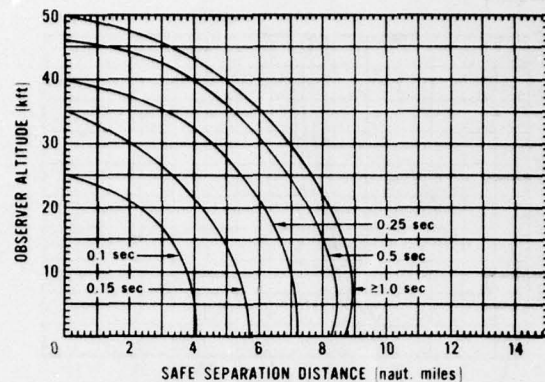


Figure A-19. 10 kt detonated at 1 kft (0.3 km).

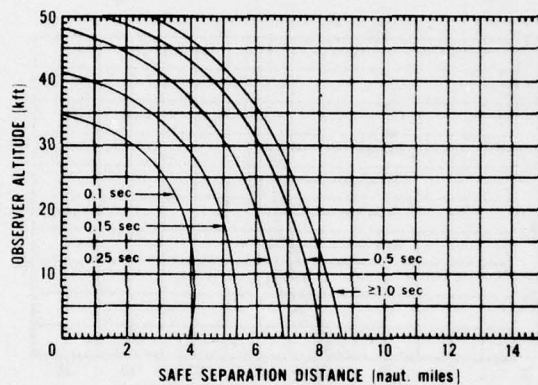
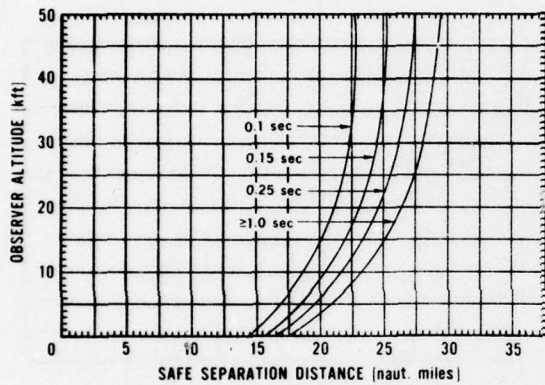


Figure A-20. 10 kt detonated at 10 kft (3 km).

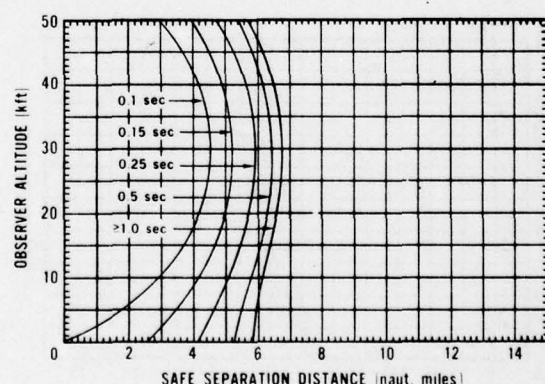
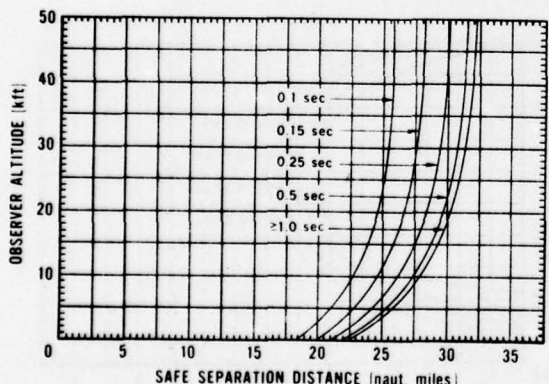
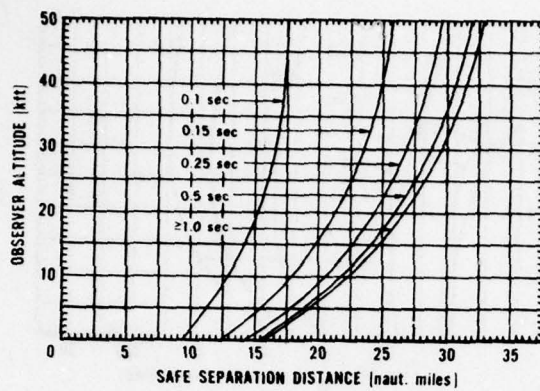


Figure A-21. 10 kt detonated at 30 kft (9.1 km).

Retinal Burn SSD



Flashblindness SSD

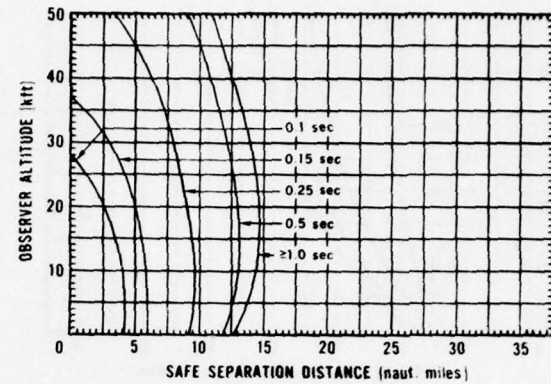


Figure A-22. 30 kt detonated at 1 kft (0.3 km).

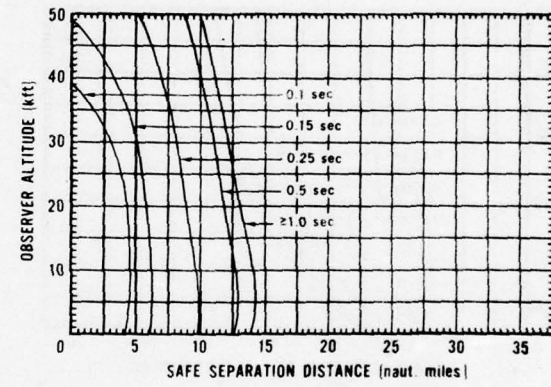
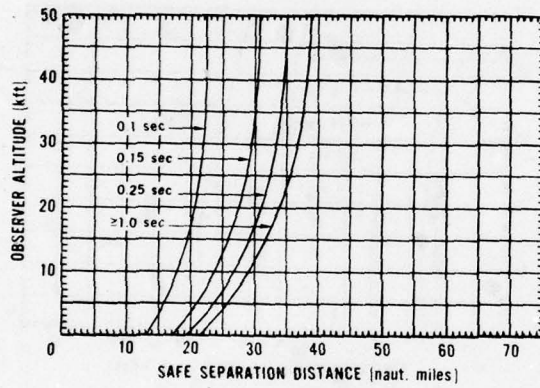


Figure A-23. 30 kt detonated at 10 kft (3 km).

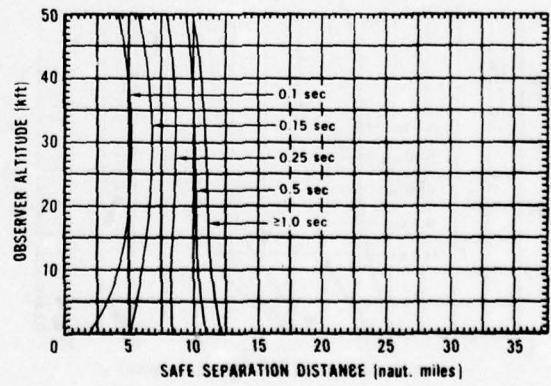
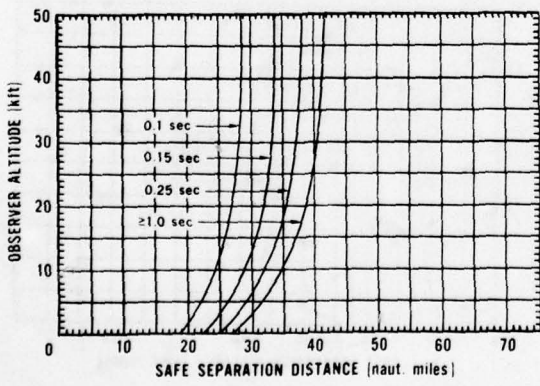
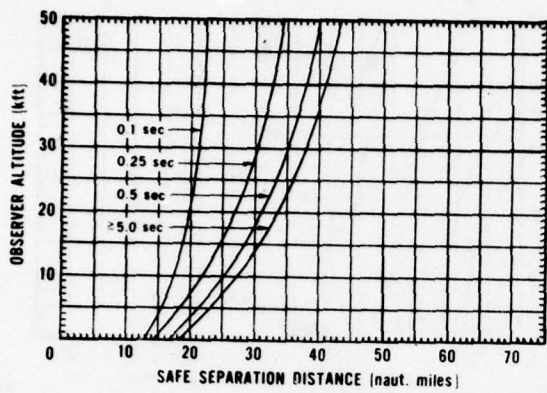


Figure A-24. 30 kt detonated at 30 kft (9.1 km).

Retinal Burn SSD



Flashblindness SSD

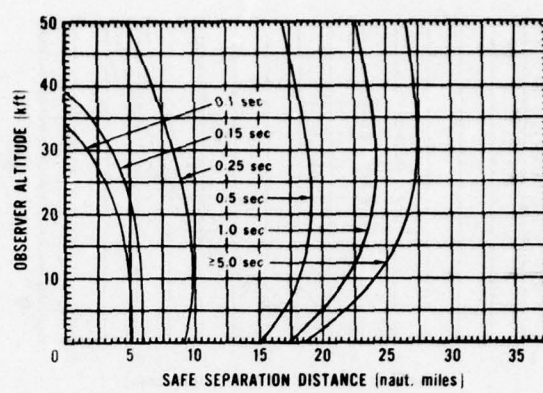


Figure A-25. 100 kt detonated at 1 kft (0.3 km).

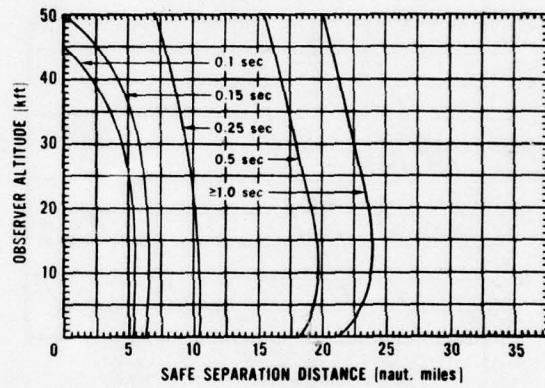
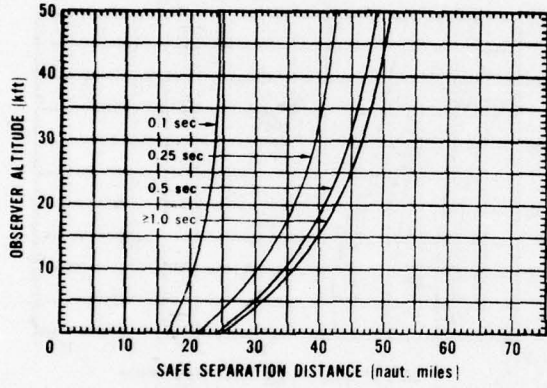


Figure A-26. 100 kt detonated at 10 kft (3 km).

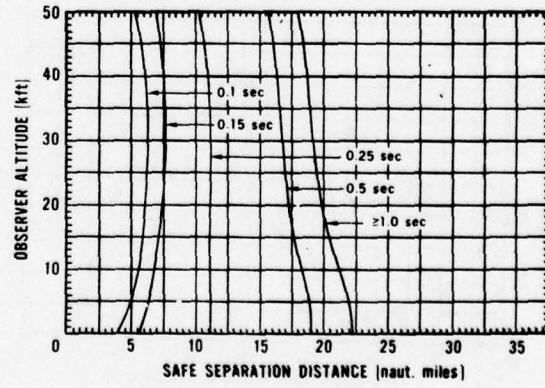
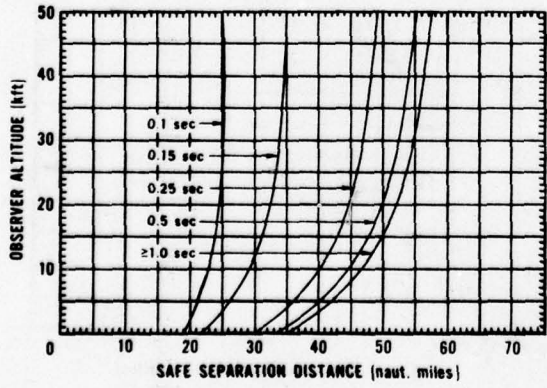
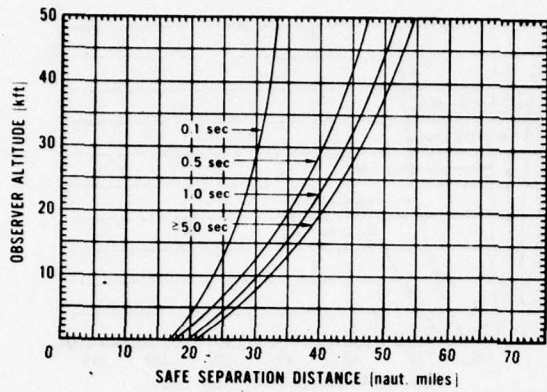


Figure A-27. 100 kt detonated at 30 kft (9.1 km).

Retinal Burn SSD



Flashblindness SSD

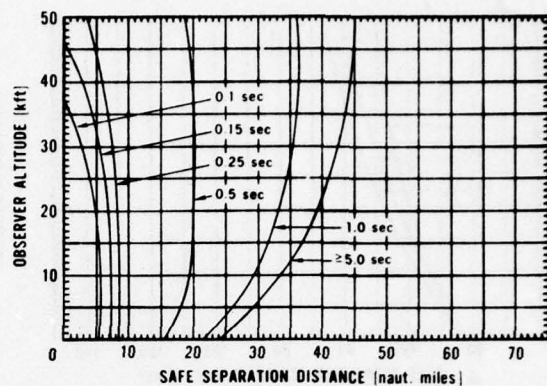


Figure A-28. 300 kt detonated at 1 kft (0.3 km).

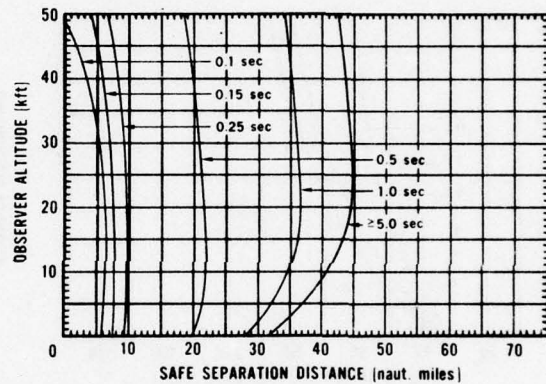
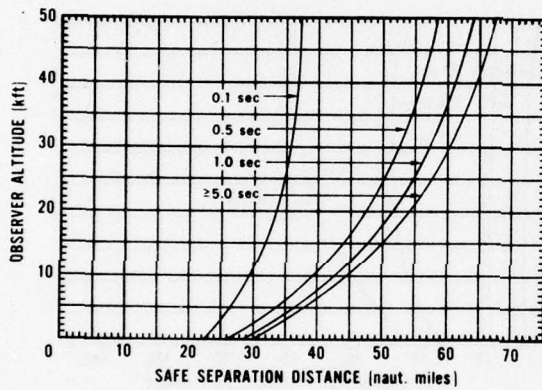


Figure A-29. 300 kt detonated at 10 kft (3 km).

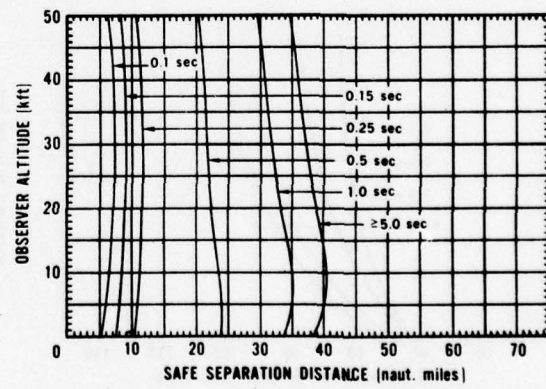
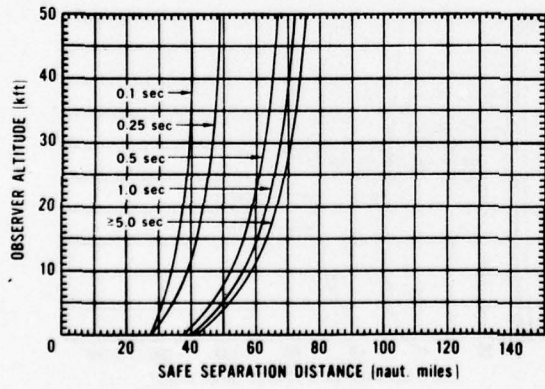
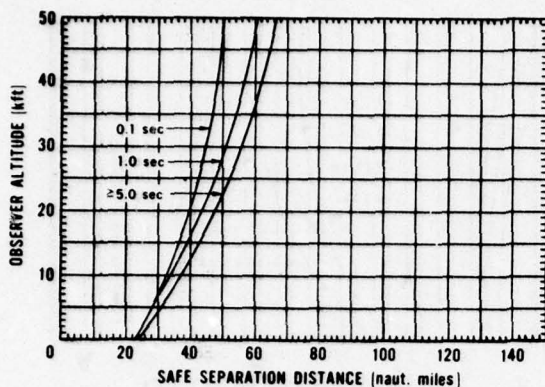


Figure A-30. 300 kt detonated at 30 kft (9.1 km).

Retinal Burn SSD



Flashblindness SSD

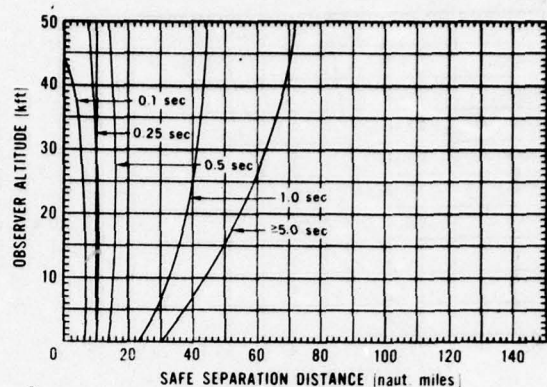


Figure A-31. 1,000 kt detonated at 1 kft (0.3 km).

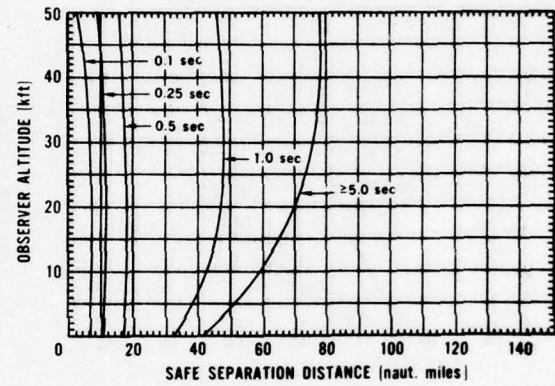
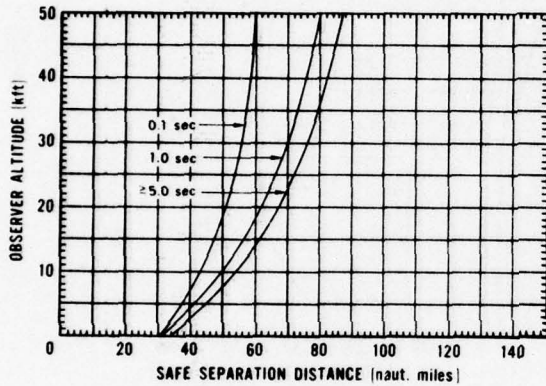


Figure A-32. 1,000 kt detonated at 10 kft (3 km).

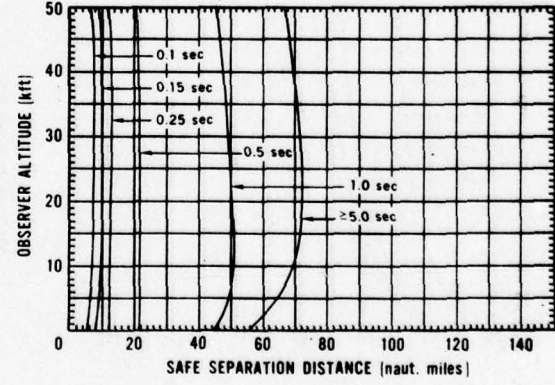
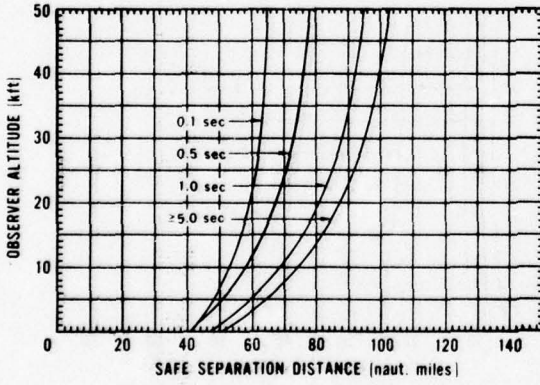
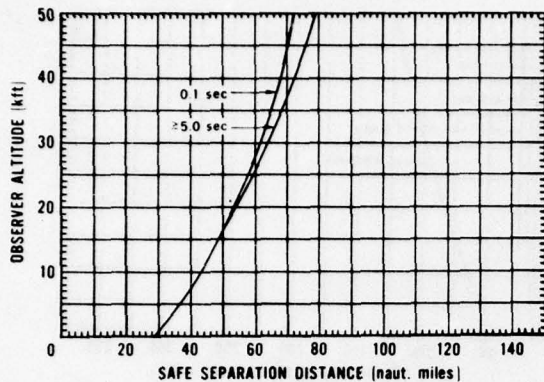


Figure A-33. 1,000 kt detonated at 30 kft (9.1 km).

Retinal Burn SSD



Flashblindness SSD

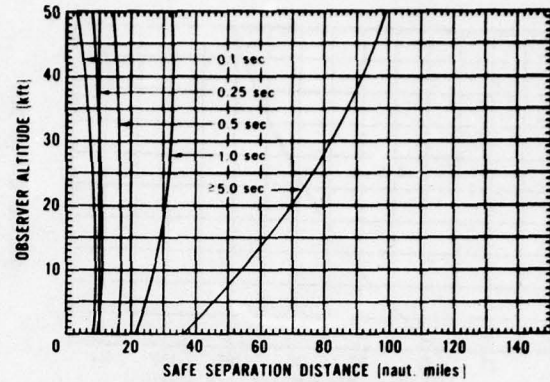


Figure A-34. 3,000 kt detonated at 1 kft (0.3 km).

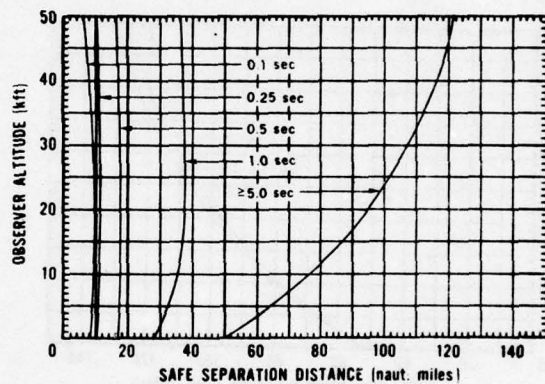
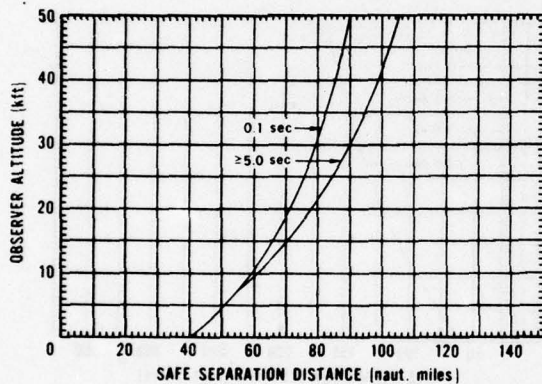


Figure A-35. 3,000 kt detonated at 10 kft (3 km).

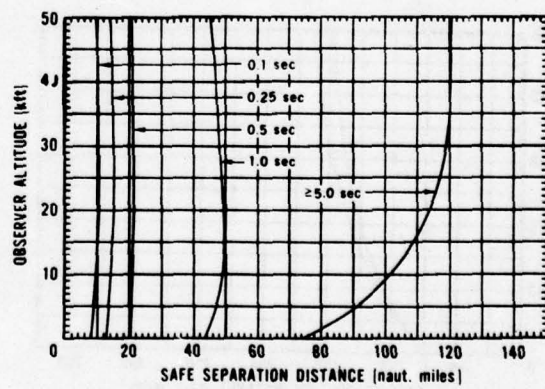
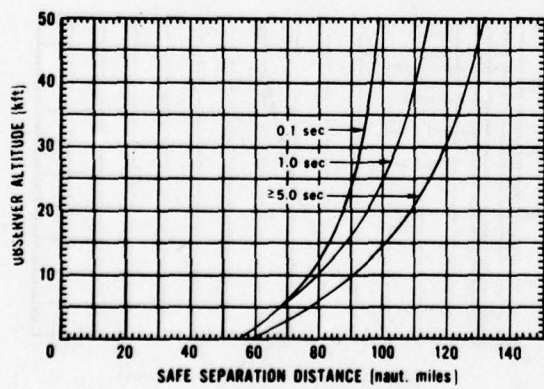
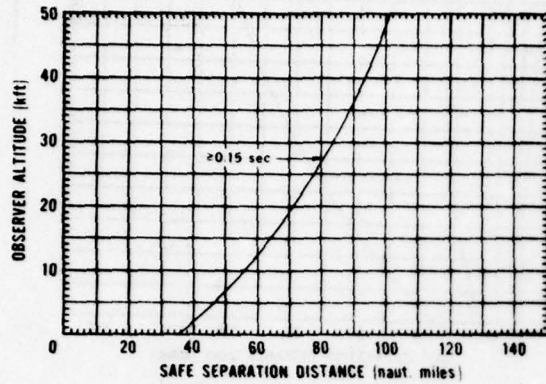


Figure A-36. 3,000 kt detonated at 30 kft (9.1 km).

Retinal Burn SSD



Flashblindness SSD

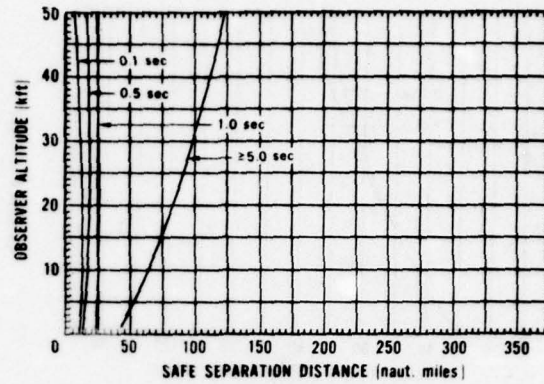


Figure A-37. 10,000 kt detonated at 1 kft (0.3 km).

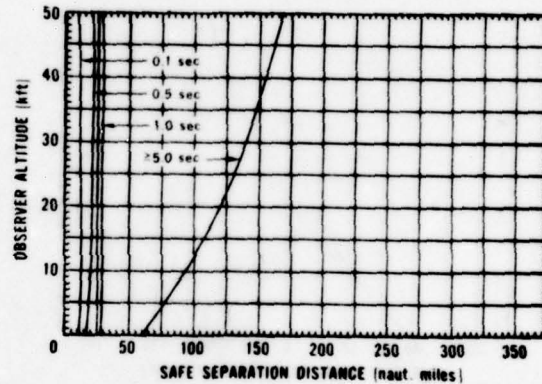
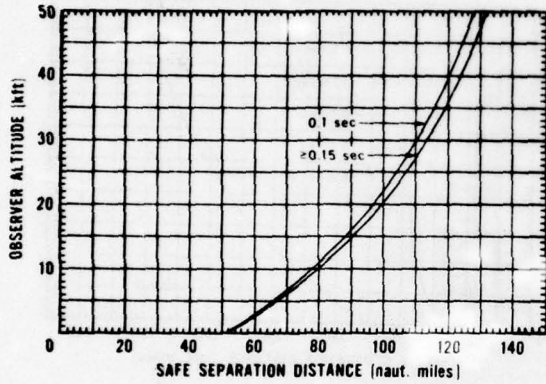


Figure A-38. 10,000 kt detonated at 10 kft (3 km).

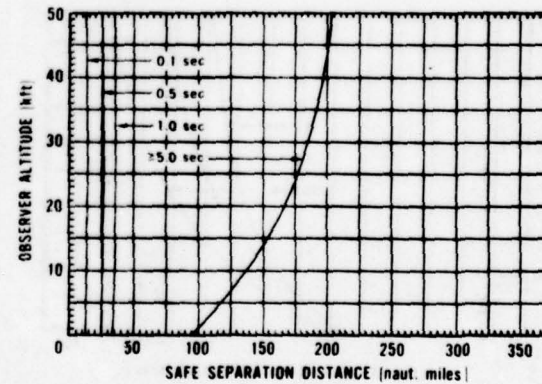
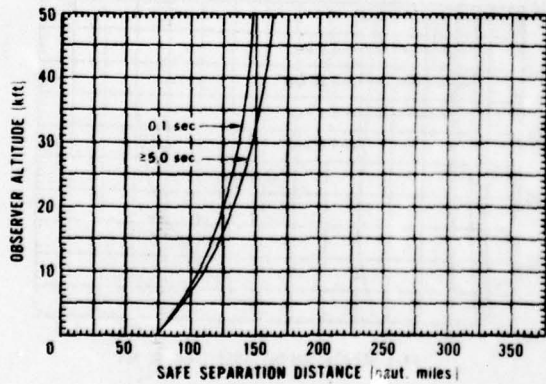
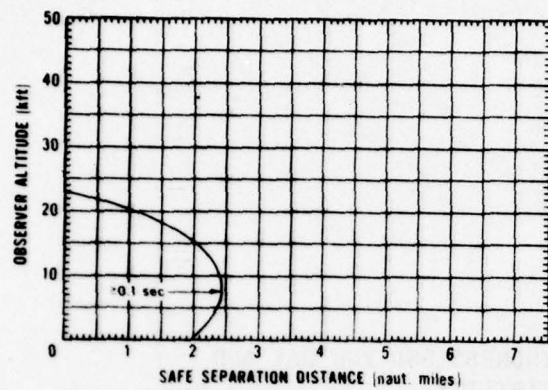


Figure A-39. 10,000 kt detonated at 30 kft (9.1 km).

**APPENDIX B: RETINAL BURN AND FLASHBLINDNESS SSD FOR DAY AND  
5-NAUT.-MILE (9.3-KM) VISIBILITY**

Curves in Figures B-1 through B-39 show minimum SSD plotted vs. observer altitude for retinal burns and flashblindness during daylight (3-mm pupil dia.) and 5-naut.-mile visibility for detonation yields, altitudes, and blink times as indicated.

Retinal Burn SSD



Flashblindness SSD

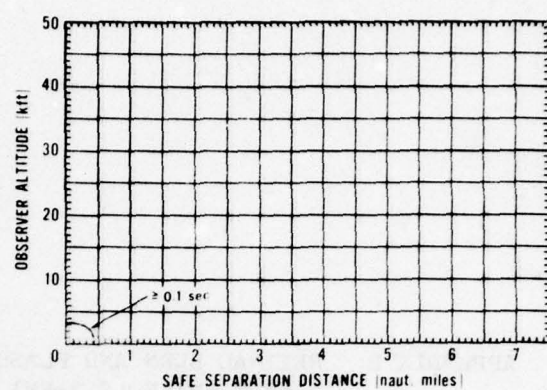


Figure B-1. 0.01 kt detonated at 1 kft (0.3 km).

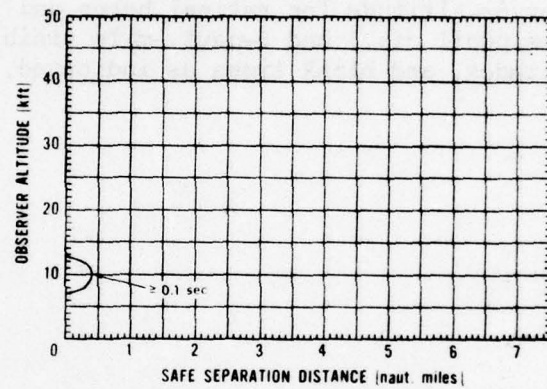
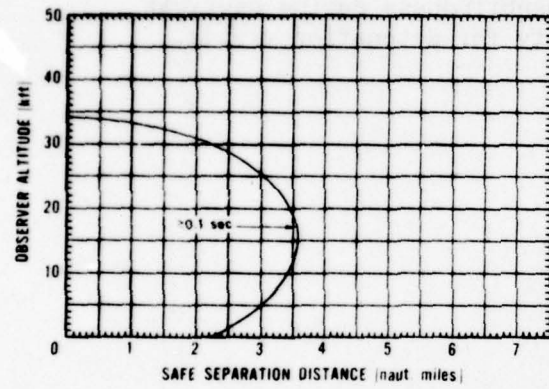


Figure B-2. 0.01 kt detonated at 10 kft (3 km).

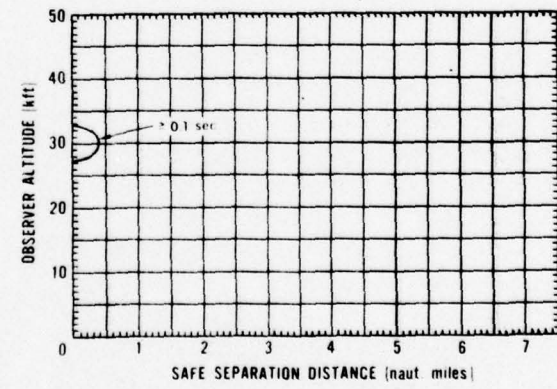
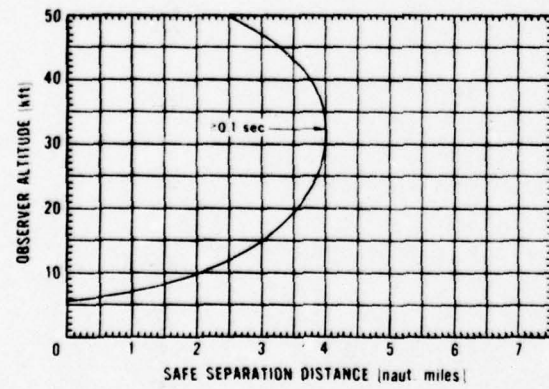
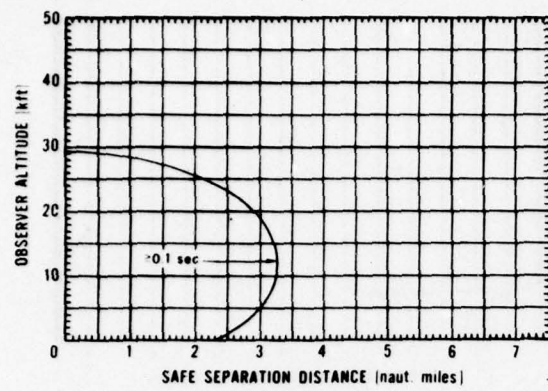


Figure B-3. 0.01 kt detonated at 30 kft (9.1 km).

Retinal Burn SSD



Flashblindness SSD

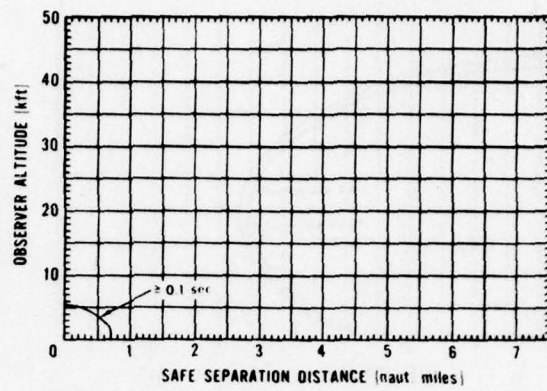


Figure B-4. 0.03 kt detonated at 1 kft (0.3 km).

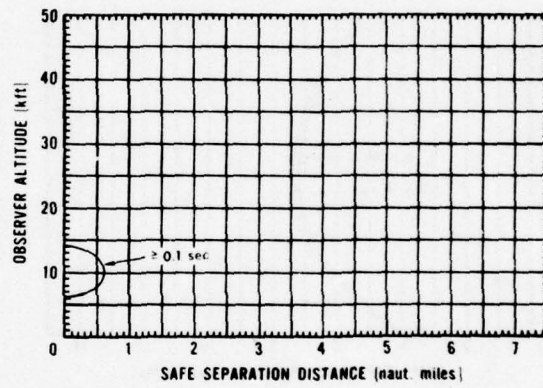
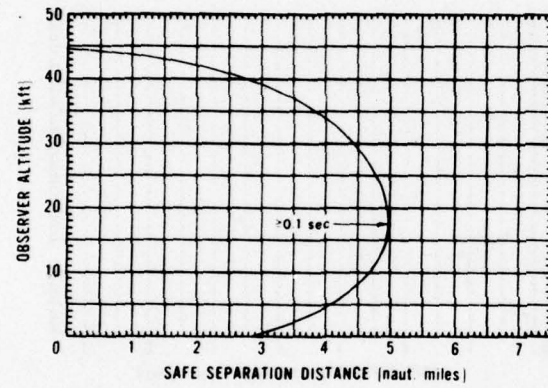


Figure B-5. 0.03 kt detonated at 10 kft (3 km).

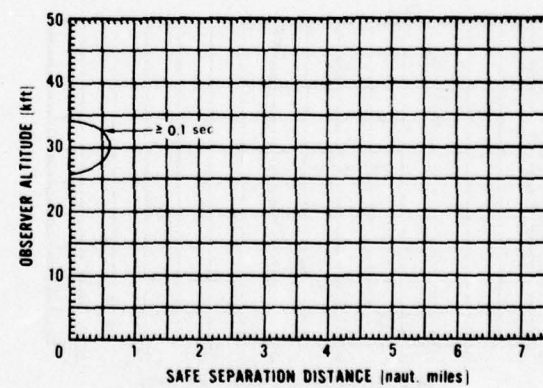
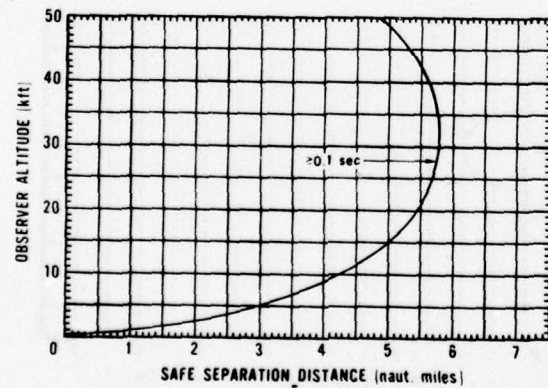
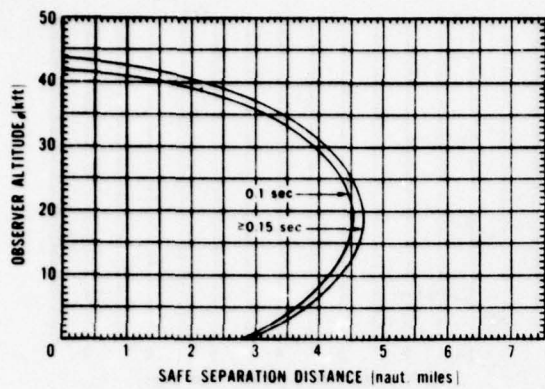


Figure B-6. 0.03 kt detonated at 30 kft (9.1 km).

Retinal Burn SSD



Flashblindness SSD

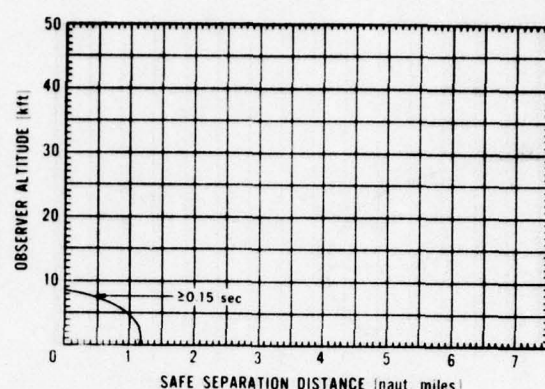


Figure B-7. 0.1 kt detonated at 1 kft (0.3 km).

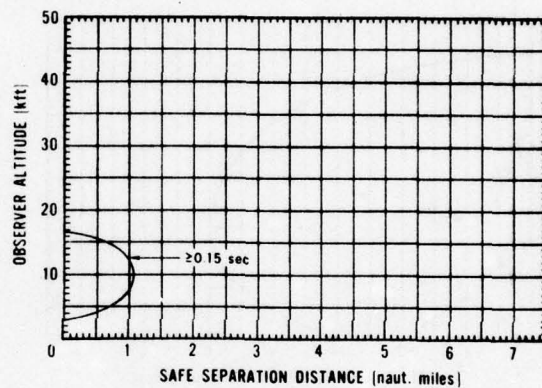
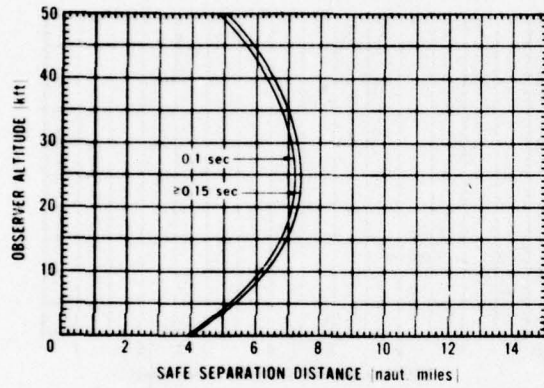


Figure B-8. 0.1 kt detonated at 10 kft (3 km).

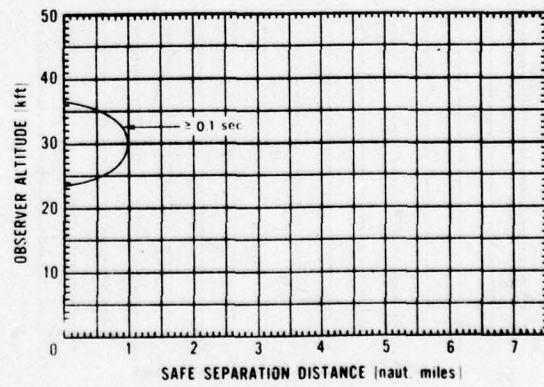
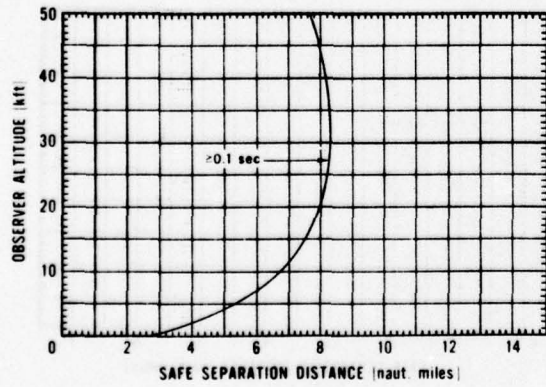
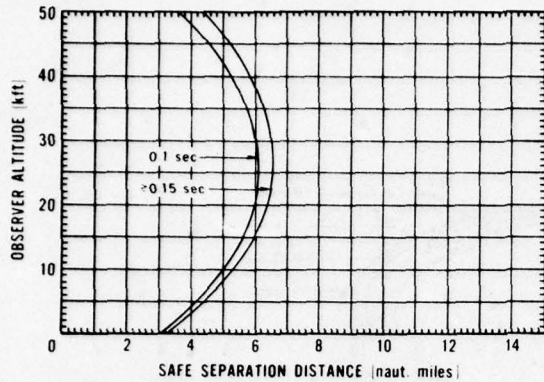


Figure B-9. 0.1 kt detonated at 30 kft (9.1 km).

Retinal Burn SSD



Flashblindness SSD

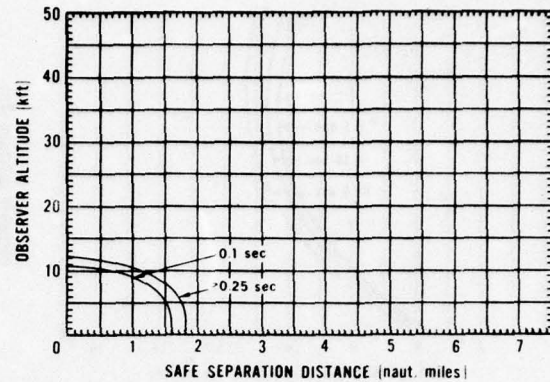


Figure B-10. 0.3 kt detonated at 1 kft (0.3 km).

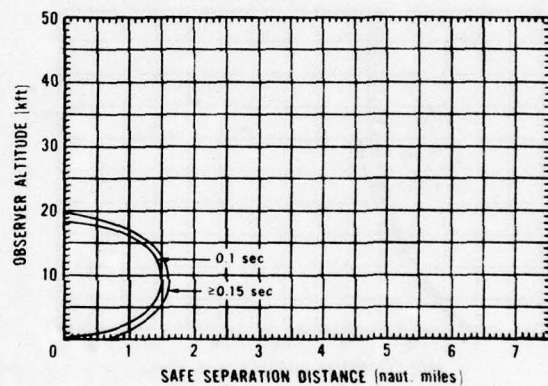
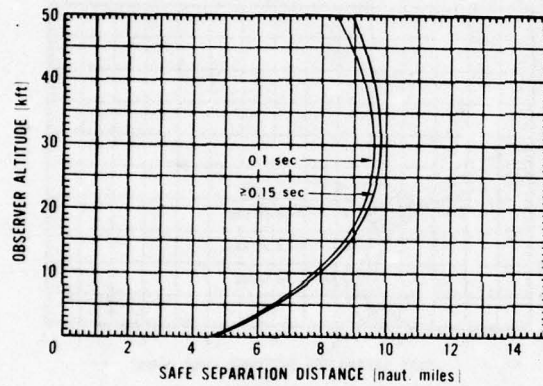


Figure B-11. 0.3 kt detonated at 10 kft (3 km).

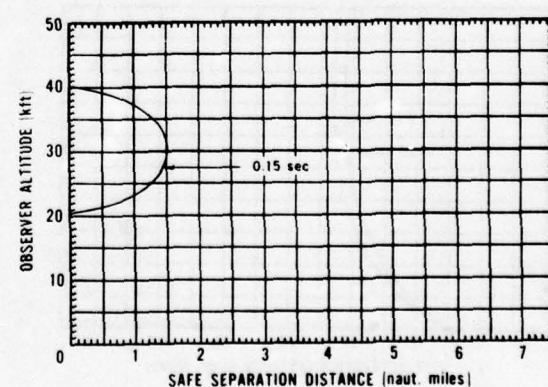
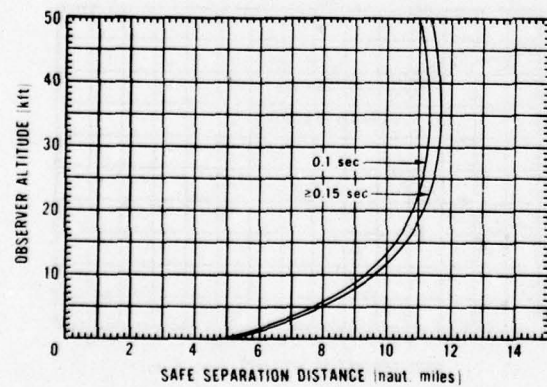
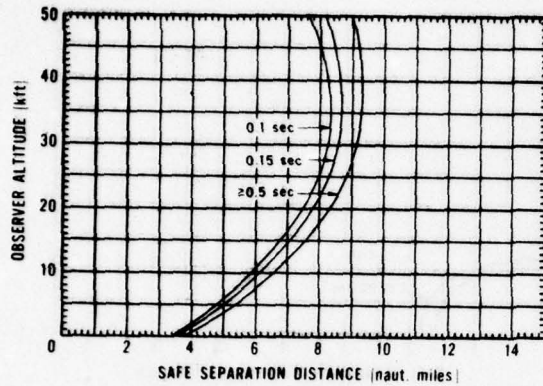


Figure B-12. 0.3 kt detonated at 30 kft (9.1 km).

Retinal Burn SSD



Flashblindness SSD

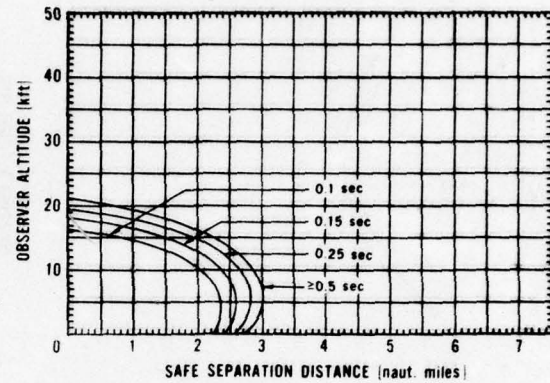


Figure B-13. 1 kt detonated at 1 kft (0.3 km).

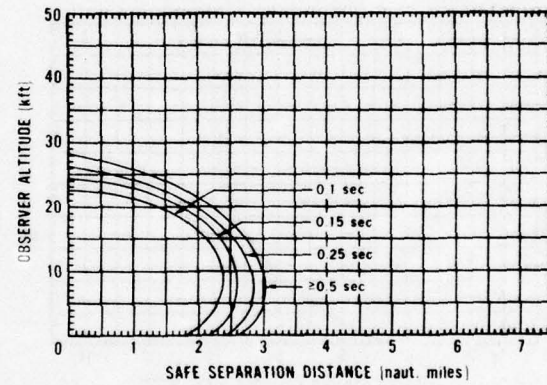
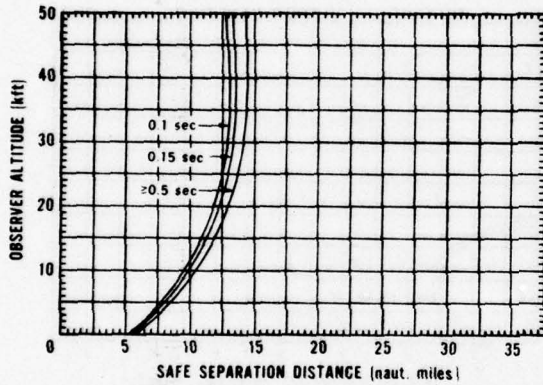


Figure B-14. 1 kt detonated at 10 kft (3 km).

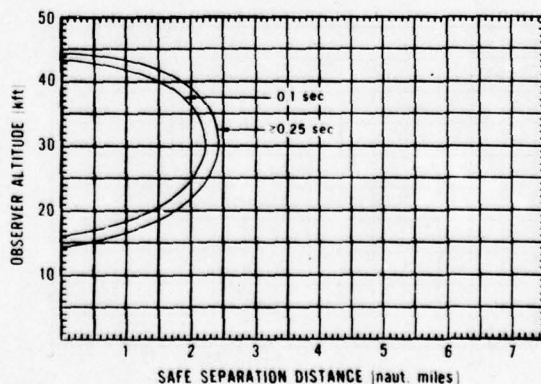
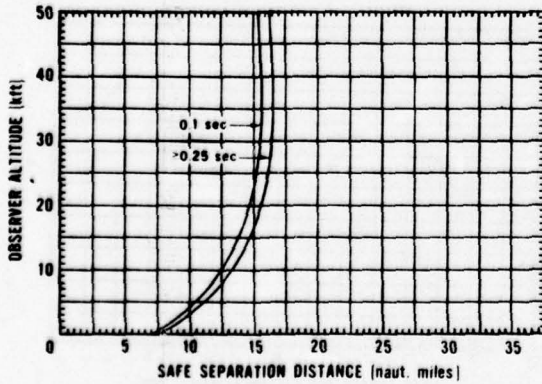
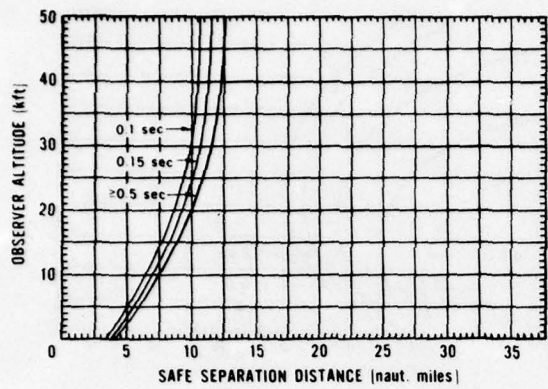


Figure B-15. 1 kt detonated at 30 kft (9.1 km).

Retinal Burn SSD



Flashblindness SSD

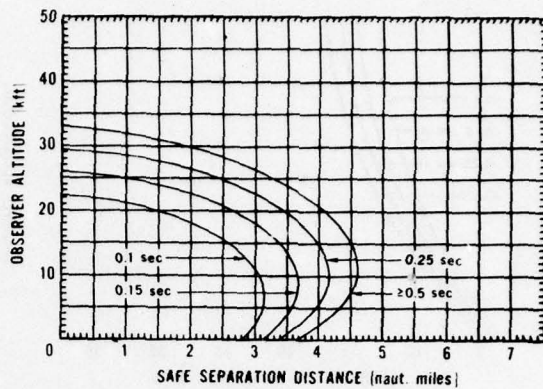


Figure B-16. 3 kt detonated at 1 kft (0.3 km).

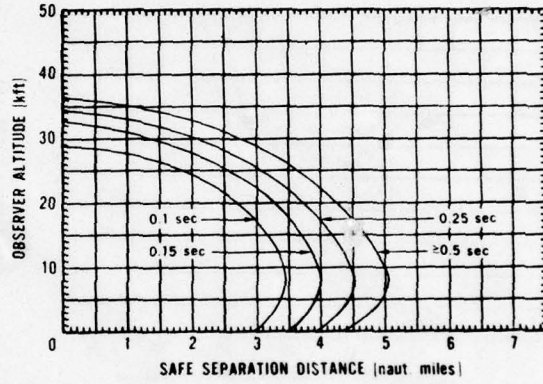
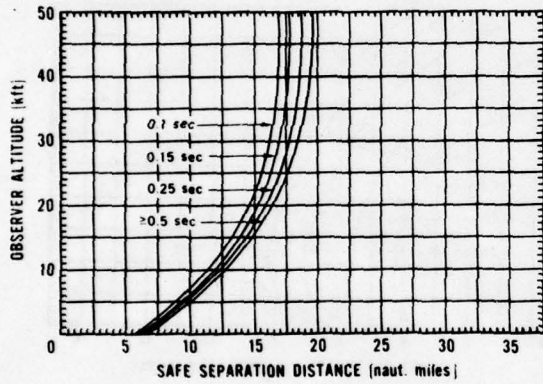


Figure B-17. 3 kt detonated at 10 kft (3 km).

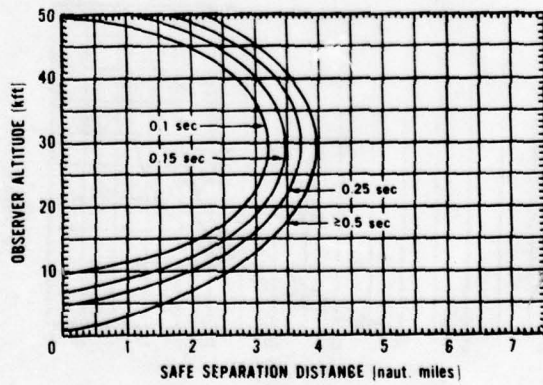
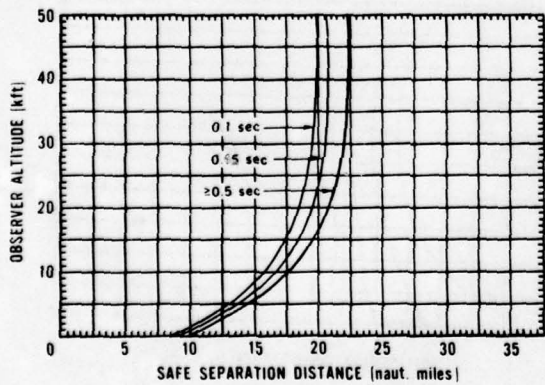
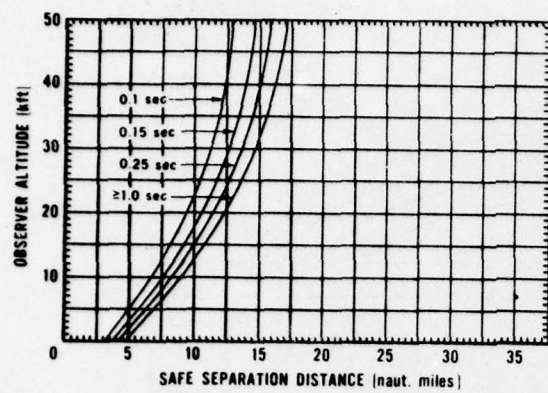


Figure B-18. 3 kt detonated at 30 kft (9.1 km).

Retinal Burn SSD



Flashblindness SSD

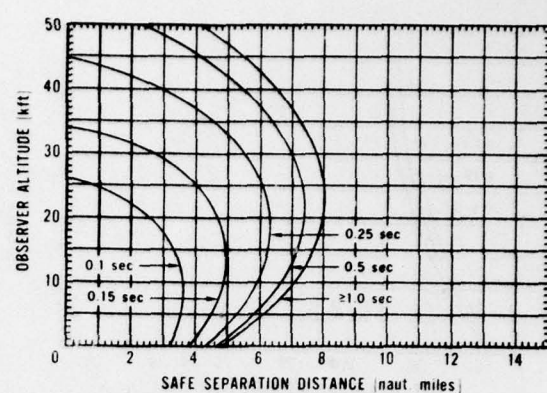


Figure B-19. 10 kt detonated at 1 kft (0.3 km).

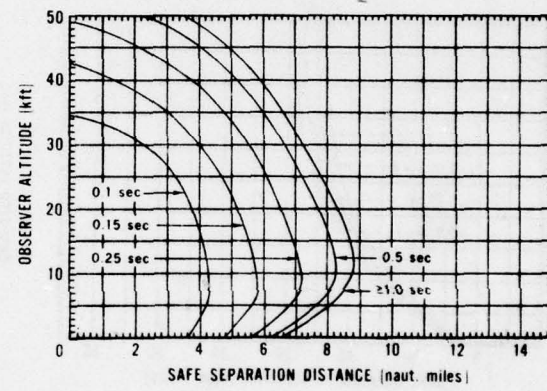
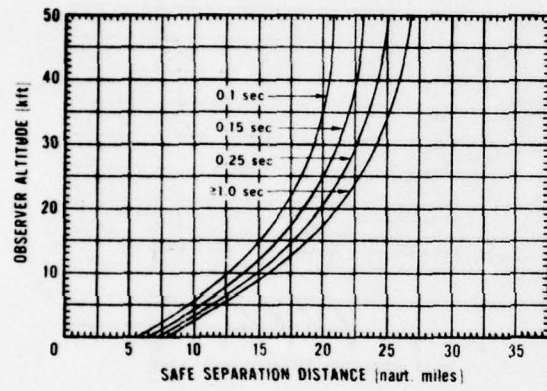


Figure B-20. 10 kt detonated at 10 kft (3 km).

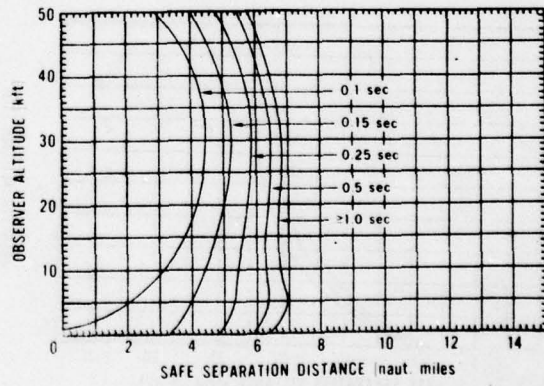
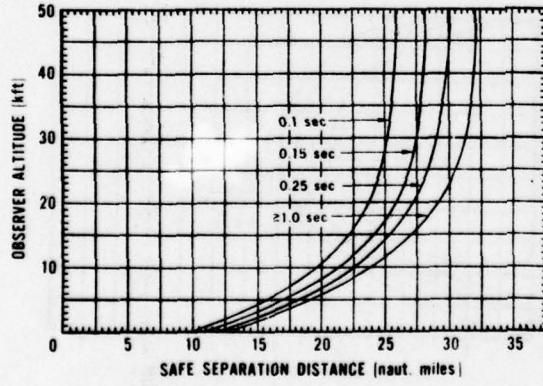
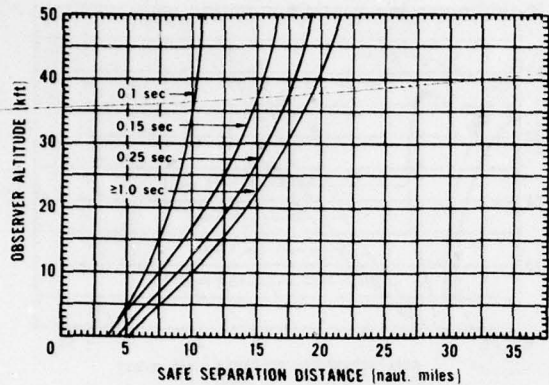


Figure B-21. 10 kt detonated at 30 kft (9.1 km).

Retinal Burn SSD



Flashblindness SSD

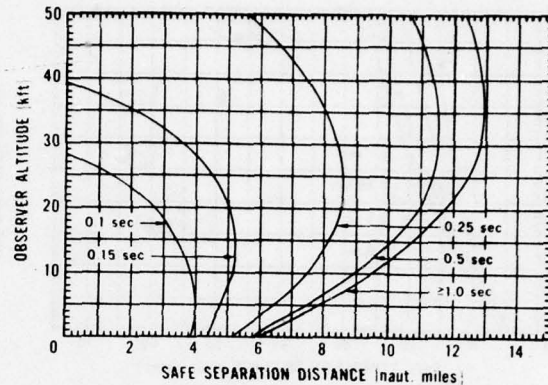


Figure B-22. 30 kt detonated at 1 kft (0.3 km).

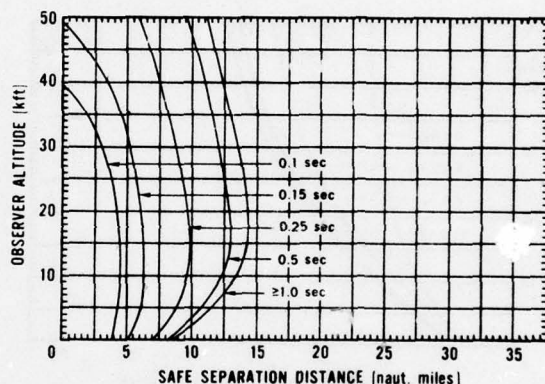
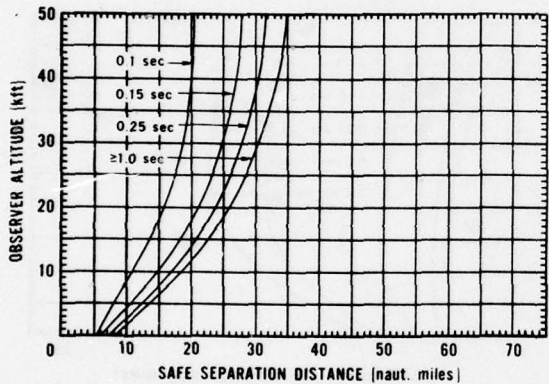


Figure B-23. 30 kt detonated at 10 kft (3 km).

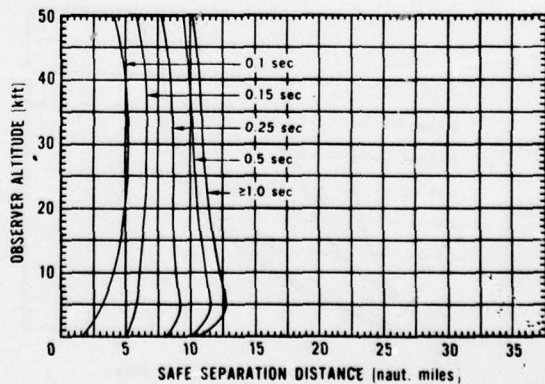
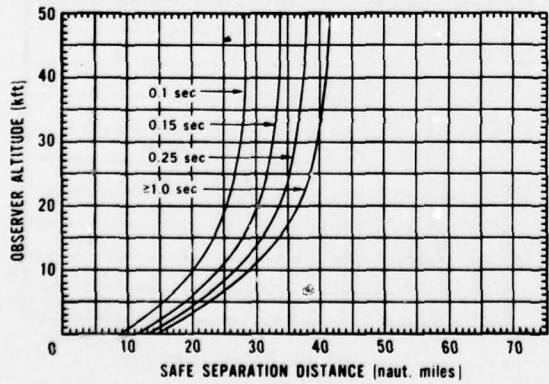
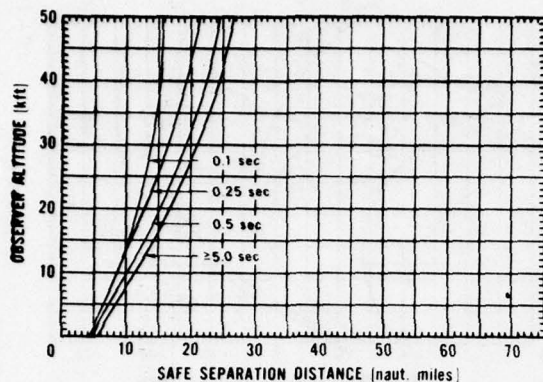


Figure B-24. 30 kt detonated at 30 kft (9.1 km).

Retinal Burn SSD



Flashblindness SSD

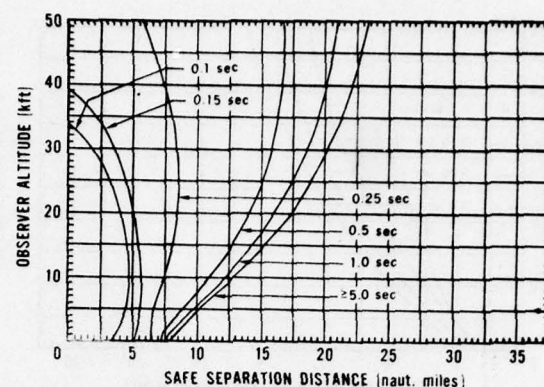


Figure B-25. 100 kt detonated at 1 kft (0.3 km).

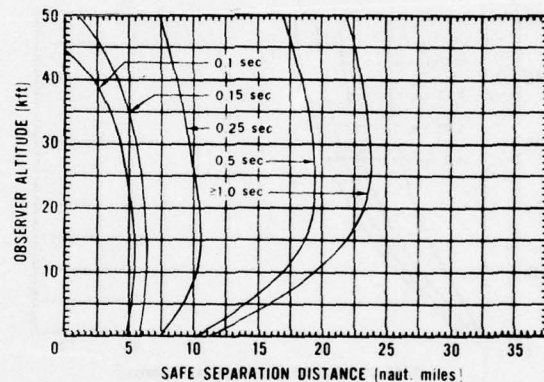
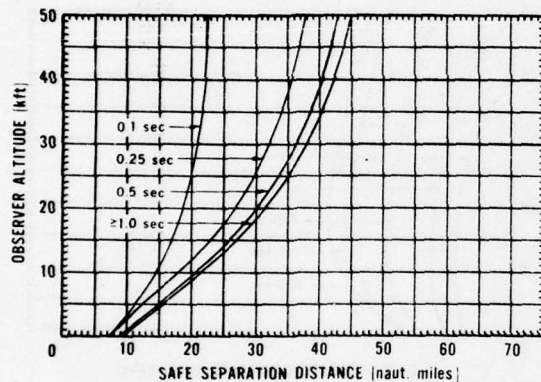


Figure B-26. 100 kt detonated at 10 kft (3 km).

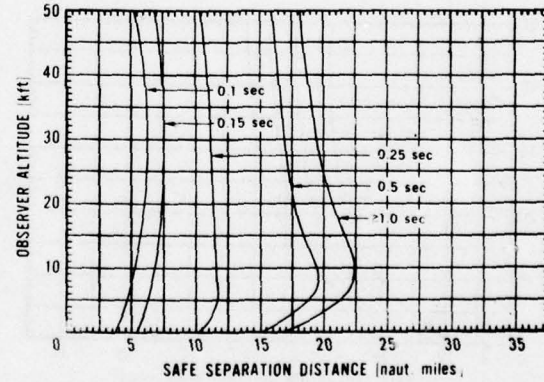
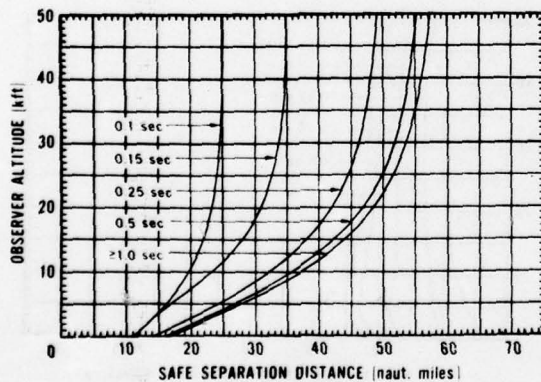
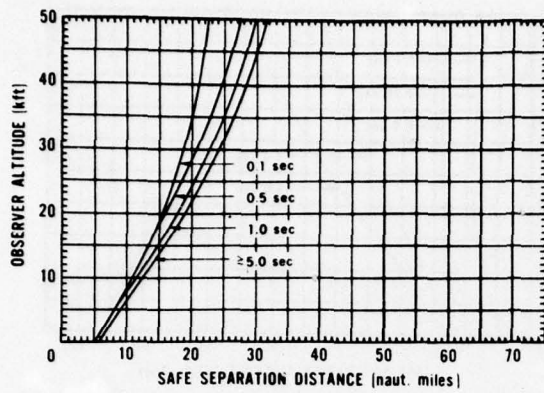


Figure B-27. 100 kt detonated at 30 kft (9.1 km).

Retinal Burn SSD



Flashblindness SSD

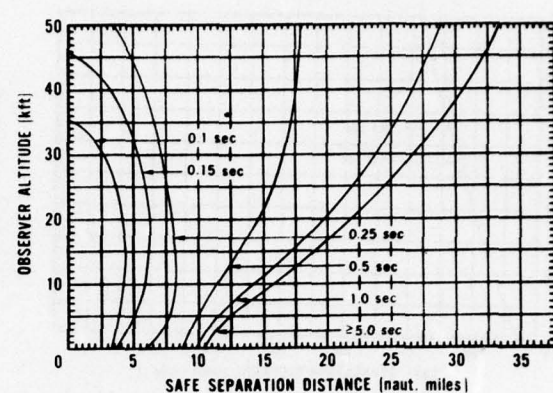


Figure B-28. 300 kt detonated at 1 kft (0.3 km).

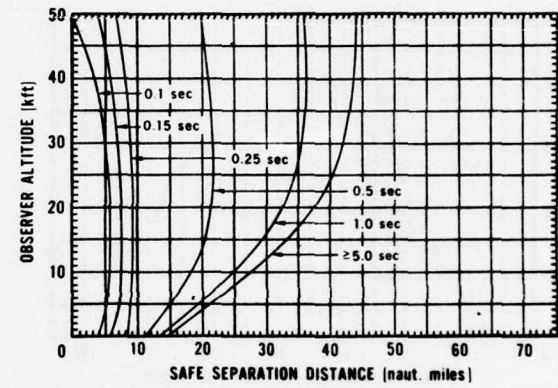
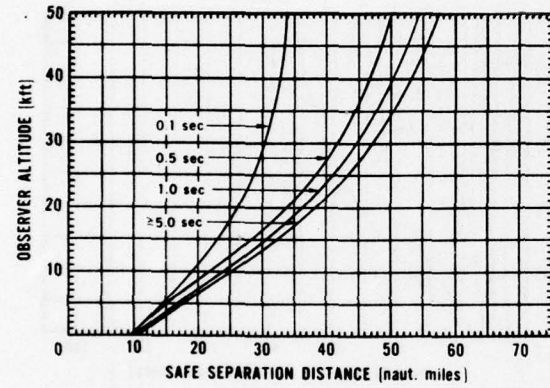


Figure B-29. 300 kt detonated at 10 kft (3 km).

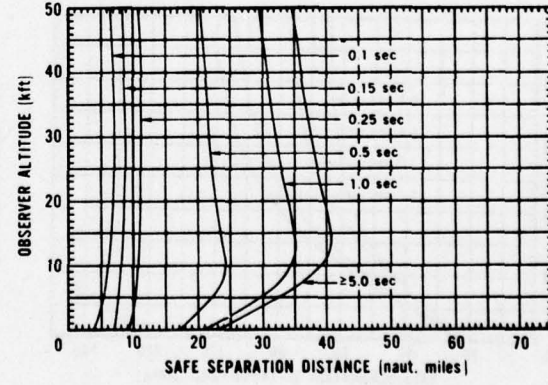
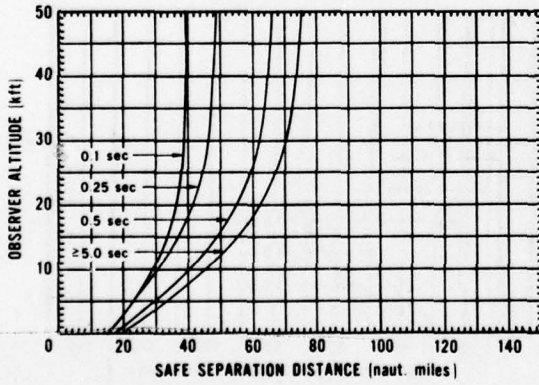
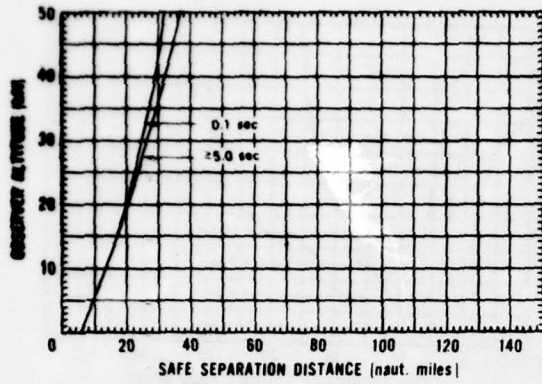


Figure B-30. 300 kt detonated at 30 kft (9.1 km).

Retinal Burn SSD



Flashblindness SSD

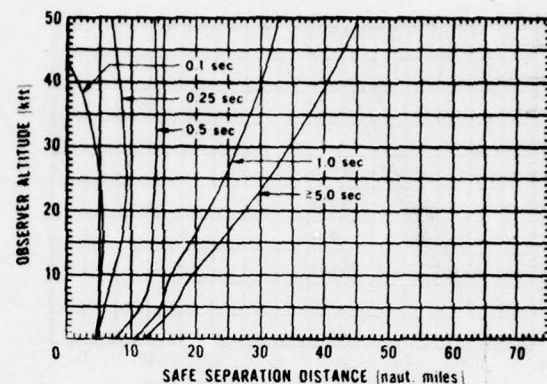


Figure B-31. 1,000 kt detonated at 1 kft (0.3 km).

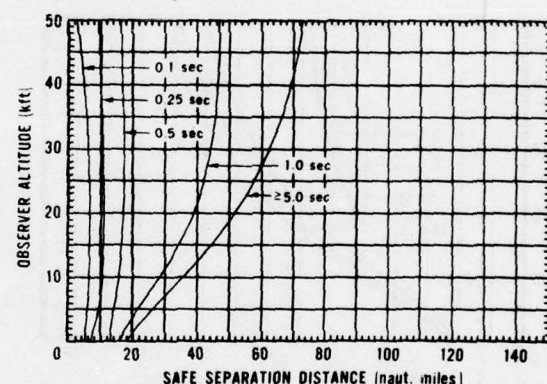
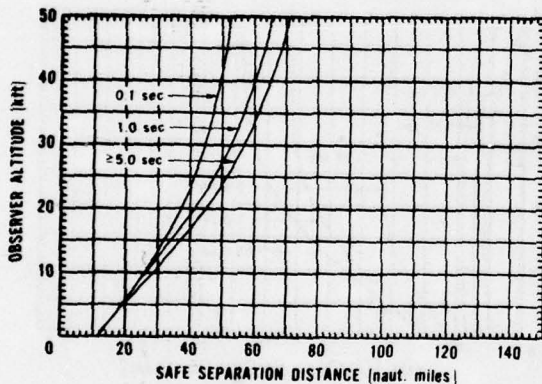


Figure B-32. 1,000 kt detonated at 10 kft (3 km).

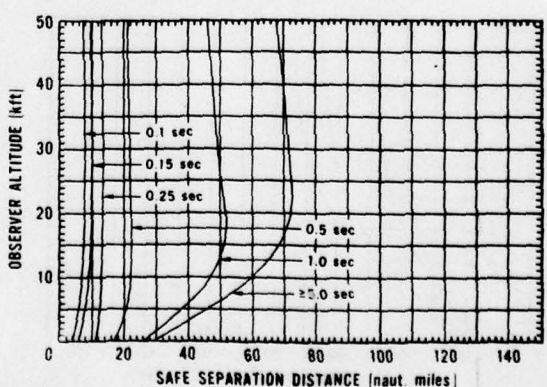
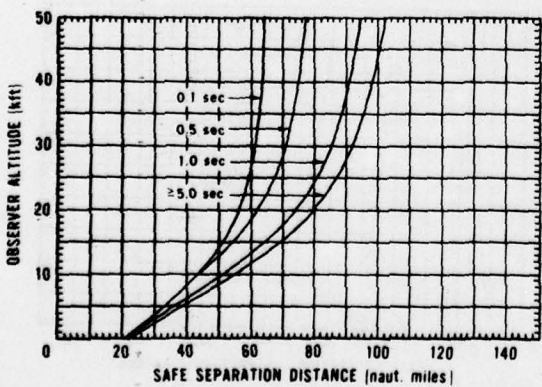
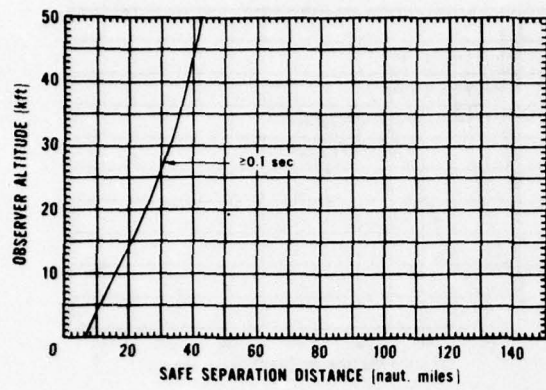


Figure B-33. 1,000 kt detonated at 30 kft (9.1 km).

Retinal Burn SSD



Flashblindness SSD

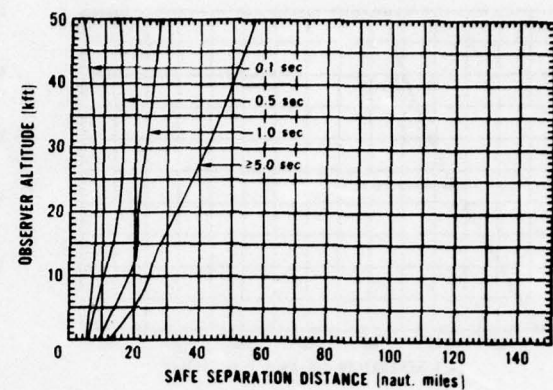


Figure B-34. 3,000 kt detonated at 1 kft (0.3 km).

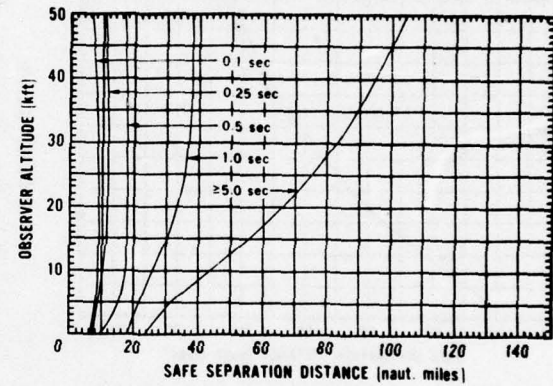
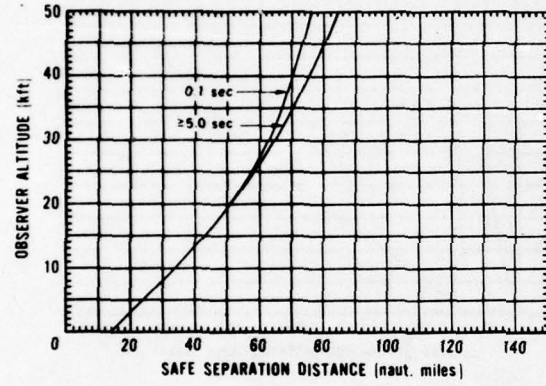


Figure B-35. 3,000 kt detonated at 10 kft (3 km).

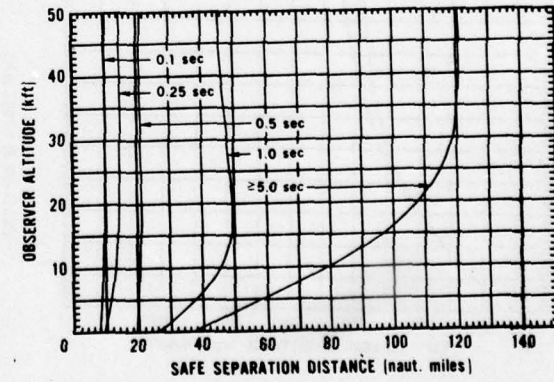
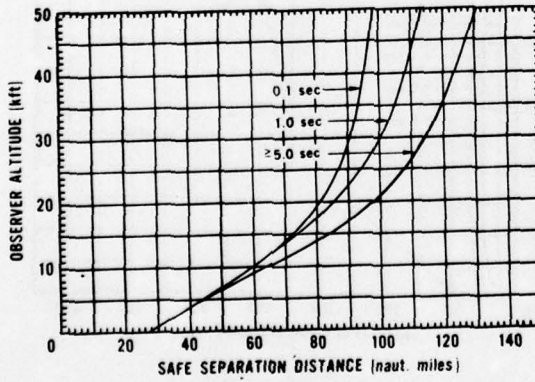
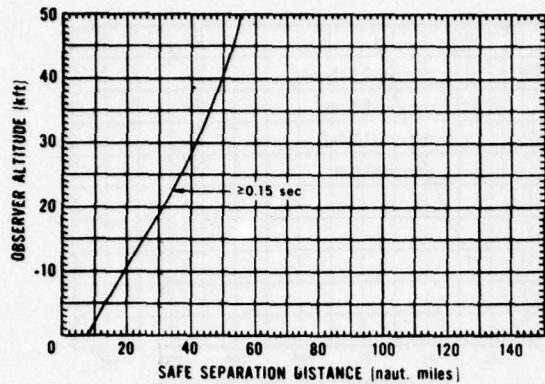


Figure B-36. 3,000 kt detonated at 30 kft (9.1 km).

Retinal Burn SSD



Flashblindness SSD

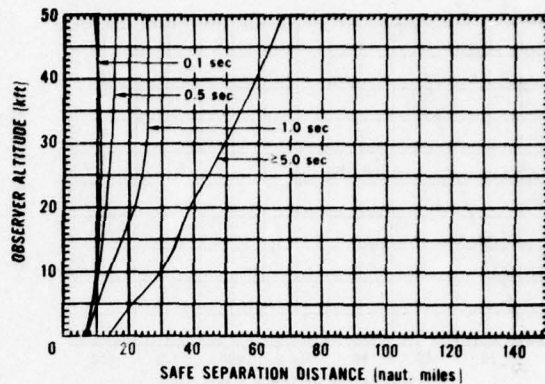


Figure B-37. 10,000 kt detonated at 1 kft (0.3 km).

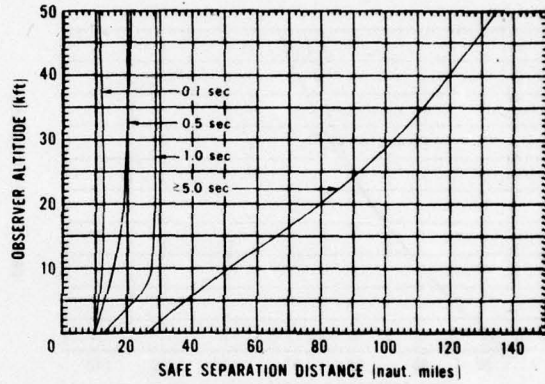
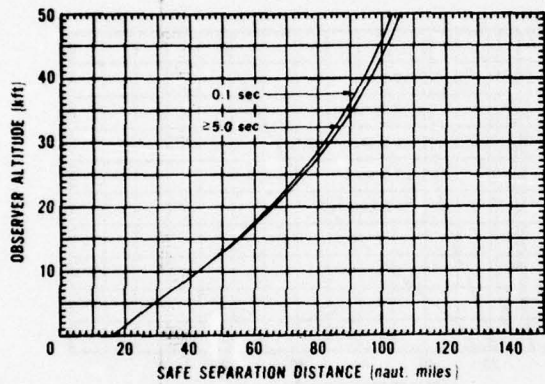


Figure B-38. 10,000 kt detonated at 10 kft (3 km).

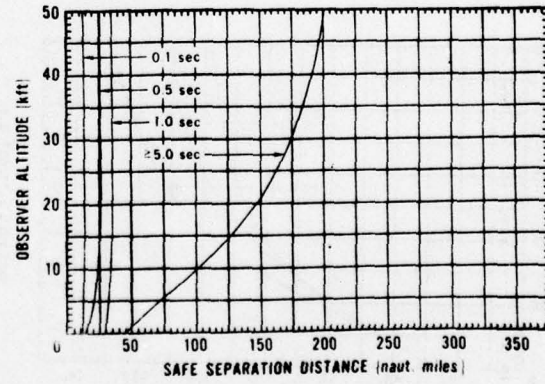
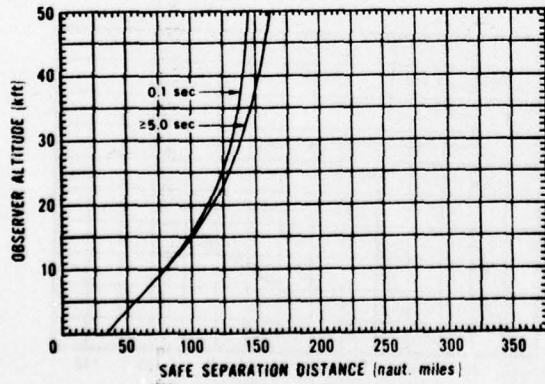
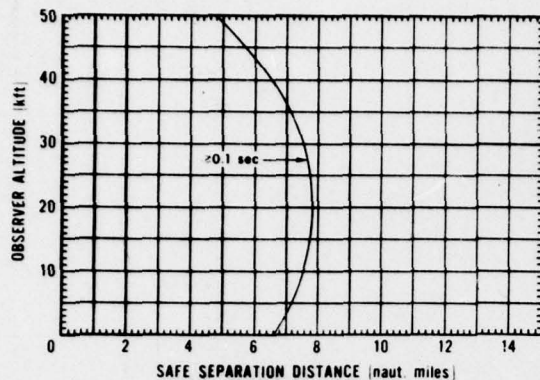


Figure B-39. 10,000 kt detonated at 30 kft (9.1 km).

APPENDIX C: RETINAL BURN AND FLASHBLINDNESS SSD FOR NIGHT AND  
25-NAUT.-MILE (46.3-KM) VISIBILITY

Curves in Figures C-1 through C-39 show minimum SSD plotted vs. observer altitude for retinal burns and flashblindness at night (7-mm pupil dia.) and 25-naut.-mile visibility for detonation yields, altitudes, and blink times as indicated.

Retinal Burn SSD



Flashblindness SSD

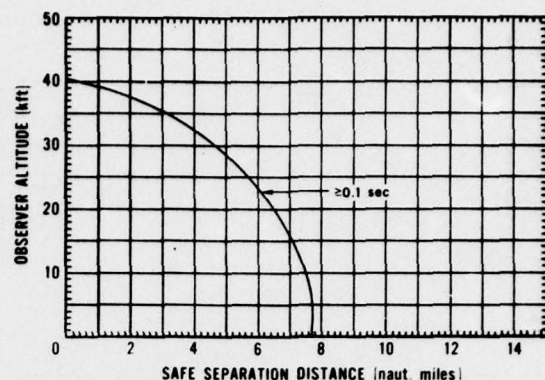


Figure C-1. 0.01 kt detonated at 1 kft (0.3 km).

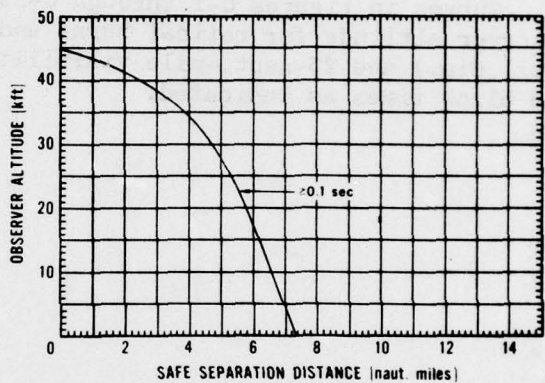
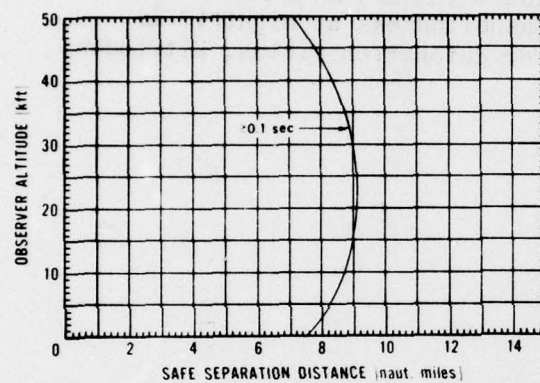


Figure C-2. 0.01 kt detonated at 10 kft (3 km).

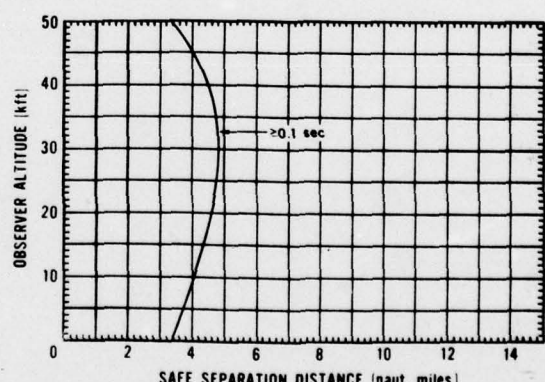
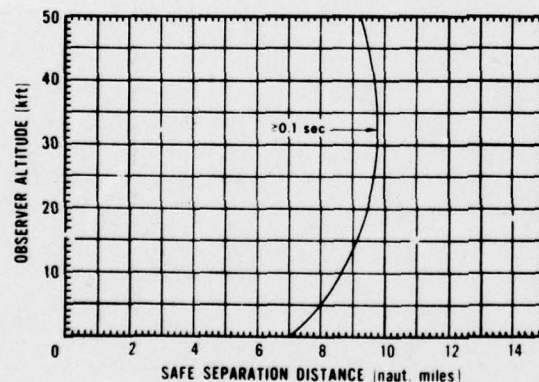
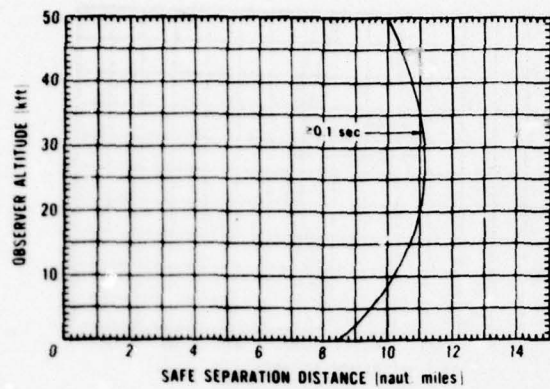


Figure C-3. 0.01 kt detonated at 30 kft (9.1 km).

Retinal Burn SSD



Flashblindness SSD

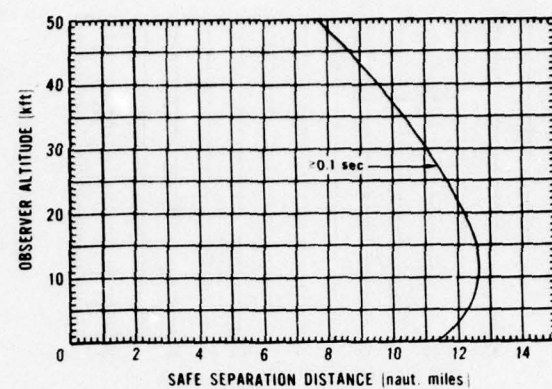


Figure C-4. 0.03 kt detonated at 1 kft (0.3 km).

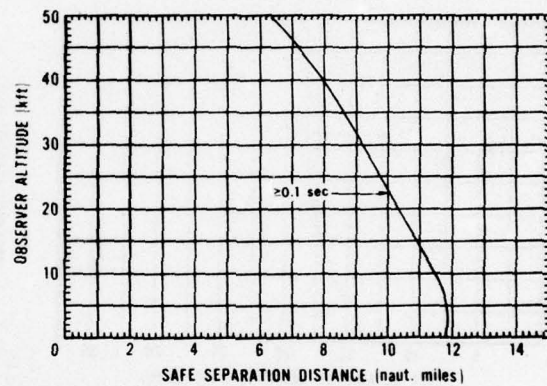
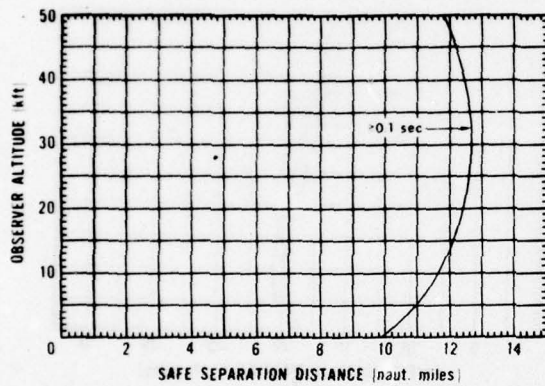


Figure C-5. 0.03 kt detonated at 10 kft (3 km).

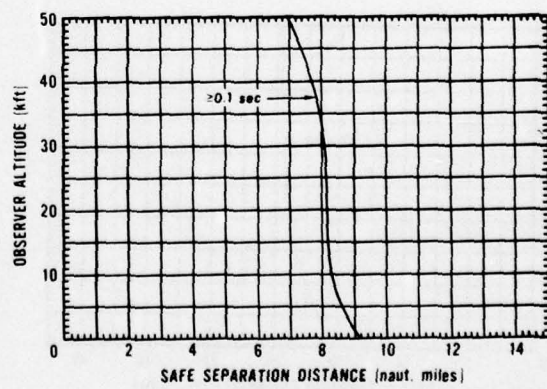
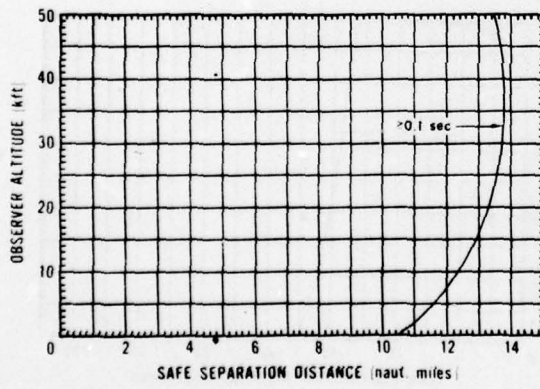
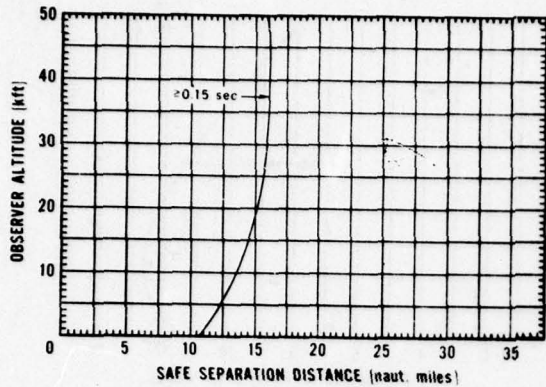


Figure C-6. 0.03 kt detonated at 30 kft (9.1 km).

Retinal Burn SSD



Flashblindness SSD

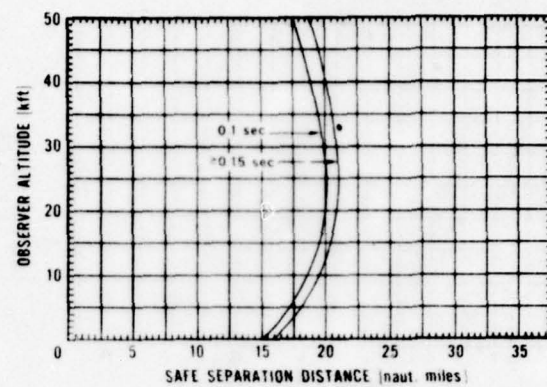


Figure C-7. 0.1 kt detonated at 1 kft (0.3 km).

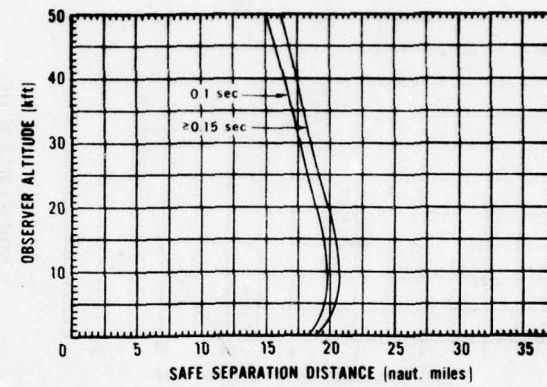
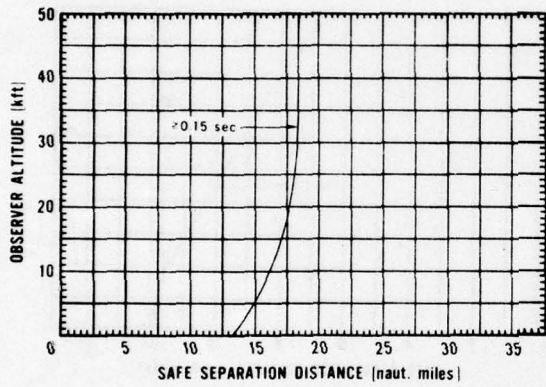


Figure C-8. 0.1 kt detonated at 10 kft (3 km).

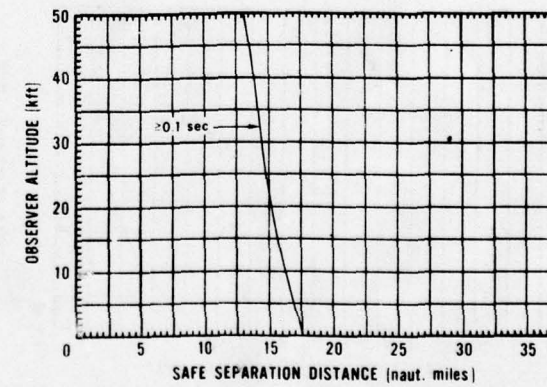
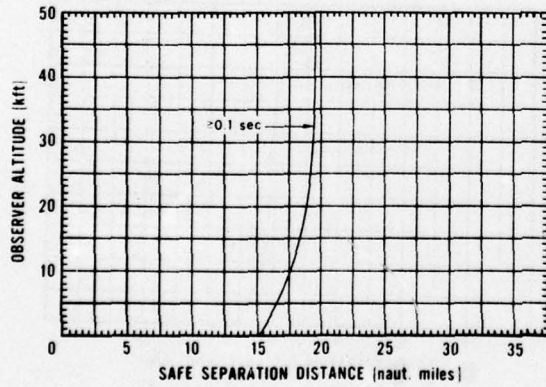
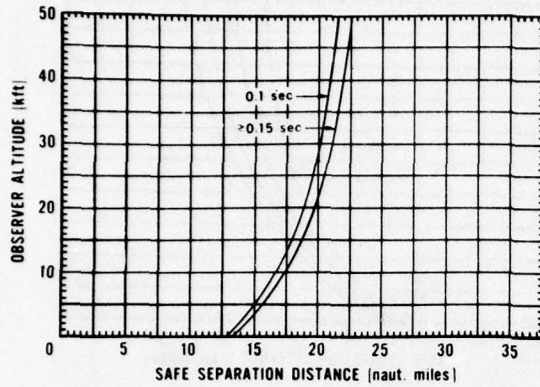


Figure C-9. 0.1 kt detonated at 30 kft (9.1 km).

Retinal Burn SSD



Flashblindness SSD

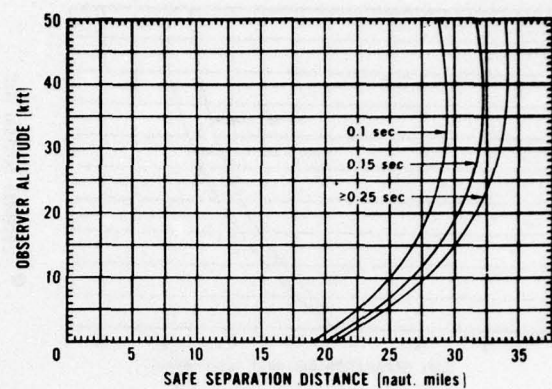


Figure C-10. 0.3 kt detonated at 1 kft (0.3 km).

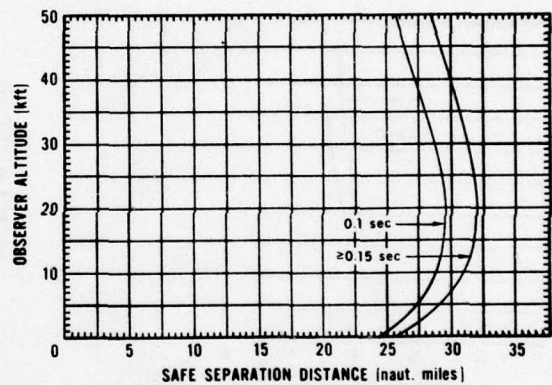
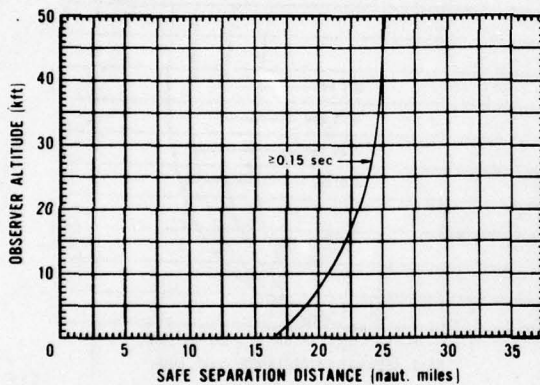


Figure C-11. 0.3 kt detonated at 10 kft (3 km).

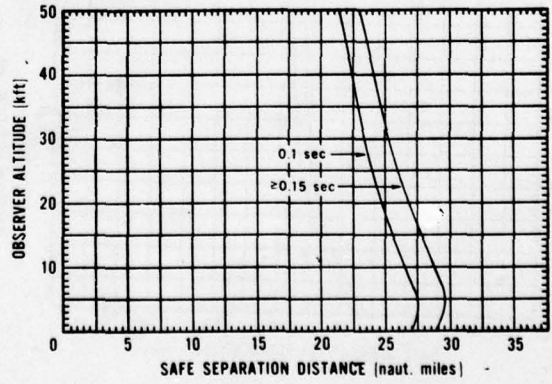
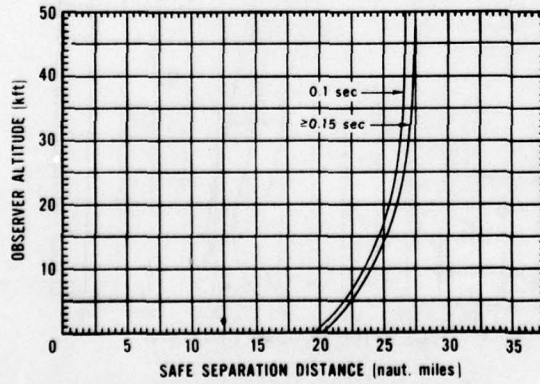
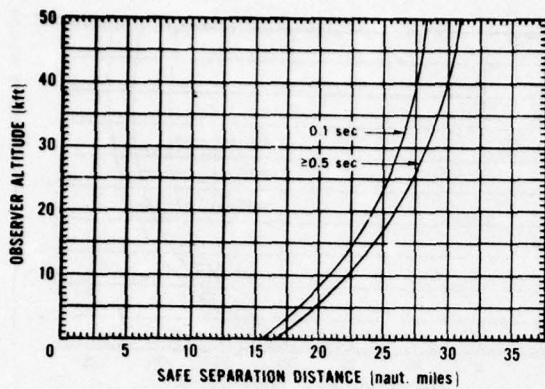


Figure C-12. 0.3 kt detonated at 30 kft (9.1 km).

Retinal Burn SSD



Flashblindness SSD

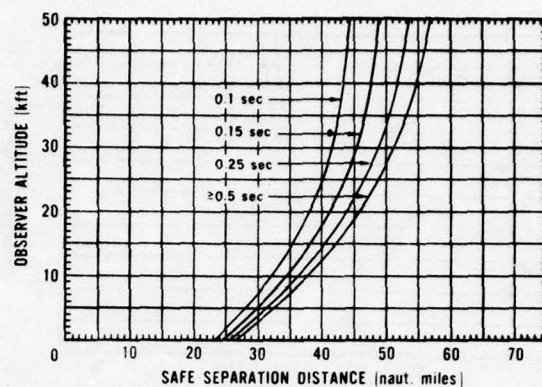


Figure C-13. 1 kt detonated at 1 kft (0.3 km).

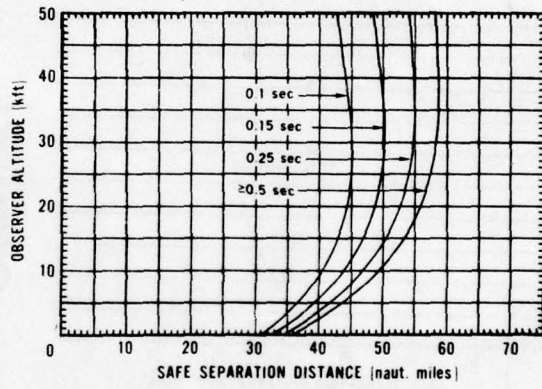
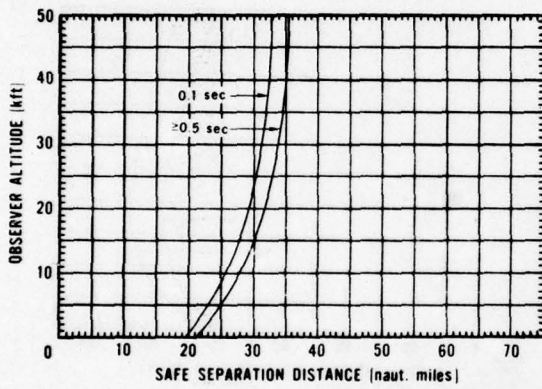


Figure C-14. 1 kt detonated at 10 kft (3 km).

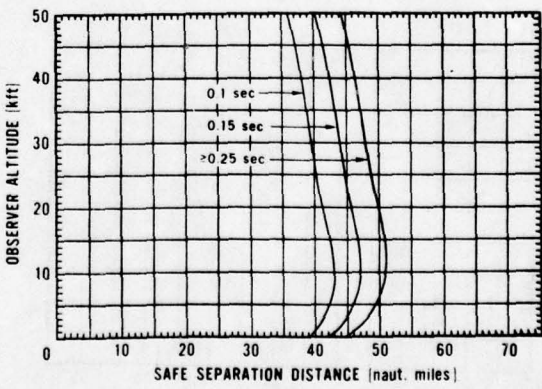
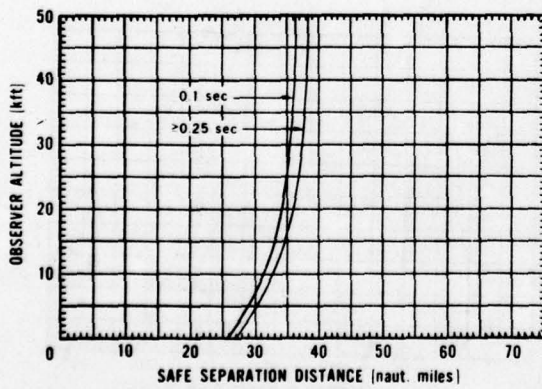
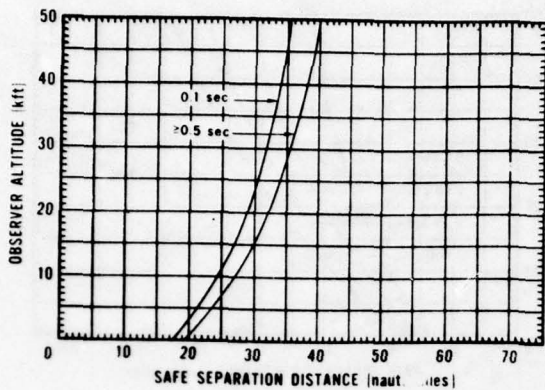


Figure C-15. 1 kt detonated at 30 kft (9.1 km).

Retinal Burn SSD



Flashblindness SSD

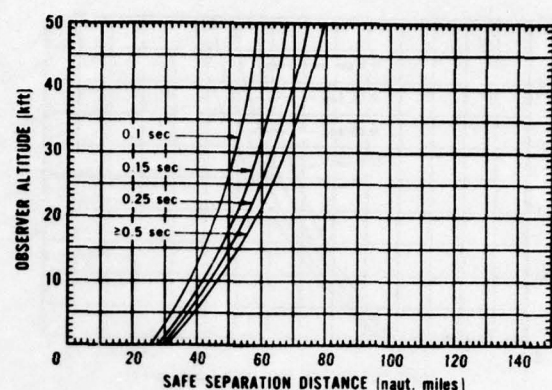


Figure C-16. 3 kt detonated at 1 kft (0.3 km).

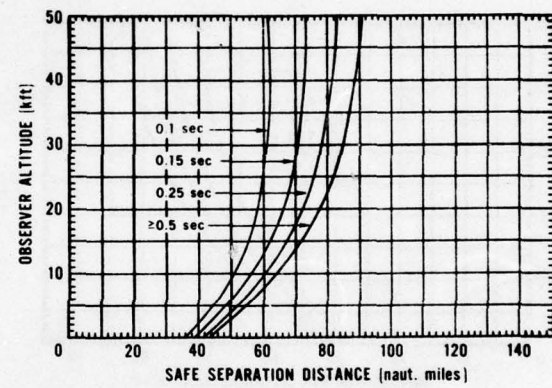
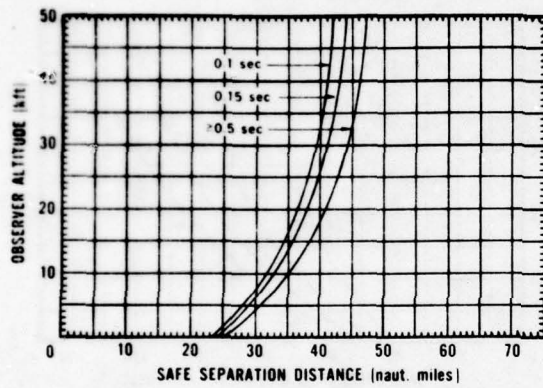


Figure C-17. 3 kt detonated at 10 kft (3 km).

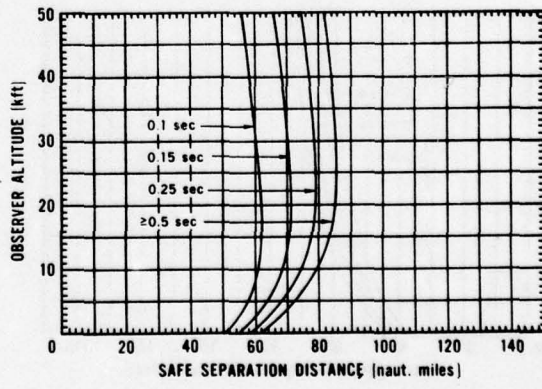
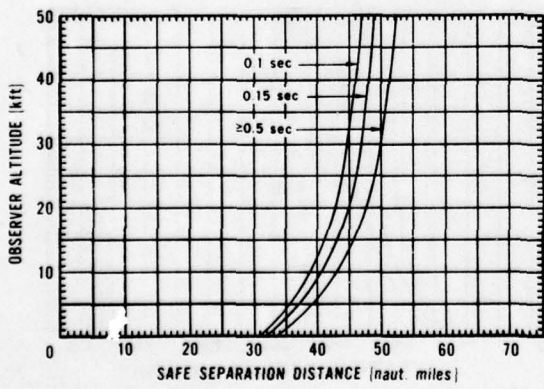
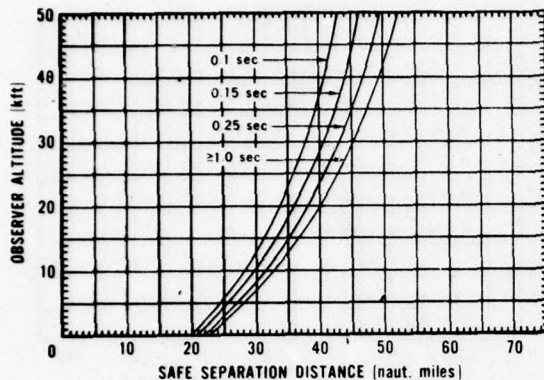


Figure C-18. 3 kt detonated at 30 kft (9.1 km).

Retinal Burn SSD



Flashblindness SSD

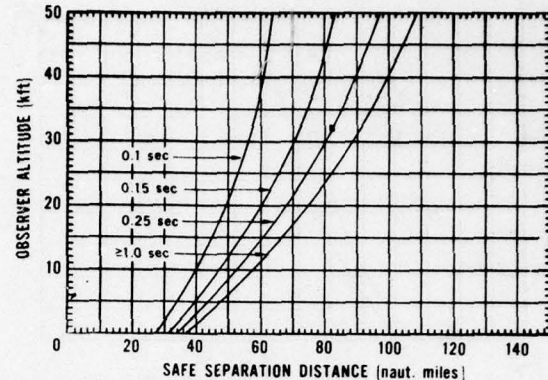


Figure C-19. 10 kt detonated at 1 kft (0.3 km).

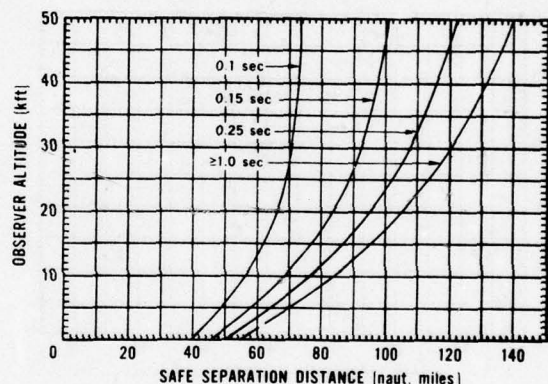
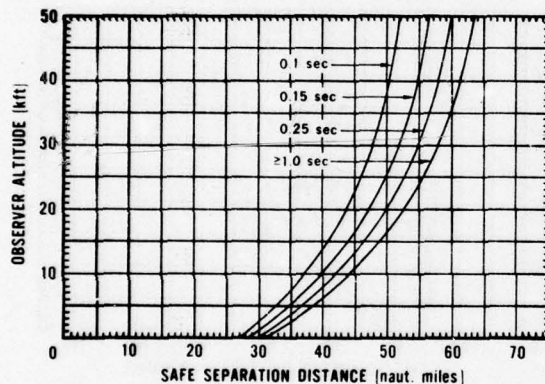


Figure C-20. 10 kt detonated at 10 kft (3 km).

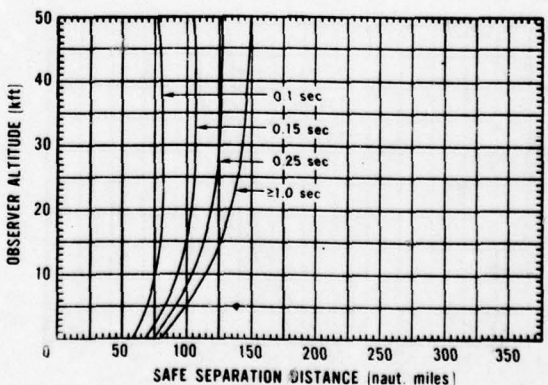
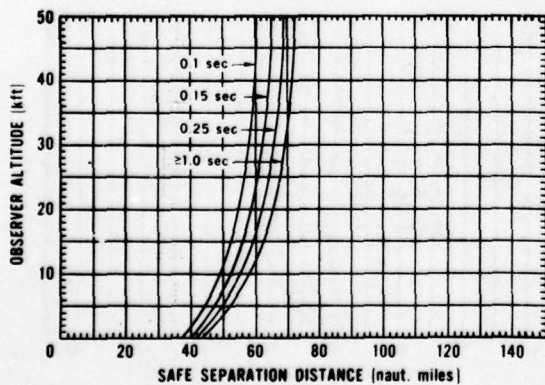


Figure C-21. 10 kt detonated at 30 kft (9.1 km).

Retinal Burn SSD

Flashblindness SSD

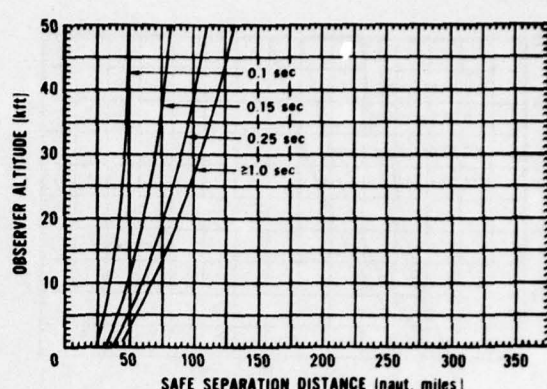
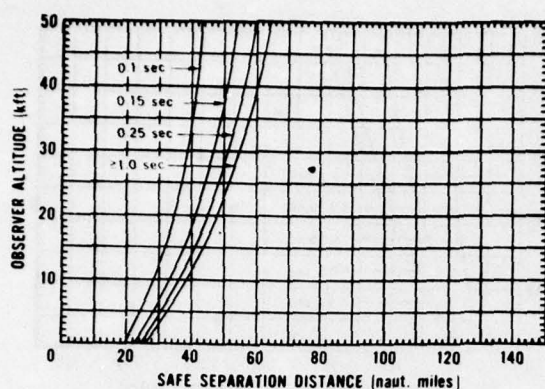


Figure C-22. 30 kt detonated at 1 kft (0.3 km).

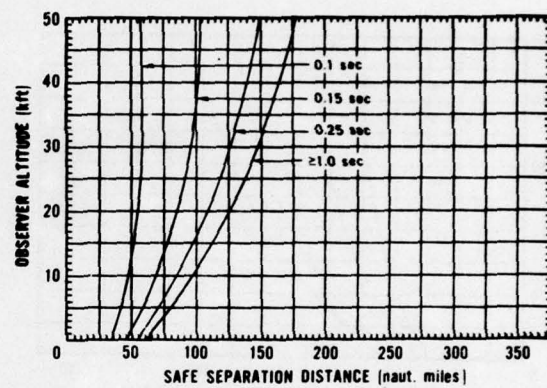
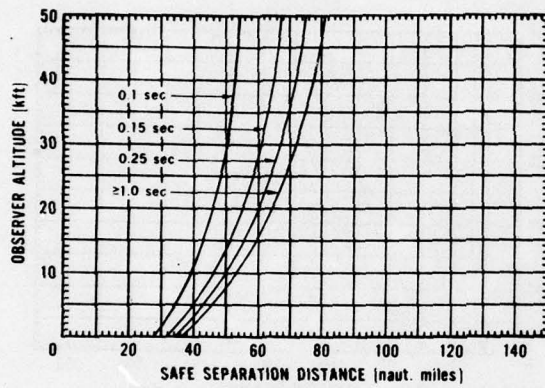


Figure C-23. 30 kt detonated at 10 kft (3 km).

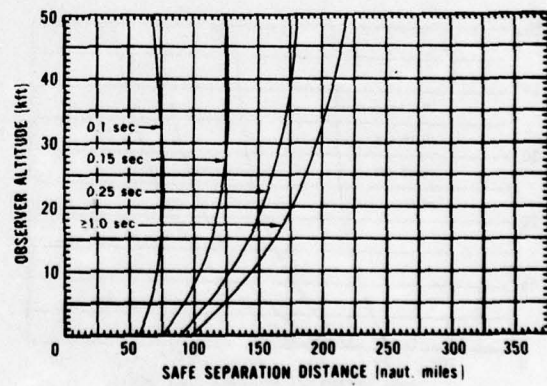
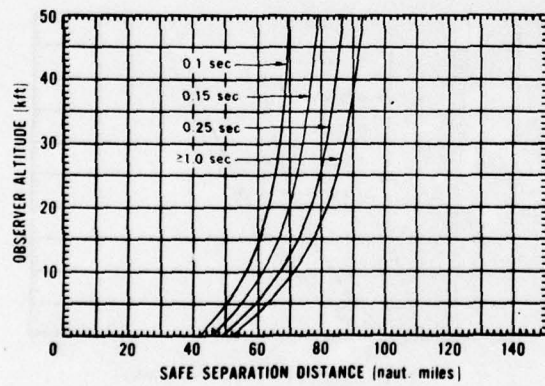
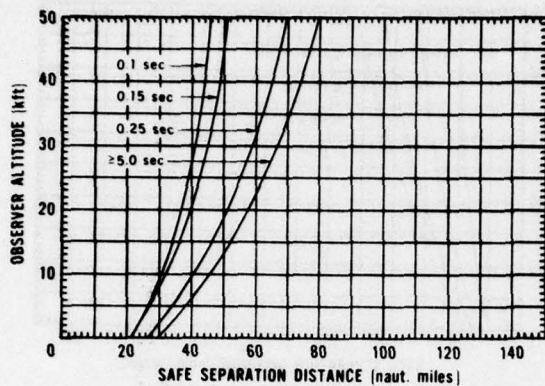


Figure C-24. 30 kt detonated at 30 kft (9.1 km).

Retinal Burn SSD



Flashblindness SSD

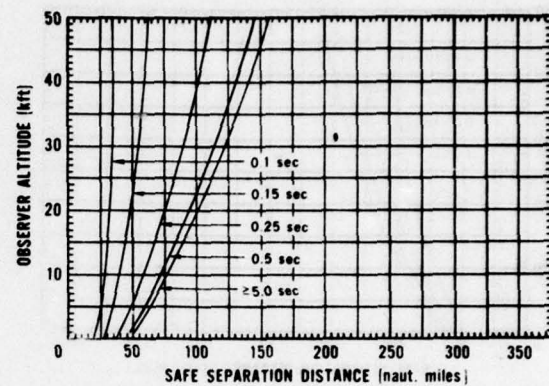


Figure C-25. 100 kt detonated at 1 kft (0.3 km).

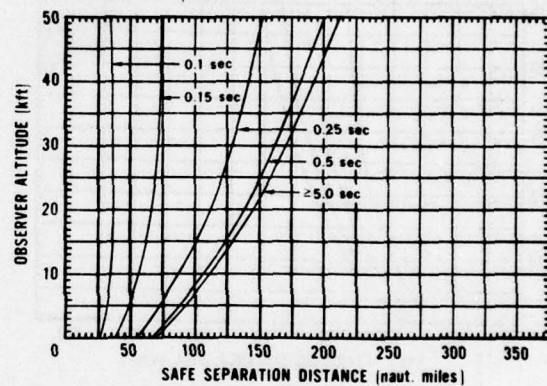
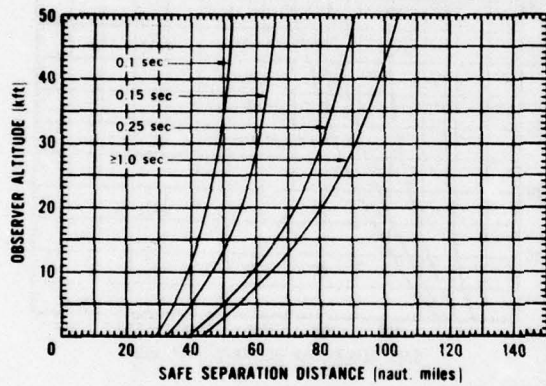


Figure C-26. 100 kt detonated at 10 kft (3 km).

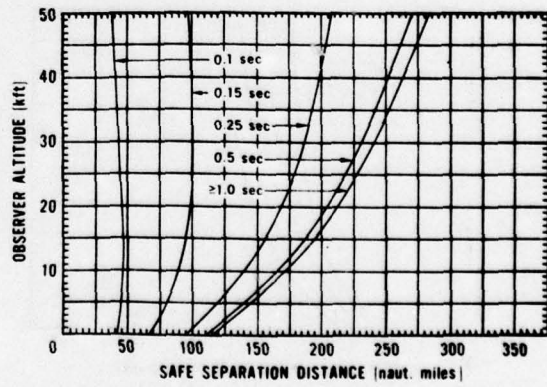
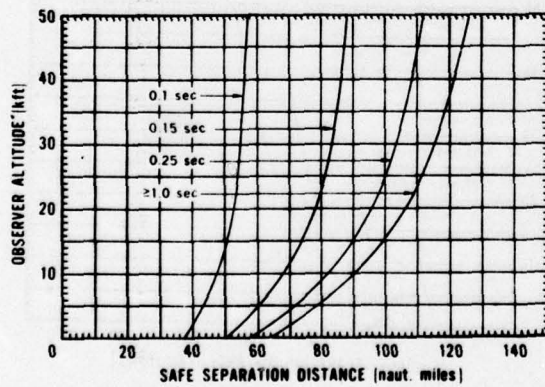
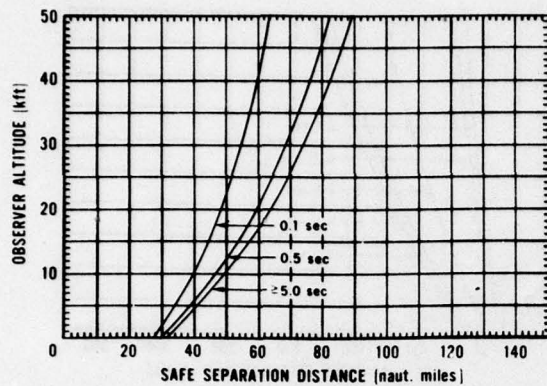


Figure C-27. 100 kt detonated at 30 kft (9.1 km).

Retinal Burn SSD



Flashblindness SSD

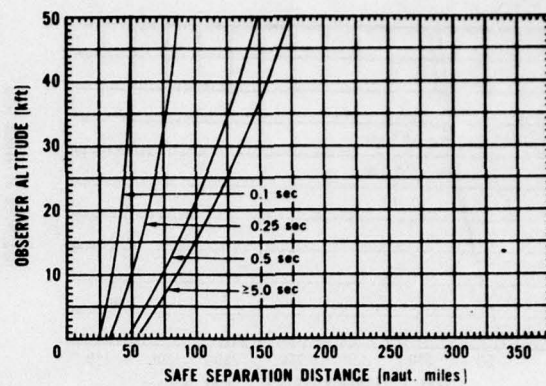


Figure C-28. 300 kt detonated at 1 kft (0.3 km).

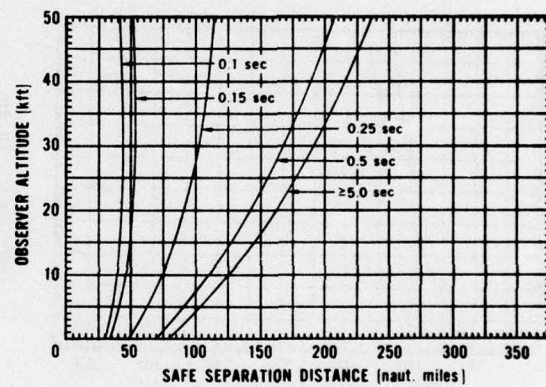
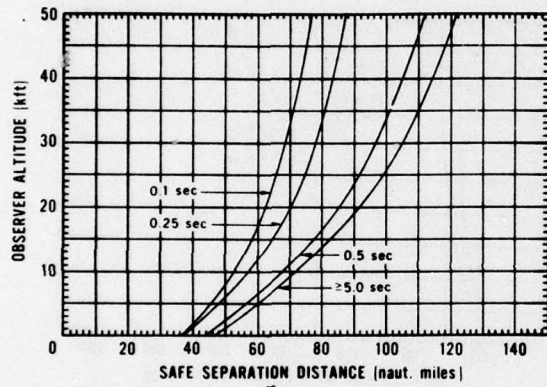


Figure C-29. 300 kt detonated at 10 kft (3 km).

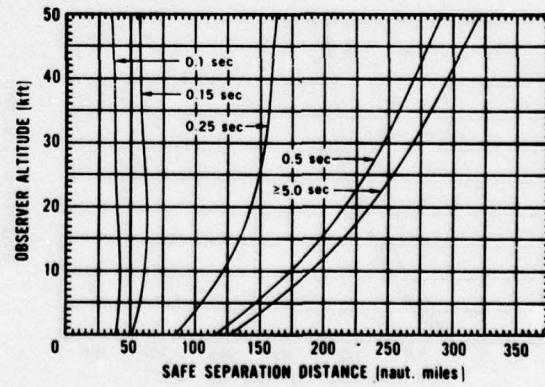
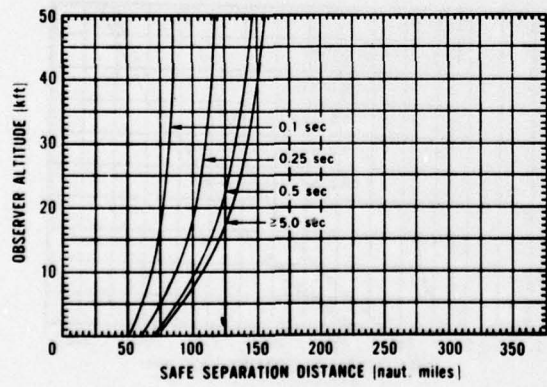
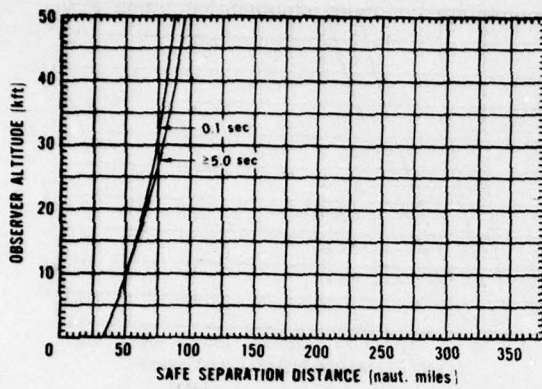


Figure C-30. 300 kt detonated at 30 kft (9.1 km).

Retinal Burn SSD



Flashblindness SSD

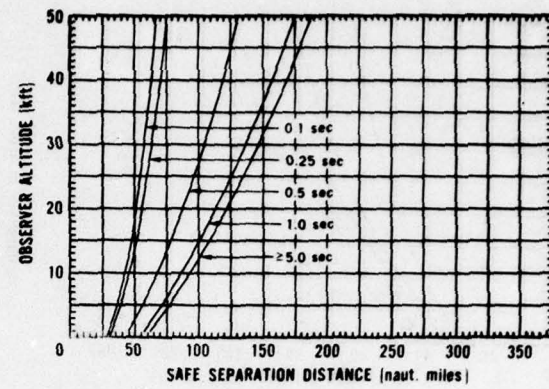


Figure C-31. 1,000 kt detonated at 1 kft (0.3 km).

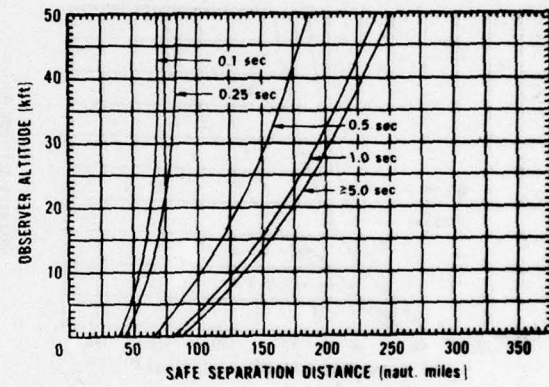
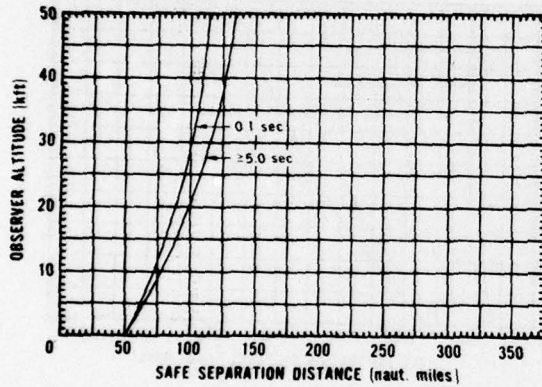


Figure C-32. 1,000 kt detonated at 10 kft (3 km).

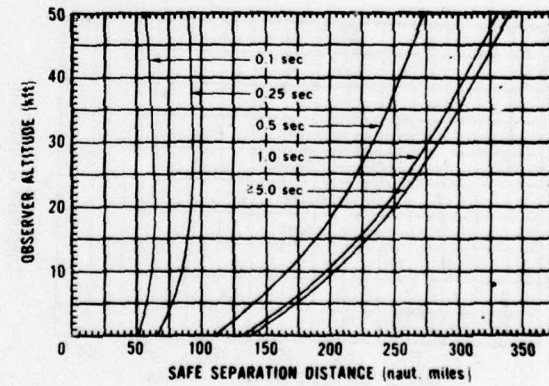
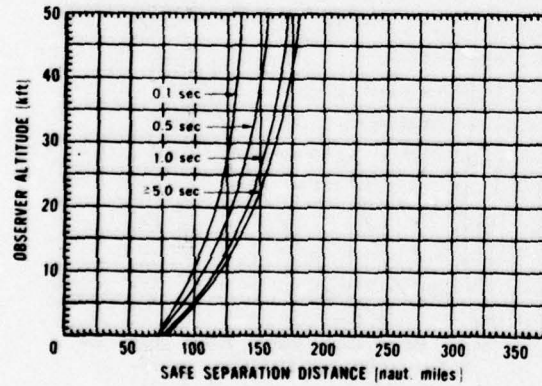
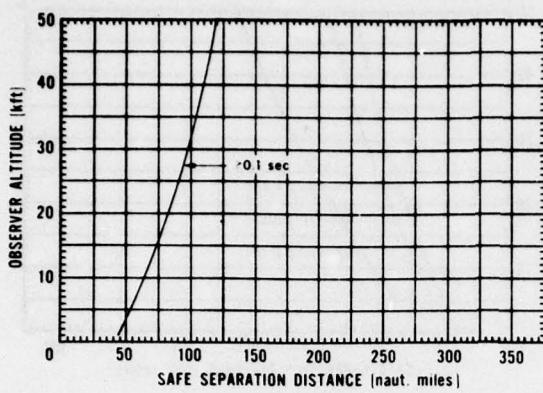


Figure C-33. 1,000 kt detonated at 30 kft (9.1 km).

Retinal Burn SSD



Flashblindness SSD

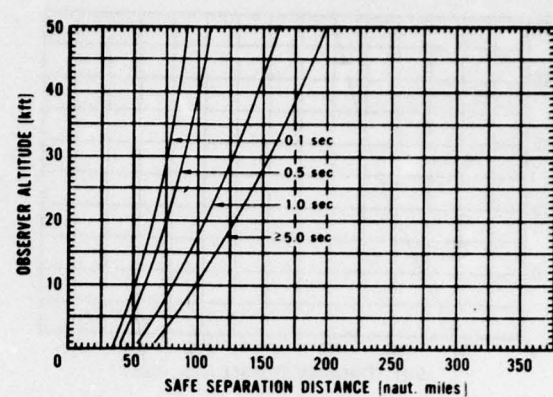


Figure C-34. 3,000 kt detonated at 1 kft (0.3 km).

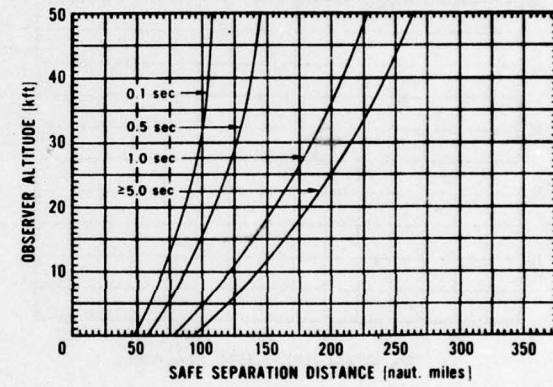
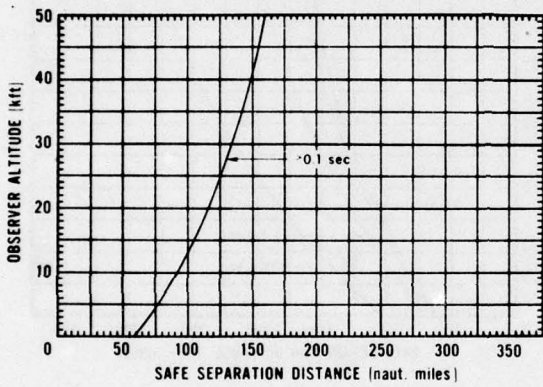


Figure C-35. 3,000 kt detonated at 10 kft (3 km).

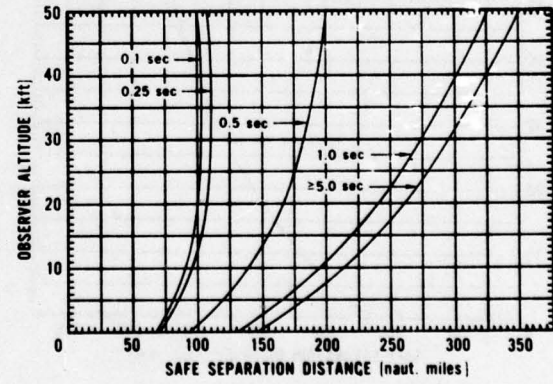
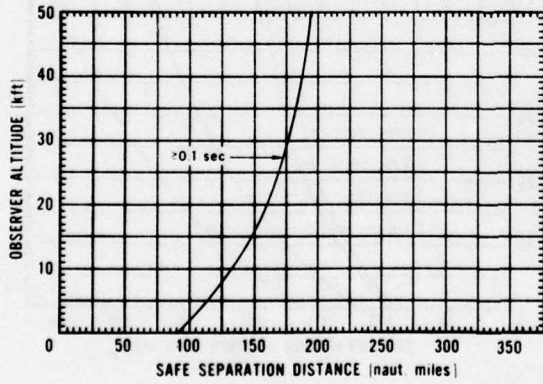
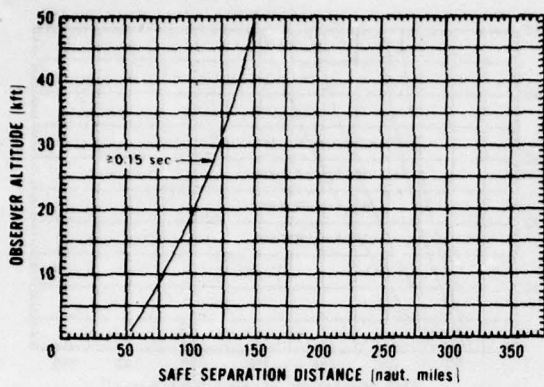


Figure C-36. 3,000 kt detonated at 30 kft (9.1 km).

Retinal Burn SSD



Flashblindness SSD

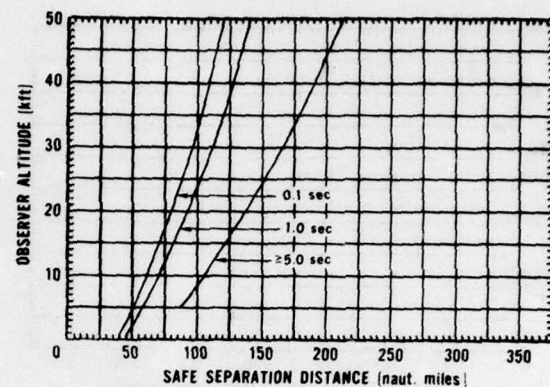


Figure C-37. 10,000 kt detonated at 1 kft (0.3 km).

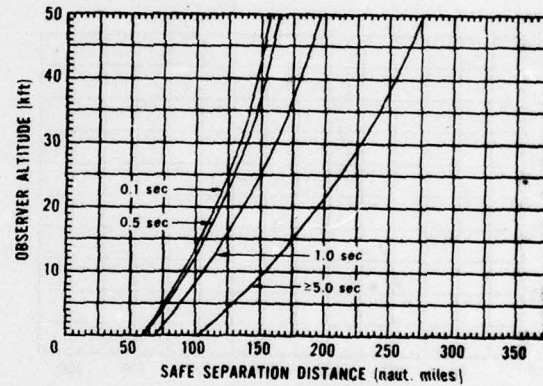
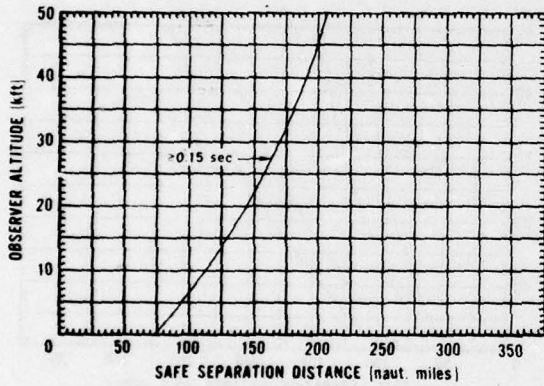


Figure C-38. 10,000 kt detonated at 10 kft (3 km).

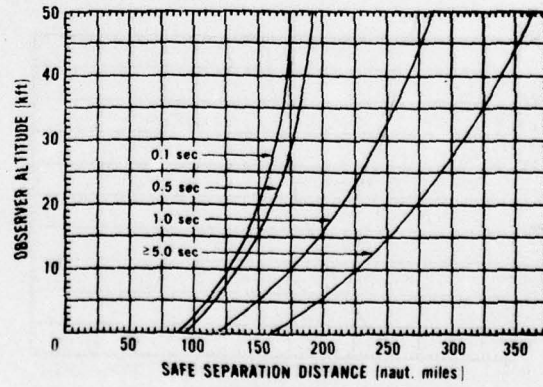
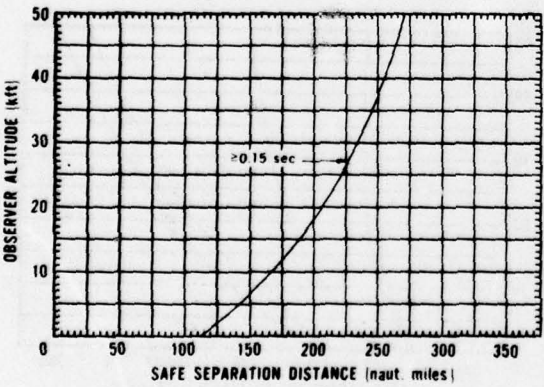
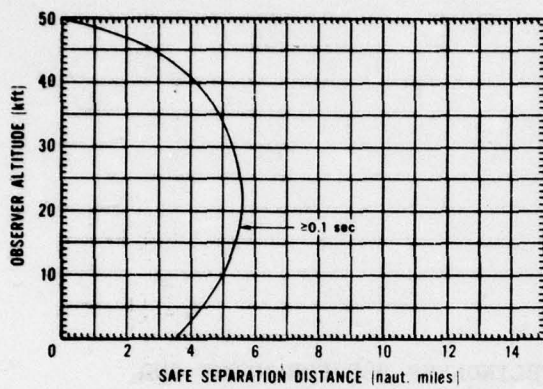


Figure C-39. 10,000 kt detonated at 30 kft (9.1 km).

**APPENDIX D: RETINAL BURN AND FLASHBLINDNESS SSD FOR NIGHT AND  
5-NAUT.-MILE (9.3-KM) VISIBILITY**

Curves in Figures D-1 through D-39 show minimum SSD plotted vs. observer altitude for retinal burns and flashblindness at night (7-mm pupil dia.) and 5-naut.-mile visibility for detonation yields, altitudes, and blink times as indicated.

Retinal Burn SSD



Flashblindness SSD

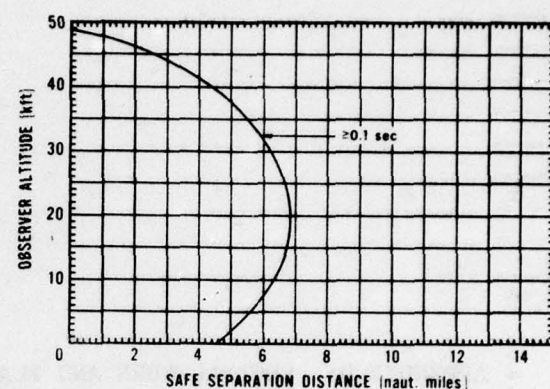


Figure D-1. 0.01 kt detonated at 1 kft (0.3 km).

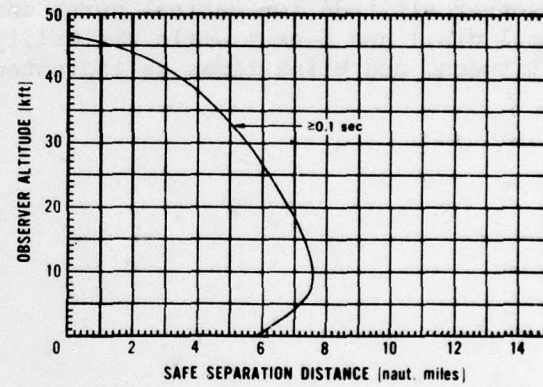
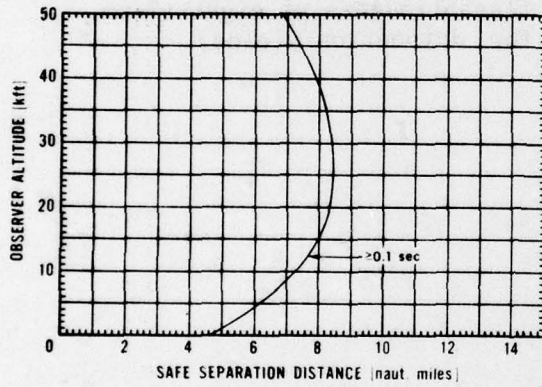


Figure D-2. 0.01 kt detonated at 10 kft (3 km).

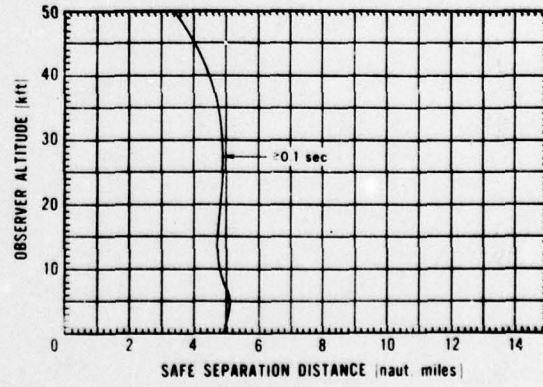
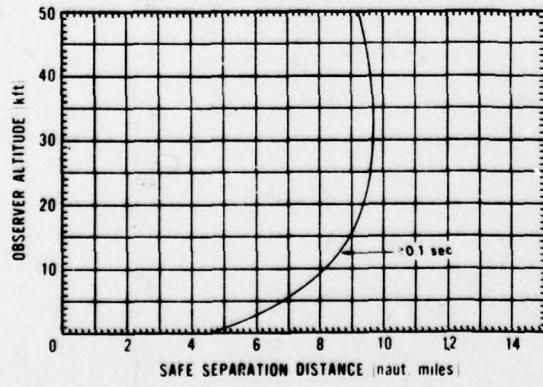
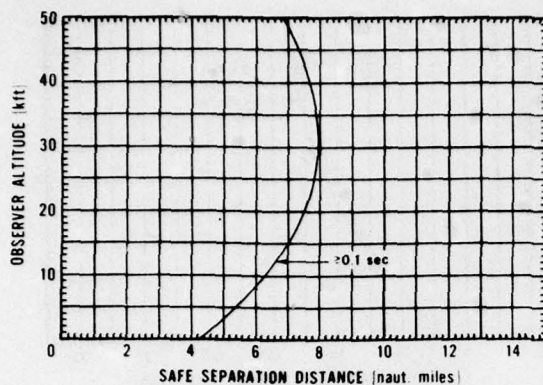


Figure D-3. 0.01 kt detonated at 30 kft (9.1 km).

Retinal Burn SSD



Flashblindness SSD

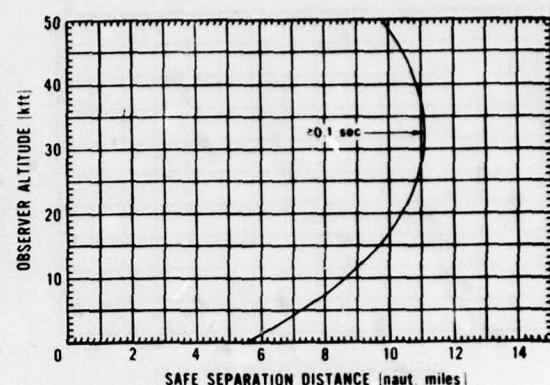


Figure D-4. 0.03 kt detonated at 1 kft (0.3 km).

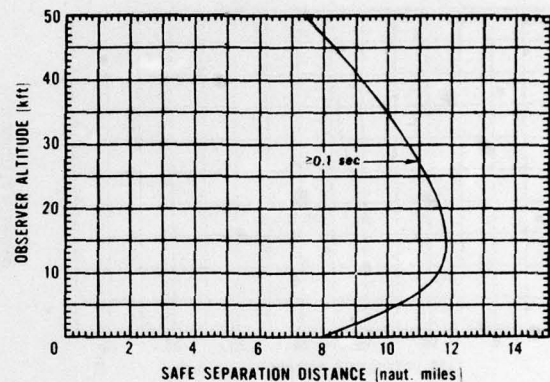
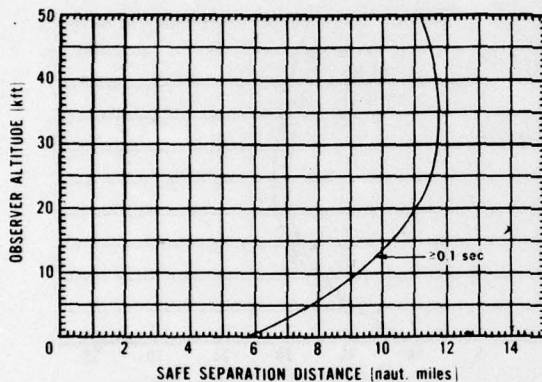


Figure D-5. 0.03 kt detonated at 10 kft (3 km).

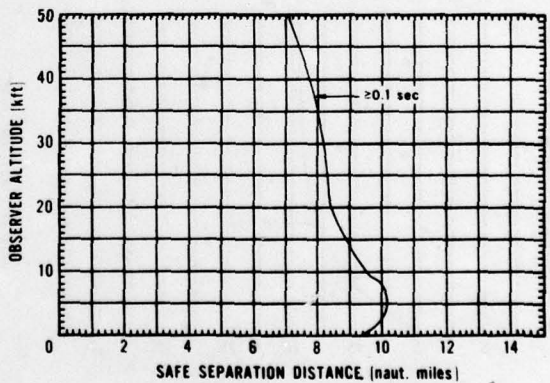
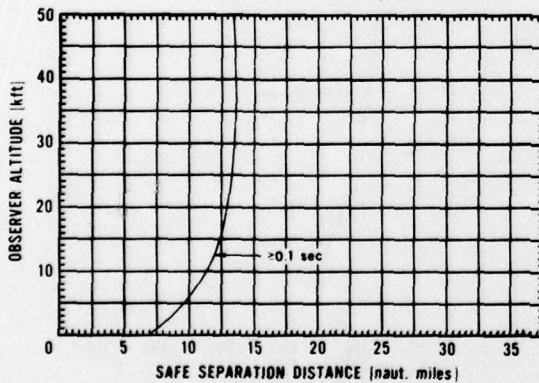
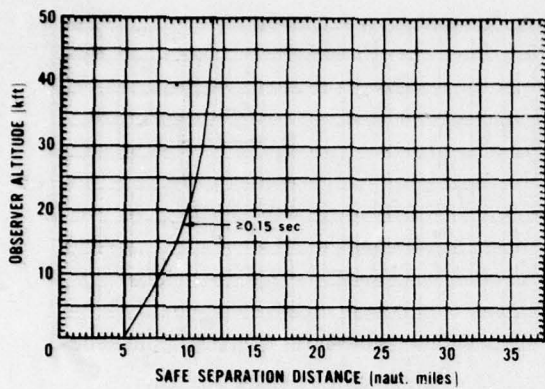


Figure D-6. 0.03 kt detonated at 30 kft (9.1 km).

Retinal Burn SSD



Flashblindness SSD

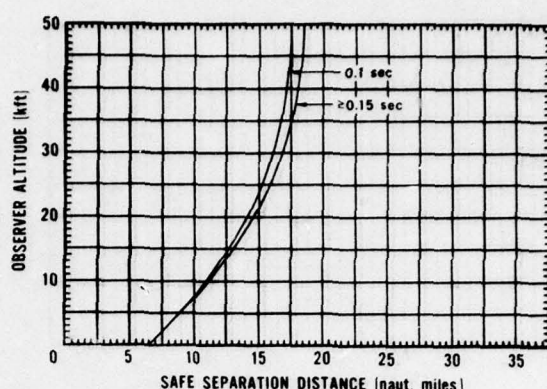


Figure D-7. 0.1 kt detonated at 1 kft (0.3 km).

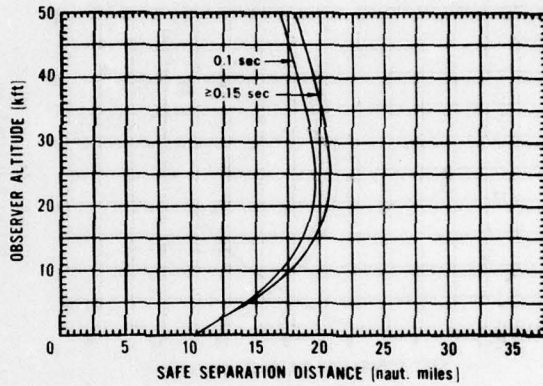
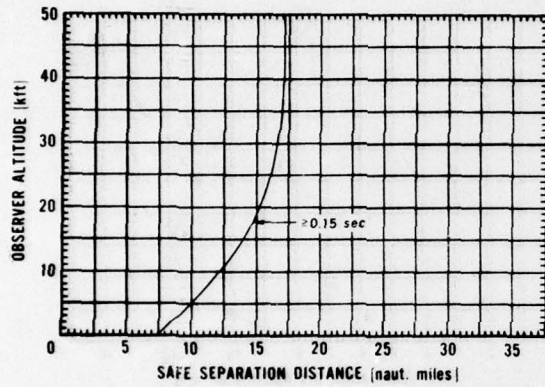


Figure D-8. 0.1 kt detonated at 10 kft (3 km).

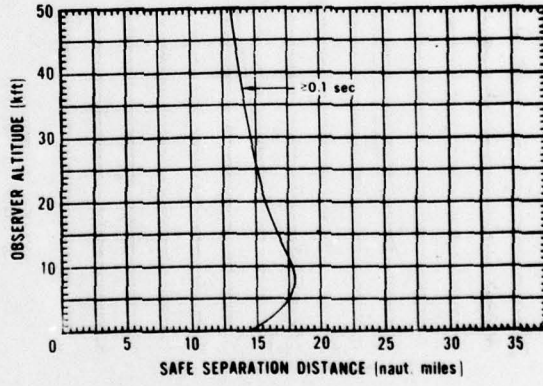
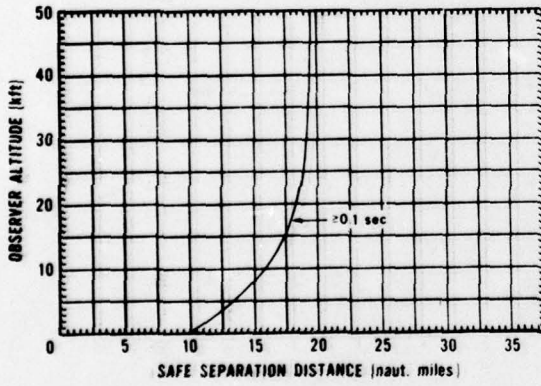
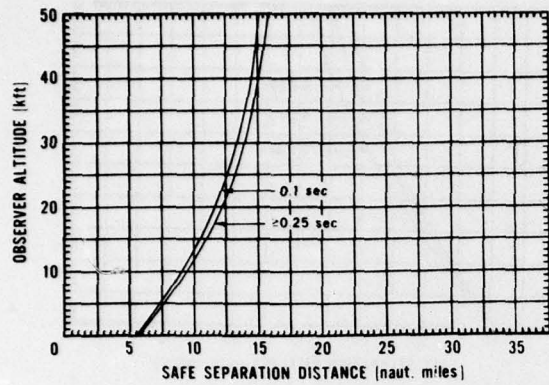


Figure D-9. 0.1 kt detonated at 30 kft (9.1 km).

Retinal Burn SSD



Flashblindness SSD

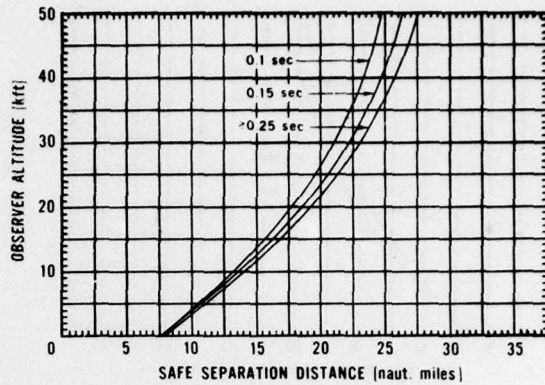


Figure D-10. 0.3 kt detonated at 1 kft (0.3 km).

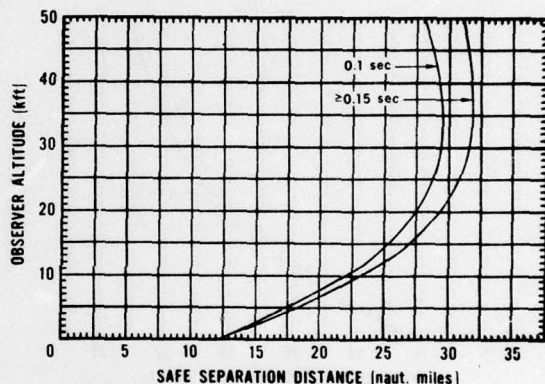
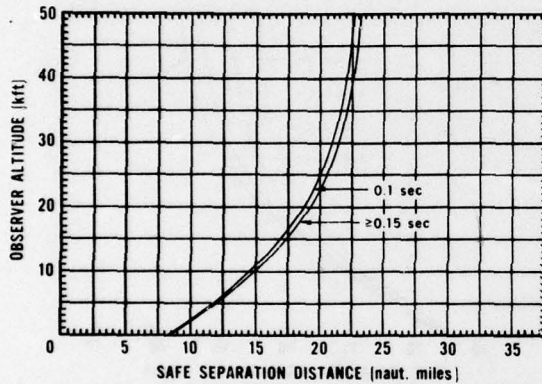


Figure D-11. 0.3 kt detonated at 10 kft (3 km).

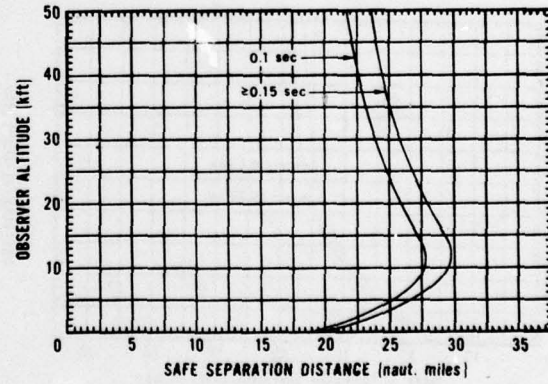
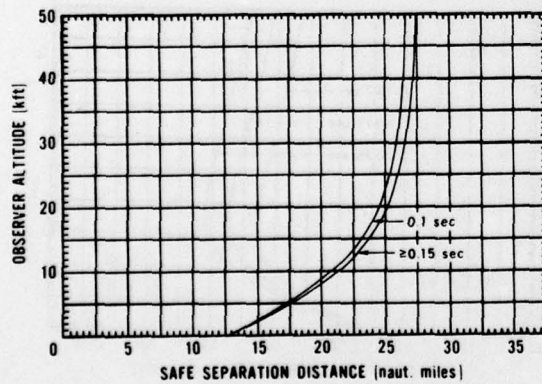
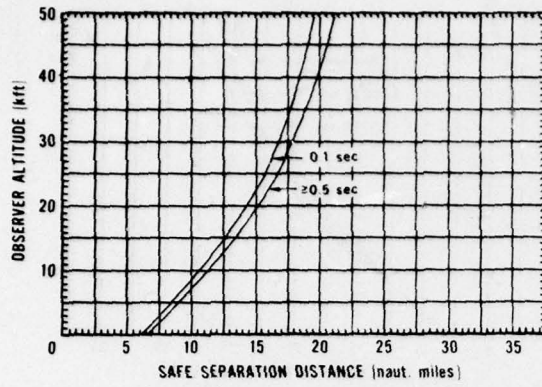


Figure D-12. 0.3 kt detonated at 30 kft (9.1 km).

Retinal Burn SSD



Flashblindness SSD

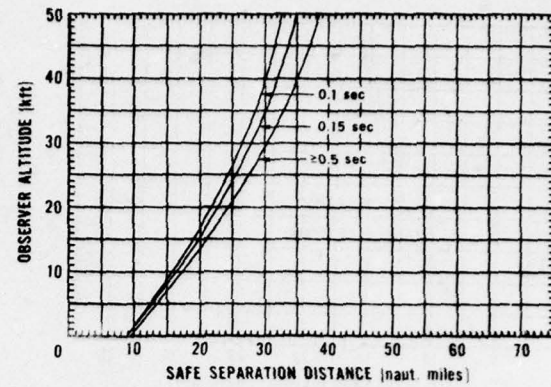


Figure D-13. 1 kt detonated at 1 kft (0.3 km).

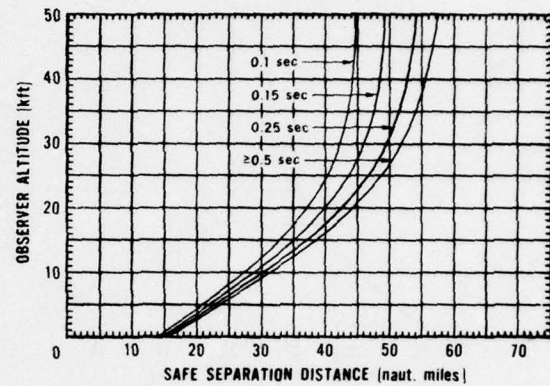
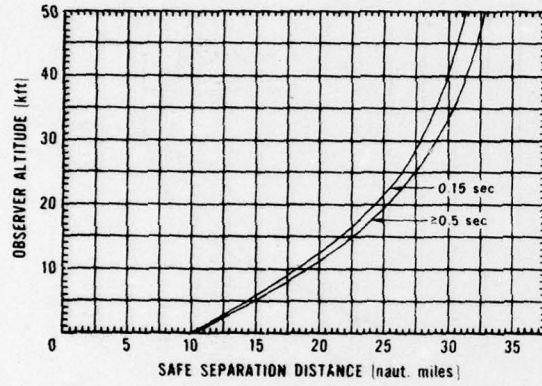


Figure D-14. 1 kt detonated at 10 kft (3 km).

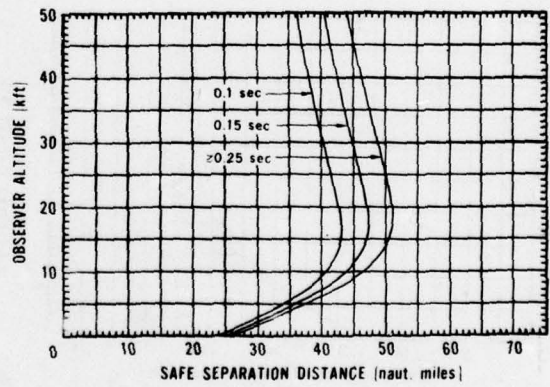
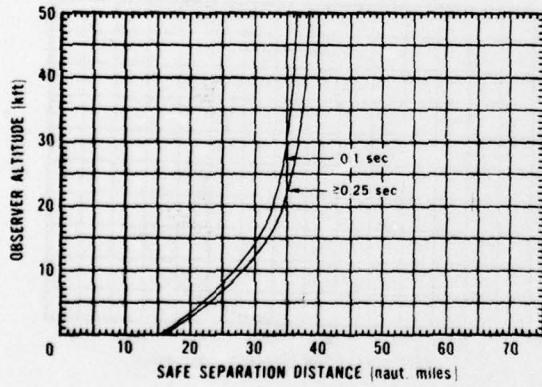
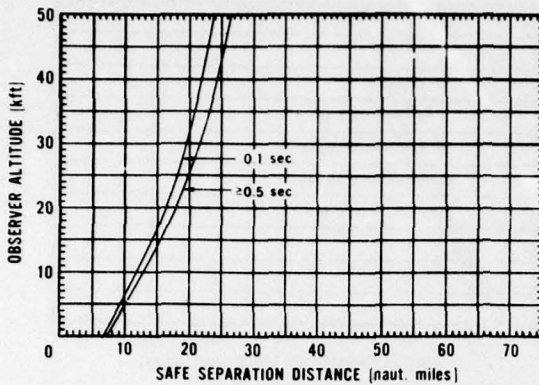


Figure D-15. 1 kt detonated at 30 kft (9.1 km).

Retinal Burn SSD



Flashblindness SSD

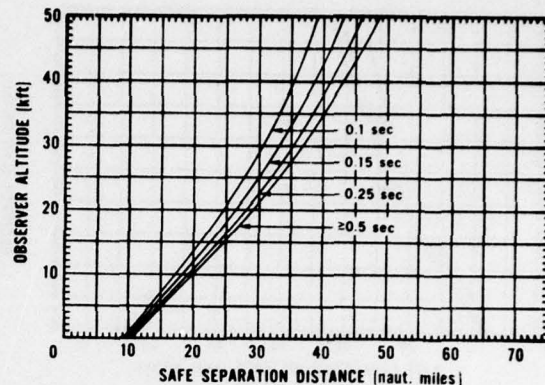


Figure D-16. 3 kt detonated at 1 kft (0.3 km).

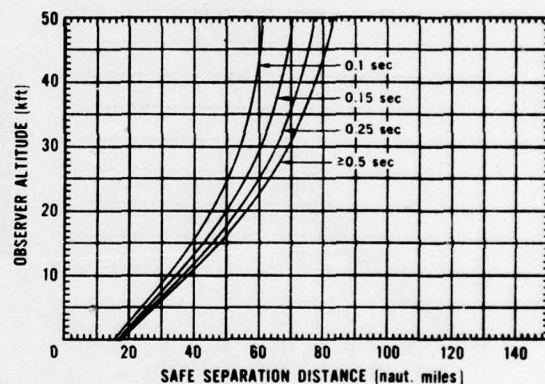
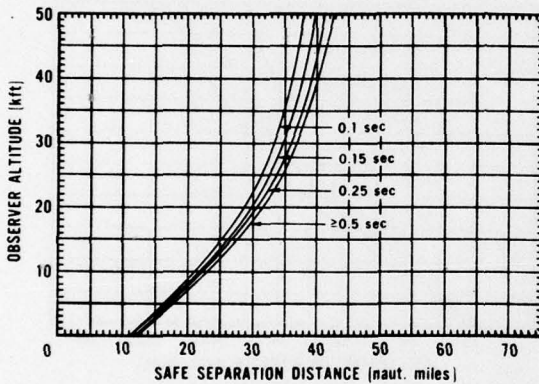


Figure D-17. 3 kt detonated at 10 kft (3 km).

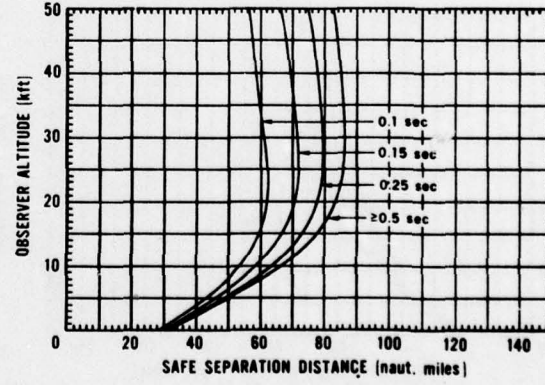
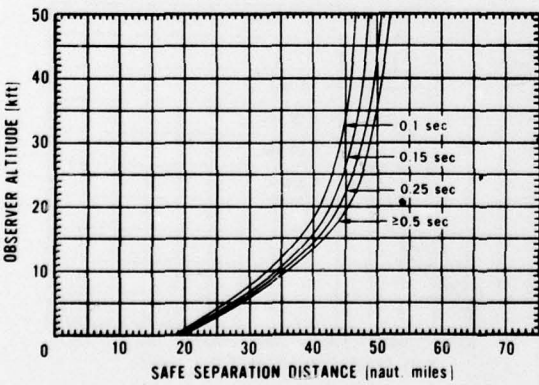
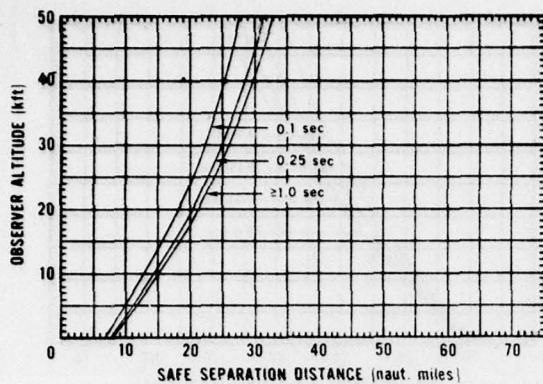


Figure D-18. 3 kt detonated at 30 kft (9.1 km).

Retinal Burn SSD



Flashblindness SSD

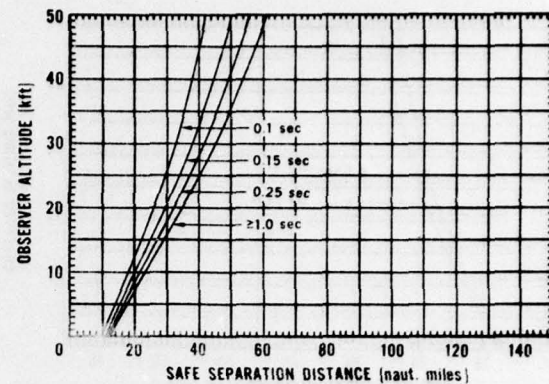


Figure D-19. 10 kt detonated at 1 kft (0.3 km).

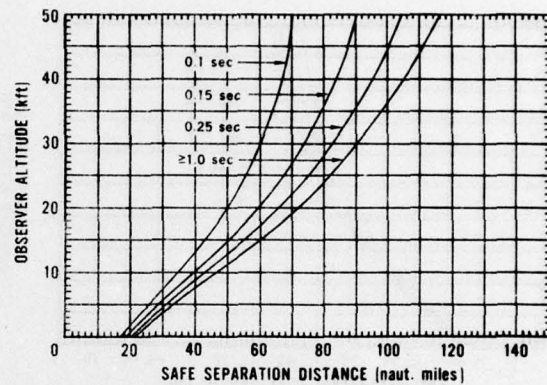
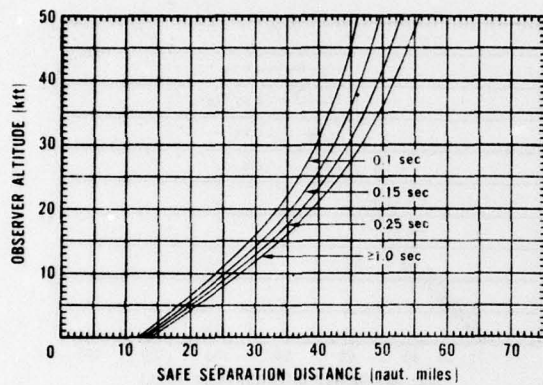


Figure D-20. 10 kt detonated at 10 kft (3 km).

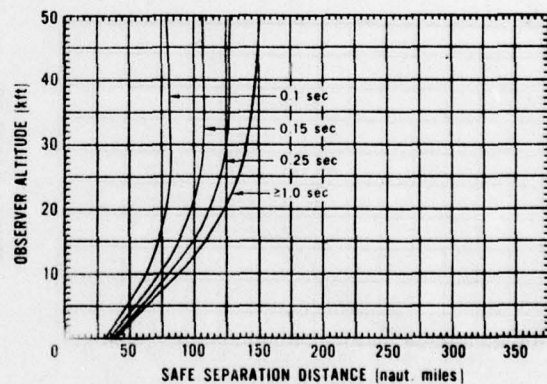
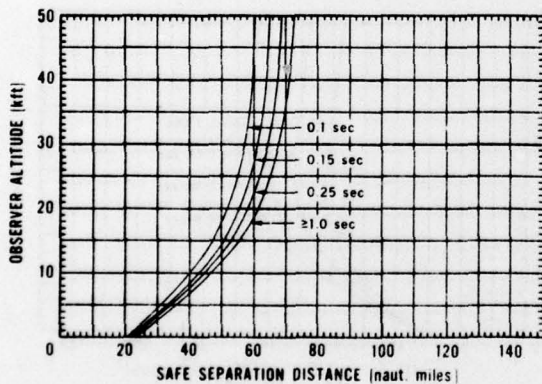
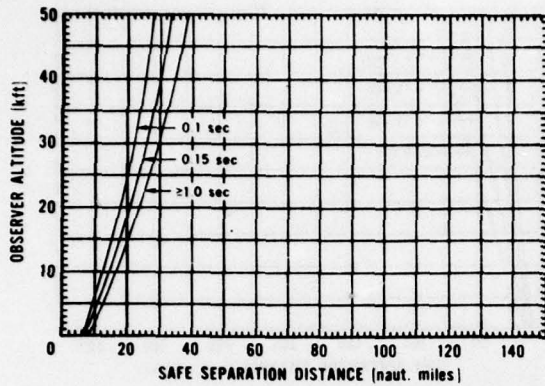


Figure D-21. 10 kt detonated at 30 kft (9.1 km).

Retinal Burn SSD



Flashblindness SSD

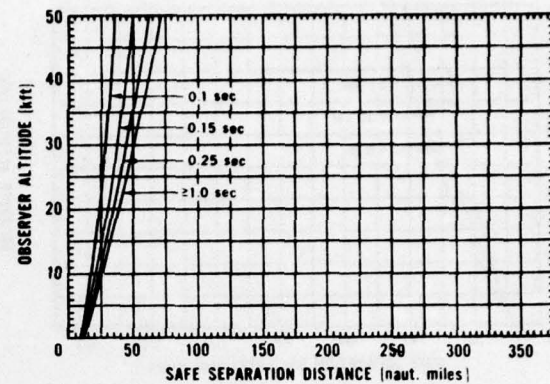


Figure D-22. 30 kt detonated at 1 kft (0.3 km).

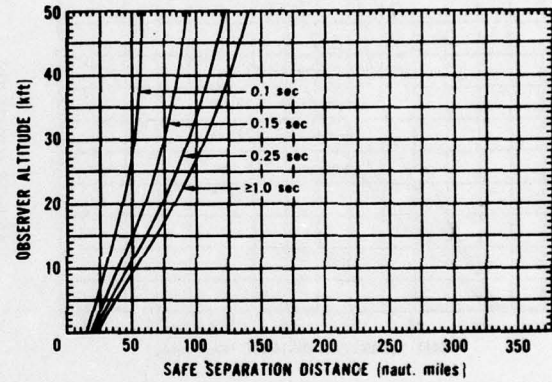
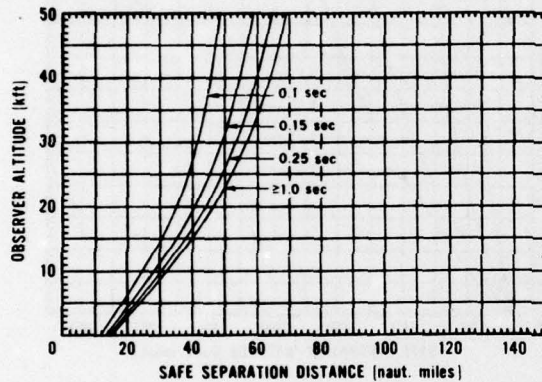


Figure D-23. 30 kt detonated at 10 kft (3 km).

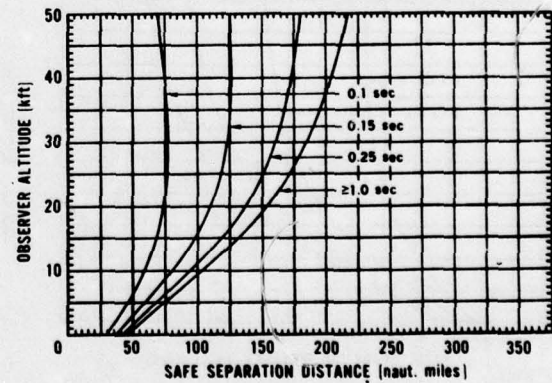
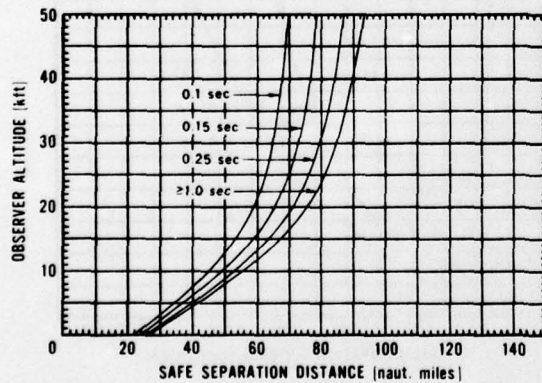
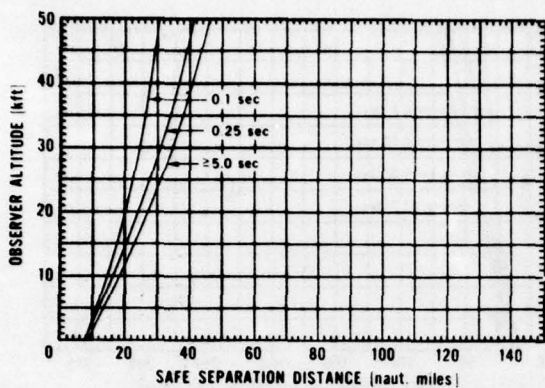


Figure D-24. 30 kt detonated at 30 kft (9.1 km).

Retinal Burn SSD



Flashblindness SSD

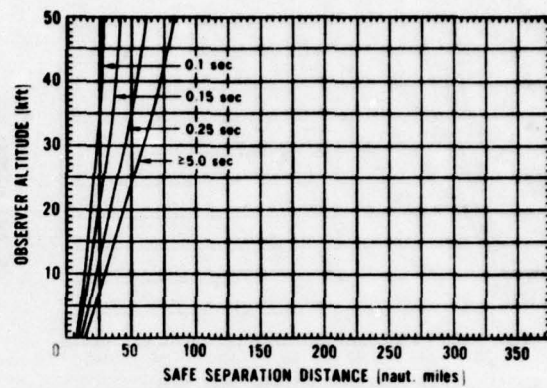


Figure D-25. 100 kt detonated at 1 kft (0.3 km).

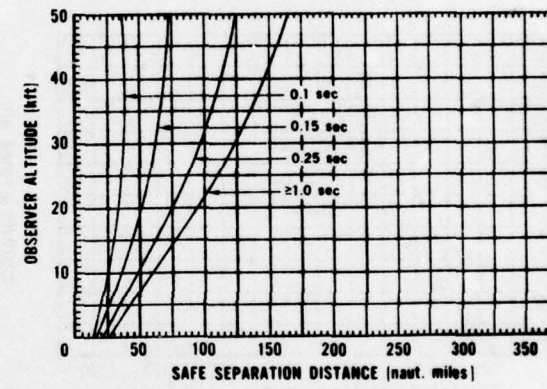
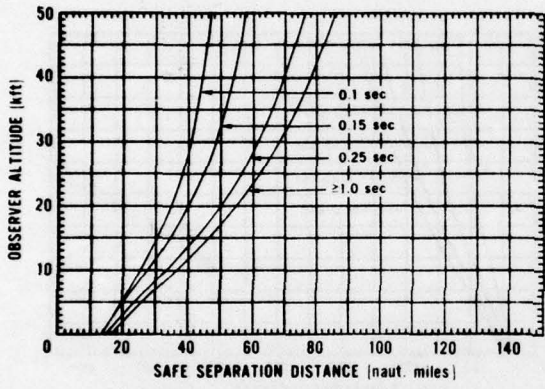


Figure D-26. 100 kt detonated at 10 kft (3 km).

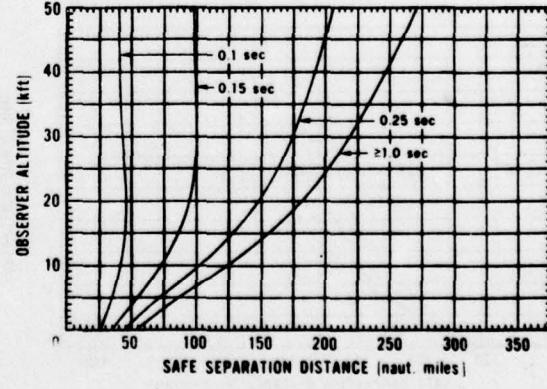
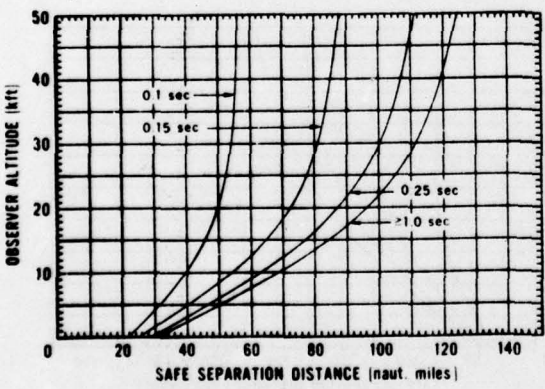
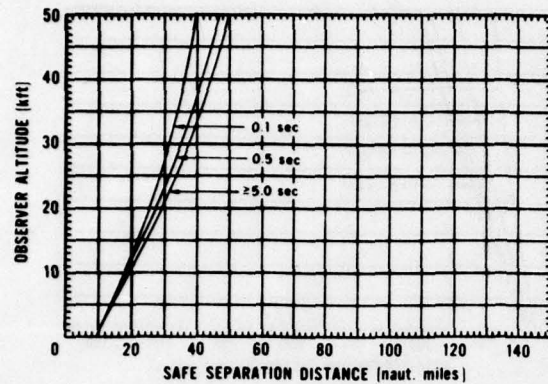


Figure D-27. 100 kt detonated at 30 kft (9.1 km).

Retinal Burn SSD



Flashblindness SSD

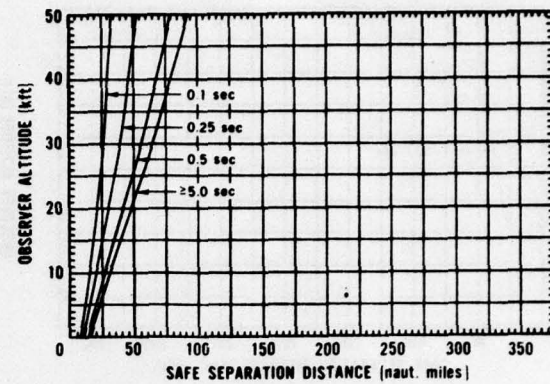


Figure D-28. 300 kt detonated at 1 kft (0.3 km).

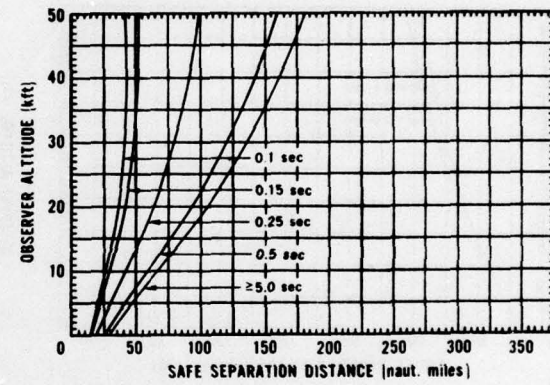
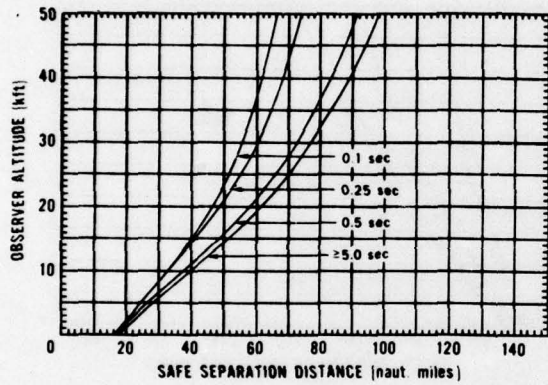


Figure D-29. 300 kt detonated at 10 kft (3 km).

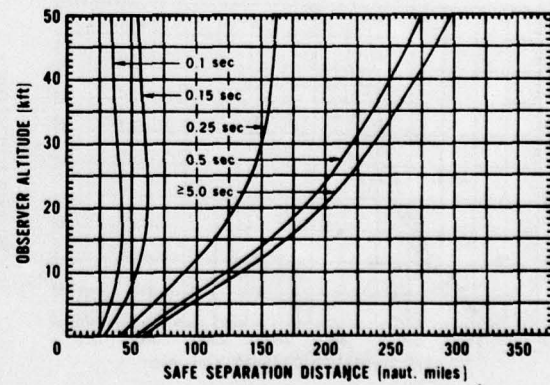
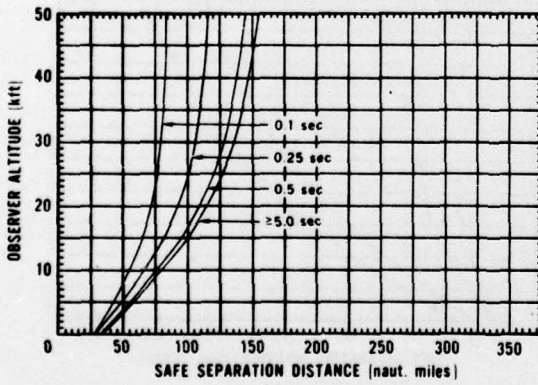
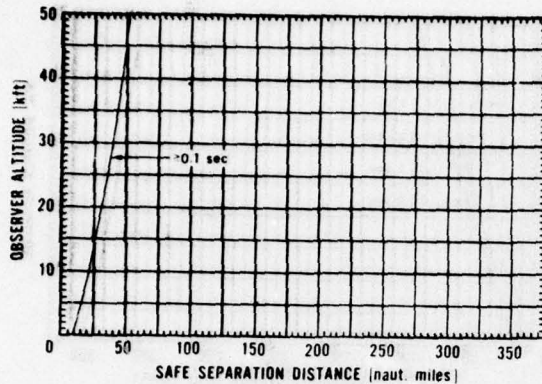


Figure D-30. 300 kt detonated at 30 kft (9.1 km).

Retinal Burn SSD



Flashblindness SSD

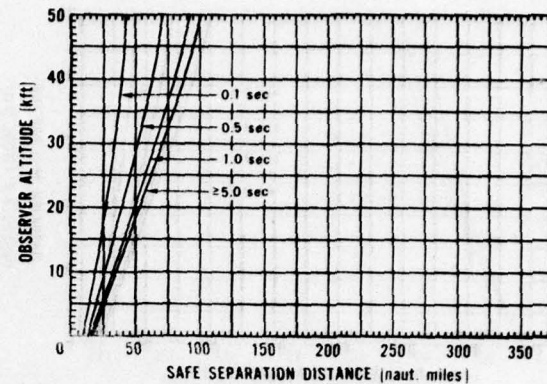


Figure D-31. 1,000 kt detonated at 1 kft (0.3 km).

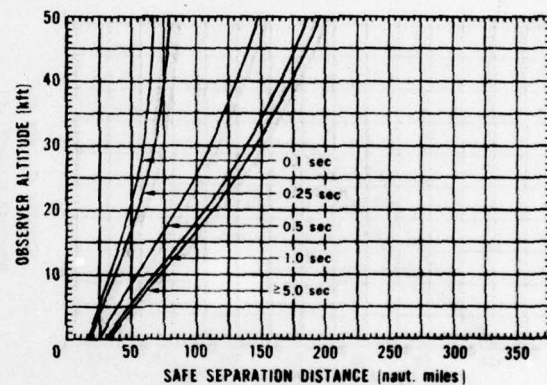
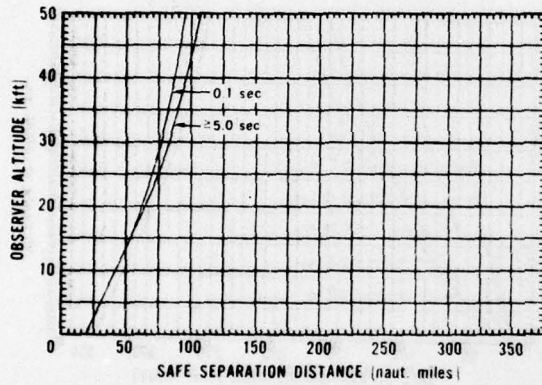


Figure D-32. 1,000 kt detonated at 10 kft (3 km).

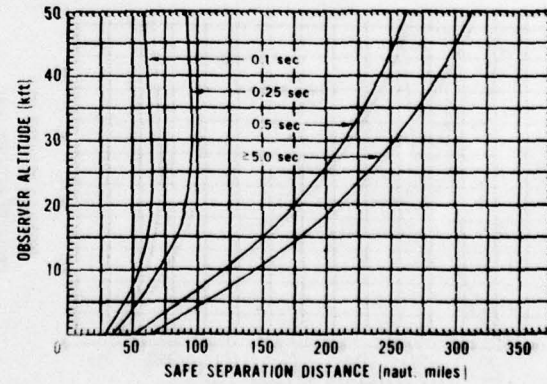
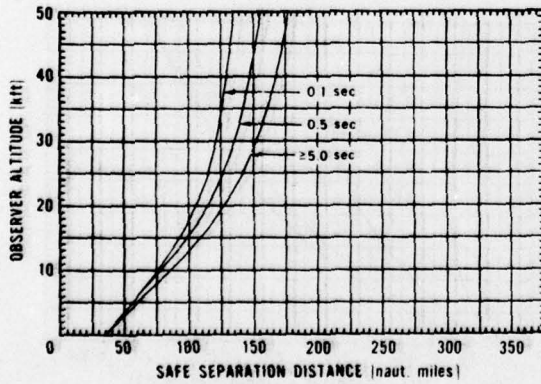
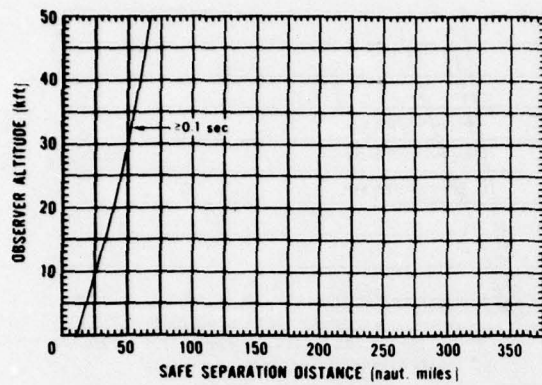


Figure D-33. 1,000 kt detonated at 30 kft (9.1 km).

Retinal Burn SSD



Flashblindness SSD

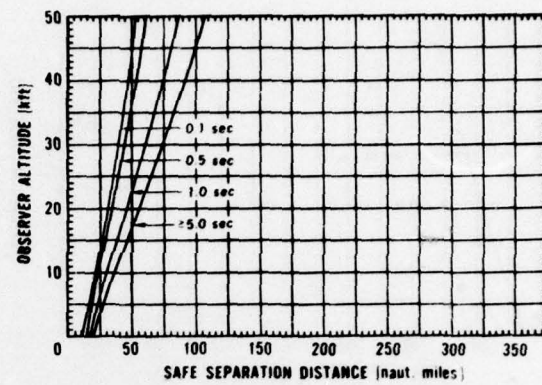


Figure D-34. 3,000 kt detonated at 1 kft (0.3 km).

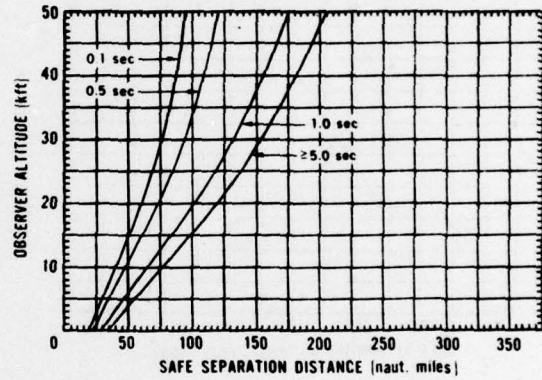
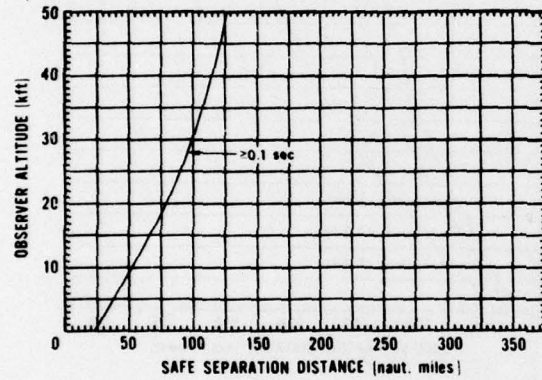


Figure D-35. 3,000 kt detonated at 10 kft (3 km).

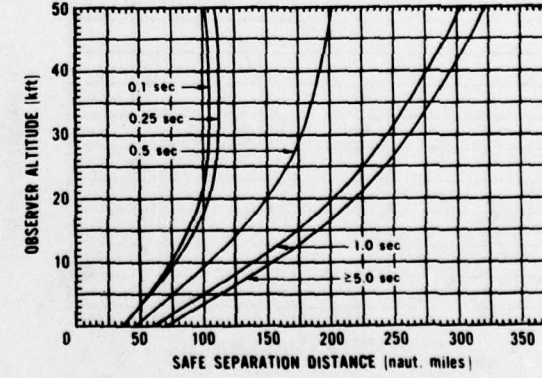
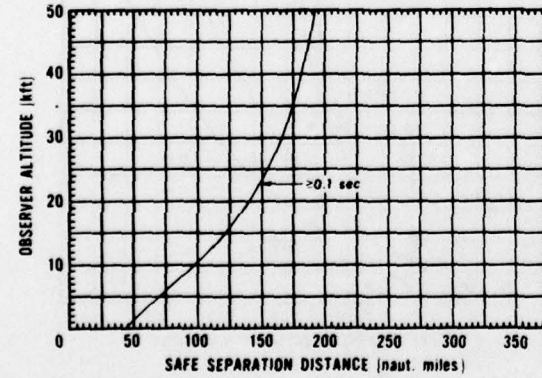
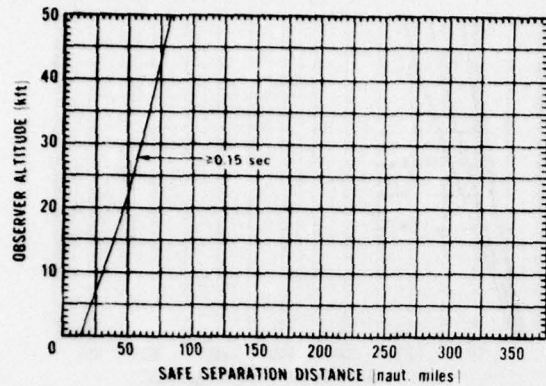


Figure D-36. 3,000 kt detonated at 30 kft (9.1 km).

Retinal Burn SSD



Flashblindness SSD

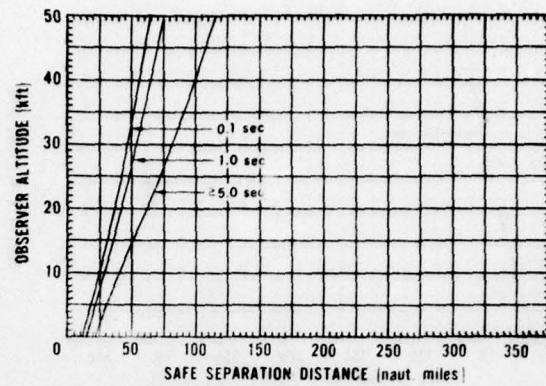


Figure D-37. 10,000 kt detonated at 1 kft (0.3 km).

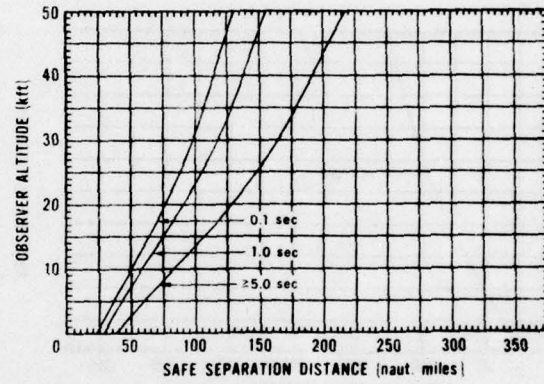
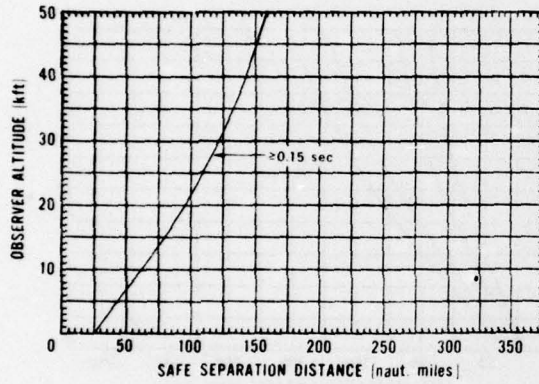


Figure D-38. 10,000 kt detonated at 10 kft (3 km).

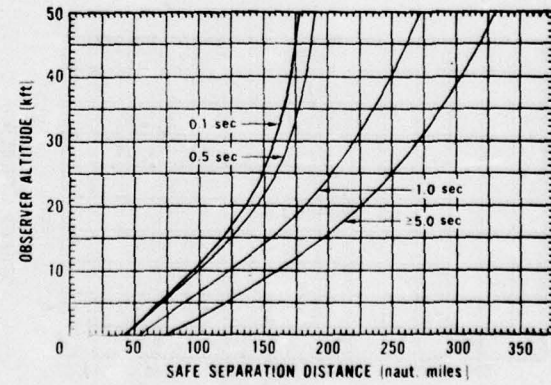
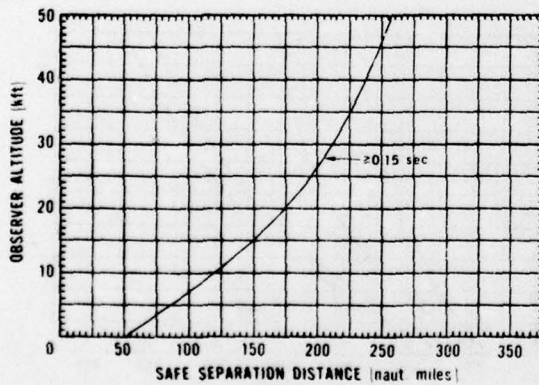


Figure D-39. 10,000 kt detonated at 30 kft (9.1 km).